THE VIENNA RECTIFIER IN AIRCRAFT APPLICATIONS: CURRENT DISTORTION MITIGATION METHODS

MOLLIGODA LIYANAGE DEVINDA ANUSHKA

School of Electrical & Electronic Engineering

A thesis submitted to the Nanyang Technological University
in partial fulfilment of the requirement for the degree of
Doctor of Philosophy

2021

Statement of Originality

I hereby certify that the work embodied in this thesis is the result of original research, is free of plagiarised materials, and has not been submitted for a higher degree to any other University or Institution.

19-08-21

. . . . . .

Date

. . . . . .

Molligoda Liyanage Devinda Anushka

Supervisor Declaration Statement

I have reviewed the content and presentation style of this thesis and declare it is free of plagiarism and of sufficient grammatical clarity to be examined. To the best of my knowledge, the research and writing are those of the candidate except as acknowledged in the Author Attribution Statement. I confirm that the investigations were conducted in accord with the ethics policies and integrity standards of Nanyang Technological University and that the research data are presented honestly and without prejudice.

19/08/2021

Date

Prof. Josep Pou

Authorship Attribution Statement

This thesis contains material from 4 papers published in the following peer-reviewed journals / from papers accepted at conferences in which I am listed as an author.

Chapter 3 is published as D. A. Molligoda, J. Pou, C. J. Gajanayake, and A. K. Gupta, “Analysis of the Vienna Rectifier under Nonunity Power Factor Operation,” in *Proc. Asian Conf. on Energy, Power and Transport. Electrific. (ACEPT)*, Oct. 2018, pp. 1–7,

D. A. Molligoda, J. Pou, S. Ceballos, K. Satpathi, F. Sasongko, C. J. Gajanayake, and A. K. Gupta, “Current Distortion Mitigation in Grid-Connected Vienna Rectifier During Nonunity Power Factor Operation,” in *Proc. IEEE Ind. Electron. Soc. (IECON)*, 2020, pp. 4085–4090,

D. A. Molligoda, S. Ceballos, J. Pou, K. Satpathi, F. Sasongko, C. J. Gajanayake, and A. K. Gupta, “Mitigating Zero-Crossing Current Distortion in the Vienna Rectifier When Operating with Nonunity Power Factor,” *IEEE Trans. Emerg. Sel. Topics Power Electron*. (In preparation).

The contributions of the co-authors are as follows:

- Prof. Josep Pou and Dr. Salvador Ceballos provided the initial concept development, reviewed the derived equations and edited the manuscript drafts.
- I prepared the manuscript drafts. The manuscript was revised by Dr. Kuntal Satpathi and Dr. Firman Sasongko.
- I designed the experiment and performed all the laboratory work at the Rolls-Royce @ NTU Corporate Lab.
- Dr. Firman Sasongko assisted me with debugging the hardware.
- Dr. Chandana Gajanayake assisted with project direction, technical matters and Rolls-Royce alignment.
- Dr. Amit Gupta assisted in the project direction and Rolls-Royce alignment.

Chapter 4 is published as D. A. Molligoda, S. Ceballos, J. Pou, K. Satpathi, F. Sasongko, C. J. Gajanayake, and A. K. Gupta, "Hybrid Modulation Strategy to Avoid Zero Crossing Distortion in the Vienna Rectifier," in *Proc. IEEE Energy Conversion Congress and Exposition (ECCE- Asia)*, 2021, pp. 1245–1249,

D. A. Molligoda, S. Ceballos, J. Pou, K. Satpathi, F. Sasongko, C. J. Gajanayake, and A. K. Gupta, " Hybrid Modulation Strategy for the Vienna Rectifier," *IEEE Trans. Power Electron*. (Accepted - Early Access).

The contributions of the co-authors are as follows:

- Prof. Josep Pou and Dr. Salvador Ceballos provided the initial concept development, reviewed the derived equations and edited the manuscript drafts.
- I prepared the manuscript drafts. The manuscript was revised by Dr. Kuntal Satpathi and Dr. Firman Sasongko.
- I designed the experiment and performed all the laboratory work at the Rolls-Royce @ NTU Corporate Lab.
- Dr. Firman Sasongko assisted me with debugging the hardware.
- Dr. Chandana Gajanayake assisted with project direction, technical matters and Rolls-Royce alignment.
- Dr. Amit Gupta assisted in the project direction and Rolls-Royce alignment.

19-08-21

. . . . . .

Date

. . . . . .

Molligoda Liyanage Devinda Anushka

Acknowledgements

I would like to express my special appreciation and thanks to my supervisor, Professor Josep Pou for giving me an opportunity to carry on pursuing my interest in research works under his valuable guidance. His inspiring spirit and enthusiasm as well as his given advices throughout the years are especially recognized and appreciated. It is an honor and pleasure to have him as my supervisor.

I wish to express my gratitude to my Rolls-Royce managers Dr. Chandana Gajanayaka and Adjuc. Prof. Amit Gupta for giving me the opportunity to carryout my experiments in the Rolls-Royce @ NTU Corporate Lab as well as give technical guidance when required.

Dr. Salvador Ceballos from Tecnalia Research and Innovation, Spain, has given me wonderful suggestions on my research studies. I would like to express my special thanks to him for his kind contributions despite his busy schedule.

My special thanks go to my Thesis Advisory Committee member, Assistant Professor Amer Ghias, for his encouragement throughout my research.

Financial assistance provided by the Nanyang Technological University in the form of Graduate Scholarship is thankfully acknowledged. Special thanks to my fellow researchers Firman, Kunthal, Sathik, Prashanth, Ghias, Hossein, Naga, Neha, Chris, Ezequiel, Jaspreet, Wang Shuai, Yu Yang, Fan Fei and Mridul from NTU for the patient discussions and helping hands.

Last but not least, I would like to thank my loving family. Words cannot express how grateful I am to my loving wife Uthpala, daughter Isumi, son Isath, my parents and brother for their love, encouragement and support.

Abstract

Electrical power demand is steadily increasing in more electric aircraft (MEA) as conventional pneumatic, hydraulic and mechanical loads are being replaced by electrical loads. The main motivation behind this trend is to reduce emissions, fuel usage, noise, etc. The designers are increasing the voltage levels to cater the power demand with reduced ohmic losses and conductor size, resulting in weight reduction and improvement of overall system efficiency. This trend also demands high power density converters. This research is focused on identifying a suitable topology and improving the overall performance of the power converter to transfer power from a generator, to a dc distribution network in future MEA. The studied solution should provide high power density, efficiency, power quality, and reliability. After benchmarking with the widely used two-level converter, the Vienna rectifier topology has been selected.

The Vienna rectifier is based on a diode bridge rectifier and therefore it has unidirectional power flow. It can generate three voltage levels that can be operated with pulse-width modulation (PWM). Despite being able to generate three voltage levels, only the connection to the neutral-point is fully controllable using the bidirectional switches. When the neutral-point voltage is not imposed in a phase-leg, the polarity of the pulses generated depends on the diode that is conducting in that phase-leg, which is defined by the current direction. As a result, the voltage pulses generated can go in the opposite direction to what is demanded by the controller, and hence the current becomes distorted. The challenge of this research is to improve the performance of the Vienna rectifier under such operating conditions.

The Vienna rectifier is connected to a programmable ac source, where the frequency can be varied and the grid voltages can be measured. Initially, two operation modes based on a special zero sequence and reactive power injection have been proposed depending on the operating conditions of the converter. Then, a hybrid modulation method is proposed combining the above two methods, achieving a smooth transition between operating points with significant less reactive current injection. With the proposed methods, the Vienna rectifier can operate in a wide range of

power factors without compromising the quality of the source currents and within the aerospace standards. The proposed solutions are validated in an experimental setup.

Table of Contents

List of Figures

List of Tables

List of Acronyms and Notations

A. List of Acronyms

AEA	All Electric Aircraft
CB-PWM	Carrier-based Pulse-Width Modulation
DSP	Digital Signal Processor
DDSRF	Decoupled Double Synchronous Reference Frame
ESD	Electrostatic Discharge
FFT	Fast Fourier Transform
FOC	Field Oriented Control
GCU	Generator Control Unit
IG	Induction Generator
IPM	Interior Permanent Magnet
LPF	Low Pass Filter
MAF	Moving Average Filter
MEA	More Electric Aircraft
MPC	Model Predictive Control
NPC converter	Neutral-Point-Clamped converter
PCC	Point of Common Coupling
PFC	Power Factor Correction
PI controller	Proportional-integral controller
PM	Permanent Magnet
PMSG	Permanent Magnet Synchronous Generator
PWM	Pulse-Width Modulation
PD-PWM	Phase Disposition Pulse-Width Modulation
SPM	Surface Permanent Magnet
SRG	Switched Reluctance Generator
SVM	Space-Vector Modulation
TRU	Transformer Rectifier Unit
UPF	Unity Power Factor

VFG	Variable Frequency Generator
VOC	Voltage Oriented Control

B. List of Notations

E	Source RMS voltage
E_d	Active source voltage component
E_q	Reactive source voltage component
f_0	Fundamental frequency
f_s	Switching frequency
i_d	d-axis current
i_q	q-axis current
i_α	α-axis
i_β	β-axis
i_{abc}	Three-phase current
I	Input current when operating with UPF at the source side
I_1	Input current when operating with UPF at the converter side
L	Boost inductance
L_d	direct axis stator inductance
L_q	quadrature axis stator inductance
ω_{re}	electrical rotor speed
p	Active power
q	Reactive power
RI	Voltage drop due to series resistance of inductor when operating in Mode-1
RI_1	Voltage drop due to series resistance of inductor when operating in Mode-2
V	Converter terminal voltage when operating with UPF at the source side
V_1	Converter terminal voltage when operating with UPF at the converter side
v_{dc}	dc-link voltage
v_d	d-axis voltage
v_q	q-axis voltage
V_L	Inductor voltage drop when operating with UPF at the source side
V_{1L}	Inductor voltage drop when operating with UPF at the converter side
S	Apparent power
T	Temperature
t	Time
ω	Fundamental pulsating frequency
ϕ	Phase difference of source voltage and input current - UPF at converter

Chapter 1

Introduction

This chapter presents the trends in air transport electrification, and explains the benefits and challenges of more electric aircraft. Subsequently, the motivations of the present research and its objectives are introduced. The chapter also states the major contributions achieved so far in this research work.

1.1 Background and Motivation

The air traffic market is continuously growing [1], and the industry faces both economic and environmental challenges. The statistics show that commercial air traffic is steadily increasing at around 5% per annum, doubling the air traffic approximately every 15 years [2] [3] (during pre-COVID-19 pandemic times), and further increase is expected in the next two decades. During the 2013-2018 period, year-over-year average traffic growth was 6.5%. The rapid growth in air travel is mainly due to competitive low air fares as well as socioeconomic changes in growing economies boosting travel and tourism, demanding more air travel [3].

With the trend of transportation electrification, electrical power demand is steadily increasing in more electric aircraft (MEA), as shown in Fig. 1.1, as conventional pneumatic, hydraulic and mechanical loads are being replaced by electrical loads [4–8]. The main motivation behind this trend is to reduce emissions, fuel usage, noise, etc. With the rapid advancements in power electronics and battery technologies, the concept of MEA and all electric aircraft (AEA) is becoming a reality.

In a conventional MEA, while the gas turbine provides the main propulsion power,

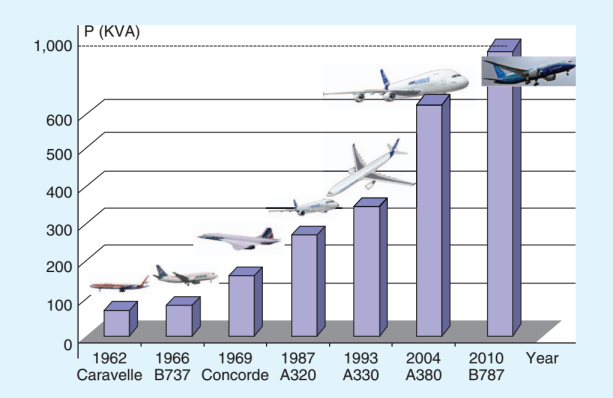

Figure 1.1: Evolution of electrical power needs in the Aircraft [1].

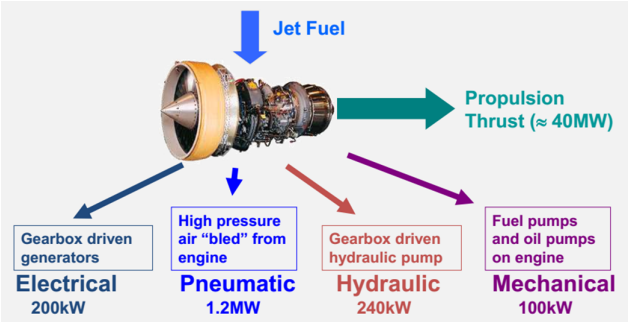

Figure 1.2: Power consumption of a typical large civilian aircraft [9].

it also gives power to electrical, pneumatic, hydraulic and mechanical loads, as illustrated in Fig. 1.2. Pneumatic loads include cabin pressurization, air conditioning, and icing protection, while hydraulic loads are flight control actuation, landing gear and braking. Examples for mechanical loads are fuel/oil pumping and engine ancillaries [4].

In aircraft power generation, the gas turbine engine is the prime mover, which speed varies across a wide range. To generate electrical power, a generator (usually a wound-field synchronous generator [5]) is connected to the prime mover through a gearbox. In most large civilian aircraft, this generator produces 115Vac three-phase voltages at 400Hz fixed frequency. Some of the newer aircraft generate 230Vac to handle higher power and they operate at variable frequency (360-800Hz) to simplify the gearbox [7] with the intention of reducing weight. The output power of the generator is processed through a rectifier, to produce a 270V dc bus, or 540V ($\pm$270V) in some newer aircraft [4] [10].

The 115/200Vac power system was standardized in MIL-STD-704, in 1959 [5]. However, as the electrical power demand in the aircraft is increasing, the designers can either increase the voltage or the current, to meet the power demand. An increase

in the current would require heavier conductors, which is unacceptable for the aircraft, as weight is a key design constraint that should be minimized. While moving towards higher voltages decreases the conduction losses and conductor size, resulting in weight reduction and improvement of overall system efficiency [11].

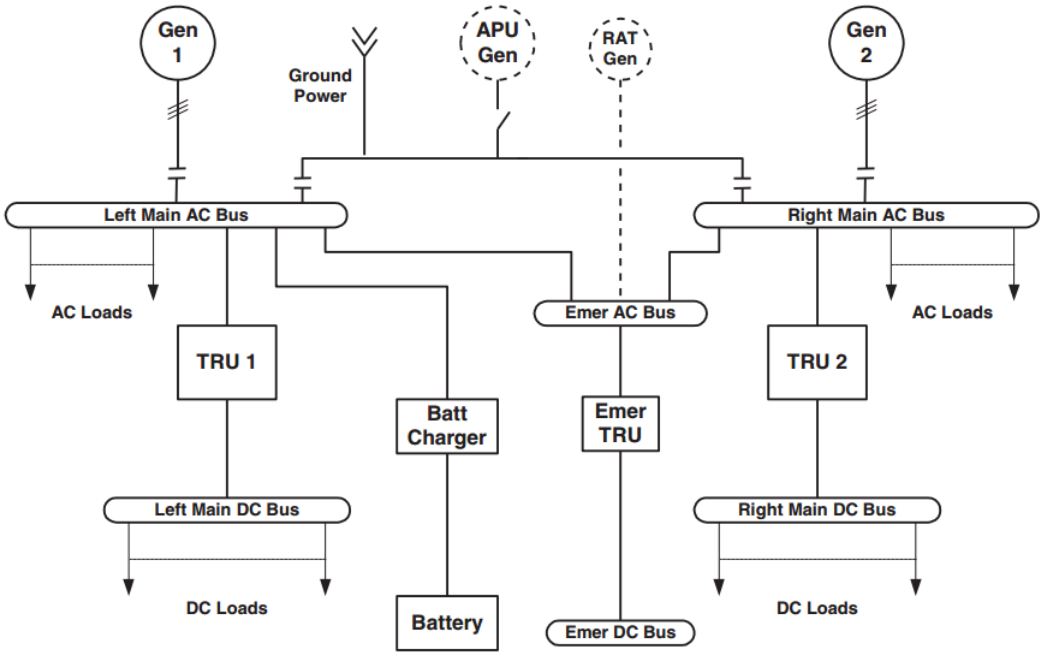

Figure 1.3: Typical aircraft electrical system [12].

An example of MEA power system is depicted in Fig. 1.3, which includes two synchronous generators controlled by generator control units (GCUs) feeding power to two split ac buses. They can be connected together using a bus tie switch. In each ac bus, there is a transformer rectifier unit (TRU) that converts the power to dc. The essential loads (e.g., electromechanical actuators) have redundant power sources, in the case of failure of one of them [12].

1.1.1 Benefits of the MEA

In studies conducted in 2016 [13] and 2018 [14, 15], it is shown that the air traffic (including domestic and international; passenger and cargo) accounts for approximately 2.5% of the global CO_2 emissions. Although this is a fraction of the total amount, with the increasing growth in the commercial air travel, the value could increase in the future unless measures are taken to minimize emissions. Furthermore, any technology change in the aerospace industry would take substantial amount of time, undergoing rigorous testing before it is implemented in an aircraft fleet. Al-

though the air traffic is growing at 5% per annum, the CO_2 emission growth due to air travel is at 2.2% per annum [3], partly because of electrification and the aircraft becoming more efficient. Other reasons include advancements of air traffic management and cabin utilization strategies by the airlines.

In terms of fuel consumption, as conventional loads are converted to electrical loads, size and weight is being reduced, thus improving the fuel economy. In [1], it is stated that for every kg of flight weight reduced saves 5,400 tons of CO_2 per year for all air traffic. Reducing these emissions would help combat climate change and make the aerospace business more economical as well as environmental friendly. Also, the environment around airports would benefit from reduced emissions and noise.

Electrical systems, when compared to hydraulic, pneumatic and mechanical systems, require significantly less maintenance. Also, with the implementation of prognostics in electrical systems, early detection of equipment failure is possible.

In summary, moving to MEA will make the future aircraft quieter, more fuel efficient, requiring less maintenance and more environmental friendly, which would lead to a reduction of the cost (both direct, e.g. fuel consumption, and indirect, e.g. maintenance), as well as improving carbon footprint, making air travel more sustainable.

1.1.2 Challenges for high power density converters in the MEA

Power electronics in aerospace applications need to withstand challenging operating conditions, which are mentioned in the DO160 standard. This standard specifies temperature, altitude (air pressure), temperature variation, humidity, shock, vibration, waterproofness, electrostatic discharge (ESD), lightning, etc. It is important for the converters to pass these tests, as they are expected to operate with low probability of failure in such harsh conditions. In the previous generations of aircraft, power generation was done using fixed frequency generation. But in the newer versions, power generation is at variable frequency, as the designers are simplifying the gearbox, coupling the prime-mover to the generator [1, 16, 17]. Hence, from a converter standpoint, this means the filters and controllers should be designed to work with variable fundamental frequency.

With the trend of moving to higher voltage in aircraft power distribution systems,

the probability of electrical discharges, which could potentially reduce the life of insulation systems over time, increases. This is due to the fact that breakdown of air is a function of the product of air pressure and gap length of the two conductors as stated in Paschen's Law [10] and depicted in Fig. 1.4. Based on this principle, the breakdown voltage for a 1-cm gap between two conductors will be approximately 40 kV at sea level, 6 kV at 50,000 ft, and 1 kV at 100,000 ft, i.e., the breakdown voltage reduces as the altitude increases for a given clearance.

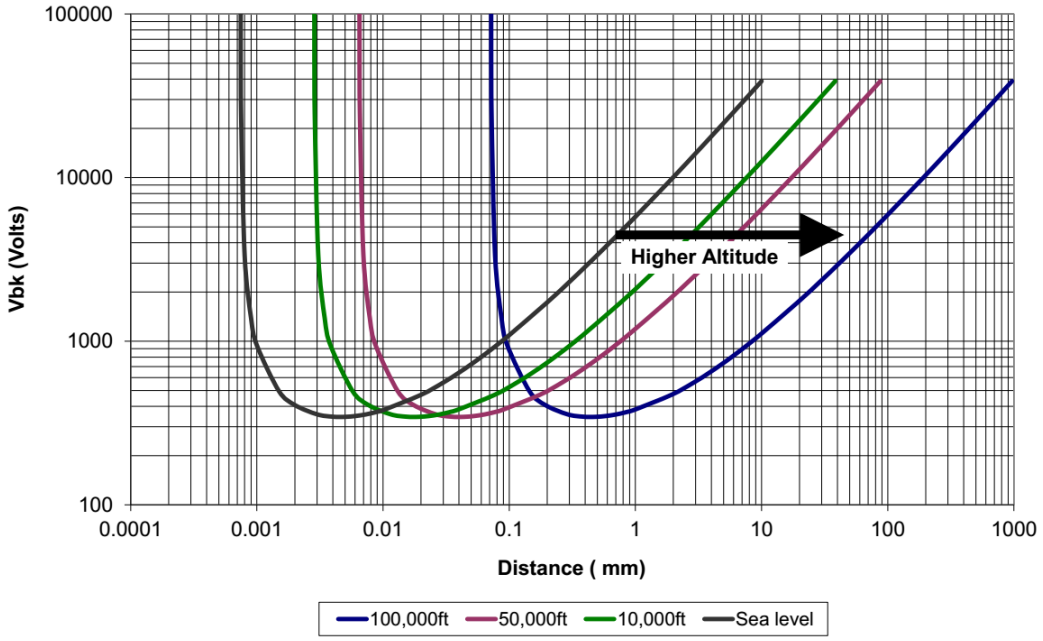

Figure 1.4: Breakdown voltage vs gap distance of air according to Paschen's law at a range of pressures [10].

It is possible to design an insulation system that will prevent discharge by having appropriate clearance and insulation in conductors. However, in electrical machines, eliminating partial discharge without an unacceptable increase in packing factor is problematic. Having a high voltage machine with the same packing factor of a low voltage machine could introduce problems related to insulation, as it may increase the risk of partial discharge in the generator's insulation system [11] [18] at high altitudes, as the required insulation distance would increase [10]. Therefore, if the generator is to produce high voltage, there is a trade-off between machine reliability and size/weight of the machine.

Fig. 1.5 shows a future aircraft generator connected to a dc bus using a power converter to transfer power to the high voltage distribution network. The power converter and the generator will have to minimize both total weight and power losses.

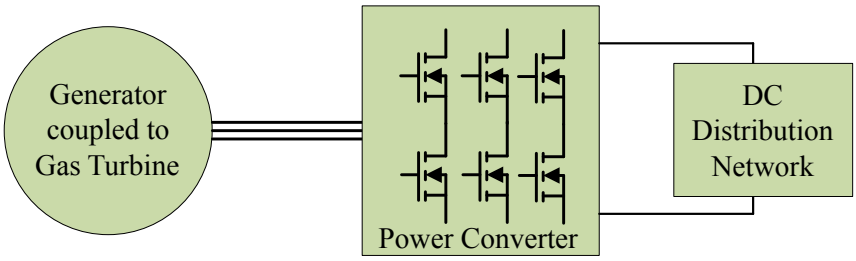

Figure 1.5: Generator connected to the dc distribution network through the rectifier.

1.1.3 State-of-the-art and beyond

Some converters that are available as off-the-shelf products are discussed next. In [19], an aerospace rectifier comprising of two stages is presented, the front end consisting of a Vienna rectifier followed by another conversion stage to isolate and step the output voltage down to 42V. As a result of the lower dc output voltage, the converter demonstrates low power densities in both gravimetric (3.3 kW/kg) and volumetric (5 kW/l) measurements. A liquid-cooled 200-kW, dc-to-dc converter for motorsport application [20], records much higher power densities (gravimetric 20 kW/kg and volumetric 21.36 kW/l) partially because of the higher dc voltage compared to the previous converter, and the absence of the isolation stage. In an oil cooled motor drive application [21], the converter delivers up to 200 kVA from a five-litre package weighing 5.75 kg. In a different high-power heavy-duty performance vehicle application [22], a converter optimized for size and weight produces 360 kW of power with a weight of 17.5kg. As the industry uses more and more wide bandgap (WBG) devices in their converters, power densities will continue to increase.

1.2 Research Objectives

The research is focused on identifying and studying suitable power converter topologies to transfer power from a generator, driven by a prime mover, to a dc distribution network in future MEA. Afterwards, the selected power converter topology is analysed in detail to further improve its performance. The main expected characteristics of this ac-to-dc converter are high power density (size and weight reduction), efficiency, power quality and reliability, while at the same time complying with the strict aerospace standards. After reviewing the candidate topologies available and the relevant literature, the Vienna rectifier is selected for the aircraft application. Then, it is benchmarked against the standard well-established two-level converter.

The Vienna rectifier has significant advantages compared to the two-level converter, mainly attributed to its simple circuit structure and three-level operation. However, only the connection to the neutral point is fully controllable using the bidirectional switches, due to the absence of the top and bottom transistors. For this reason, the Vienna rectifier does not perform well under nonunity power factor operation producing current distortion near the zero crossings. The challenge of this research is to improve the performance of the Vienna rectifier under such operating conditions.

1.3 Major Contributions

After a literature review, the Vienna rectifier has been selected for the application. As this is a nonregenerative application (the power flows in one direction), this converter can be used instead of a T-type converter or other bidirectional configurations.

The Vienna rectifier can provide three voltage levels at the ac side while generating PWM waveforms. No low-frequency distortion appears when operating at unity power factor at the ac side of the converter. However, when there is a phase displacement angle between the current and the reference voltage, the ac currents are distorted around the zero current crossings, containing unwanted low-frequency harmonics. The modulation technique proposed in [23] with the simplified version [24] is used to completely eliminate such low-frequency distortion by means of introducing a zero sequence to the reference signals. This zero sequence clamps each leg of the converter to the neutral point during certain intervals, particularly, when the current and reference voltage have opposite signs. However, when the converter is working with high modulation indexes, the zero sequence may produce overmodulation. A solution is proposed based on combining the above zero sequence (Mode-1) with reactive current injection (Mode-2) [25]. The reactive power is calculated to operate at unity power factor at the terminals of the converter, so that the converter is no longer providing the reactive power demanded by the filtering inductor. A twin controller detects potential overmodulation and decides the best mode the converter should operate, based on the operating conditions, which runs in parallel to the main controller.

As a further improvement, a hybrid modulation method is proposed combining the above two methods, achieving a smooth transition between operating points with significantly less reactive current injection. With the proposed method, the Vienna

rectifier can operate over a wide range of power factors without compromising the quality of the source currents and within the aerospace standards. This makes it suitable for the aircraft generator-fed rectifier application. The proposed techniques are simulated with Matlab/Simulink and PLECS, and then validated with an experimental setup.

1.4 Thesis Organization

This thesis is organized as follows. **Chapter 1** introduces the electrification trend in the aircraft industry and its driving factors, followed by the importance of high density power converter for the MEA. In **Chapter 2**, a literature survey is done to understand the state of the art in interfacing an aerospace generator to a dc bus, which is followed by a brief study of rectifier topologies, with more emphasis on the Vienna rectifier vs. the two-level converter. In **Chapter 3**, the low-frequency distortion problem in the Vienna rectifier is addressed, and solutions to solve this problem and extend the operational range of the Vienna rectifier to operate with large modulation indices are introduced. **Chapter 4** further improves the method mentioned in Chapter 3, by introducing a hybrid modulation and control method which require less reactive current. **Chapter 5** applies the modulation and control methods proposed in the previous two chapters to a permanent magnet synchronous generator. **Chapter 6** presents the overall conclusion of this research work as well as future work to be developed. After this chapter, the author's publications are presented along with a list of references related to this research work.

Chapter 2

Review of Rectifier Topologies and Hardware Description

This chapter discusses the state-of-the-art of three-phase rectifier topologies being used in aircraft and suitable topologies for future MEA applications. After a thorough comparison with the well established two-level converter, the Vienna rectifier is selected based on many factors including power density, simplicity, efficiency, and reliability. The operation of the Vienna rectifier is analyzed in detail, showing the problems associated with nonunity power factor operation. Various distortion mitigation strategies are discussed such as the zero sequence injection and reactive power compensation. Finally, the experimental setup is described.

2.1 Rectifier Topologies for the MEA

Rectifier topologies can be broadly categorized into passive-multipulse rectifiers, and active rectifiers with high frequency PWM switching. In land-based power systems, harmonic limitations are imposed by IEEE Standard 519, which indicates the line current total harmonic distortion (THD) should be less than 5% at the point of common coupling (PCC). In aerospace converters the standards are even more stringent, and different limitations for each harmonic are imposed by DO-160 and other OEM specific documents as stated in [26]. Table 2.1 shows the harmonic limits for harmonic orders up to 40, imposed by DO-160 [26].

It should be noted that although the DO-160F and MIL-STD-704F provide stringent requirements, for future aircraft power architectures they need to be modified

Table 2.1: Current Harmonic Limits in DO-160 Standard

Harmonic Order	Limits
3^{rd}, 5^{th}, 7^{th}	$I_3 = I_5 = I_7 = 0.02\ I_1$
Odd Triplen Harmonics (n = 9, 15, 21, ..., 39)	$I_n = 0.1\ I_1$ / n
11^{th}	$I_{11} = 0.1\ I_1$
13^{th}	$I_{13} = 0.08\ I_1$
Odd Non Triplen Harmonics 17, 19	$I_{17} = I_{19} = 0.04\ I_1$
Odd Non Triplen Harmonics 23, 25	$I_{23} = I_{25} = 0.03\ I_1$
Odd Non Triplen Harmonics 29, 31, 35, 37	$I_n = 0.3\ I_1$ / n
Even Harmonics 2 and 4	$I_n = 0.01\ I_1$ / n
Even Harmonics > 4 (n = 6, 8, 10, ..., 40)	$I_n = 0.0025\ I_1$

because not all aspects are captured, for example the increased voltage of the distribution network, as mentioned in [6].

2.1.1 Passive Rectifiers

2.1.1.1 Diode Bridge Rectifier

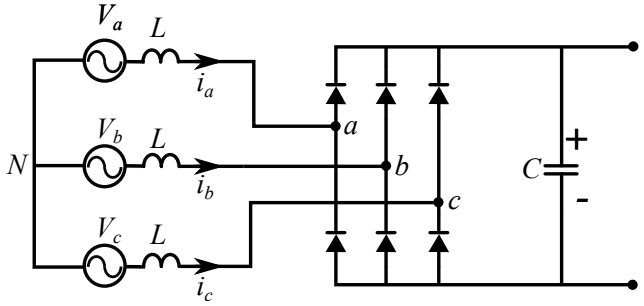

Figure 2.1: Diode bridge rectifier.

The diode bridge rectifier (DBR) (Fig. 2.1), also known as six-pulse rectifier, is the simplest form of three-phase passive rectifier. It does not introduce even harmonics and triplen harmonics to the grid, but the harmonics of order $6k \pm 1$, where k is an integer number, (i.e., harmonics 5, 7, 11, 13, etc.) are present. Although the topology is simple, it has many issues as the output voltage can neither be regulated nor boosted. Also, the line current waveforms are highly distorted, because it performs as a nonlinear load.

2.1.1.2 12-Pulse Rectifier

The 12-pulse uncontrolled rectifier, as depicted in Fig. 2.2, is an improved version of the diode bridge rectifier where two six-pulse rectifiers are cascaded. They

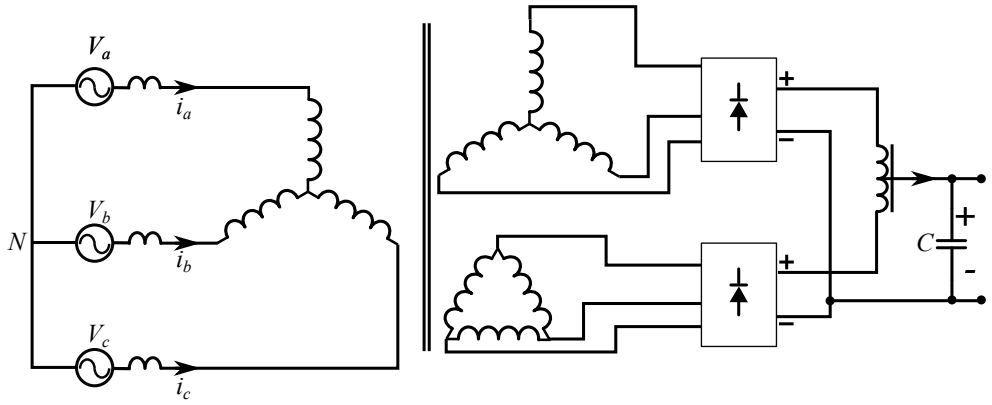

Figure 2.2: 12-pulse rectifier with isolation transformer.

are fed by a Wye-Wye/Delta isolation transformer, where the voltage waveforms are phase-shifted by 30^0 [27]. This converter produces 12 voltage pulses in a fundamental cycle. The harmonics 5, 7, 17, 19, etc. are cancelled in this configuration, which were present in the DBR. Harmonics of order $12k \pm 1$, where k is an integer number, are still present. The main drawback of this converter configuration is weight because of the transformer needed, which makes it less attractive to aerospace. Furthermore, there is no output voltage regulation and the currents are still significantly distorted. In an autotransformer-based 12-pulse rectifier, as [28] elaborates, the autotransformer with $\pi/6$ phase-shift is not suitable for voltage boosting applications. Further improvements of this solution are the 18-pulse and 24-pulse rectifiers, but none of those are suitable to boost the output voltage.

Passive rectifiers are used in aircraft applications [27] for their simple design and high reliability of passive component with reduced device count. In a typical aircraft, to generate the low voltage 28Vdc from the three-phase 400Hz 115Vac grid, a transformer-rectifier unit is used, which is based on a simple and reliable 12-pulse rectification [29–31]. However, higher system weight compared to the active rectifiers is the main constraint of this solution [30]. Besides, having the capacity to boost the dc output voltage is also needed.

In [30], it is shown that a passive rectifier has more volume compared to an active rectifier when it is working at 50Hz fundamental component, for a given output power. With new semiconductor technologies emerging, one could expect this gap to increase even further. In line with this, as shown in the next sections, harmonics and output voltage regulation would make the active rectifier a better choice.

2.1.1.3 12-Pulse Rectifier with Controlled Output Voltage

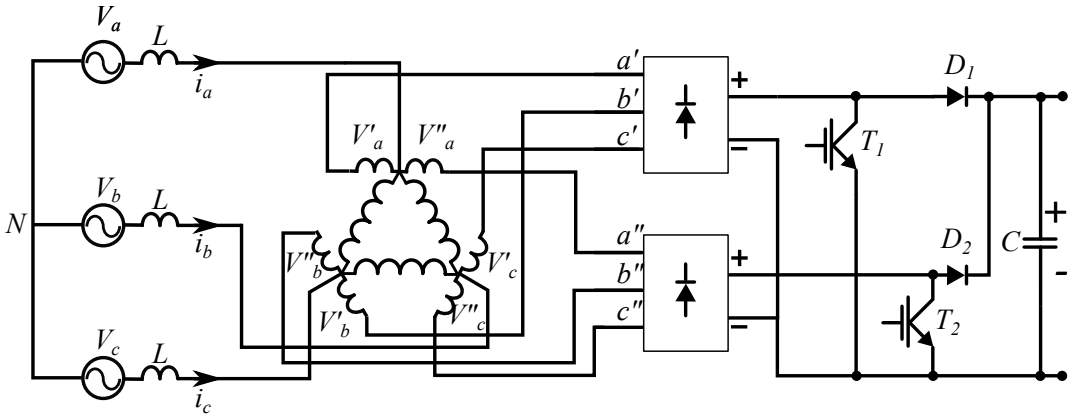

Figure 2.3: 12-pulse rectifier with controlled output voltage.

The 12-pulse rectifier topology with autotransformer shown in Fig. 2.3, with two additional diodes and switches, gives the ability to regulate the output voltage of the converter. In this application, the two switches are operated in interleaving mode [31]. Despite the capability to regulate the dc output voltage, still the current waveforms are not sinusoidal and contain significant distortion.

2.1.2 Two-Level Converters

Active rectifiers use semiconductors operated at high switching frequency to control the line currents and the dc output voltage. High frequency operation enables for a size reduction in the reactive components, i.e., inductors (magnetic components) and capacitors.

2.1.2.1 Standard PWM Rectifier Bridge

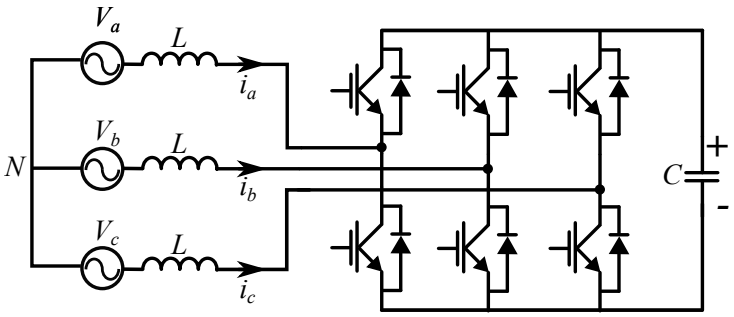

Figure 2.4: Two-level rectifier.

The two-level rectifier (Fig. 2.4) uses six semiconductor switches with associated diodes. Several PWM techniques can be used to control the switches. The dc output

voltage of the converter can be boosted and regulated, and the ac currents can be shaped to be sinusoidal.

In high power applications, the designers tend to increase the rated voltages of the systems in order to reduce power losses. In the case of the two-level converter, there are limitations to increase the output voltage to a higher value as the semiconductor switches need to block the full dc-link voltage.

2.1.2.2 Two-Level Δ Switch Rectifier

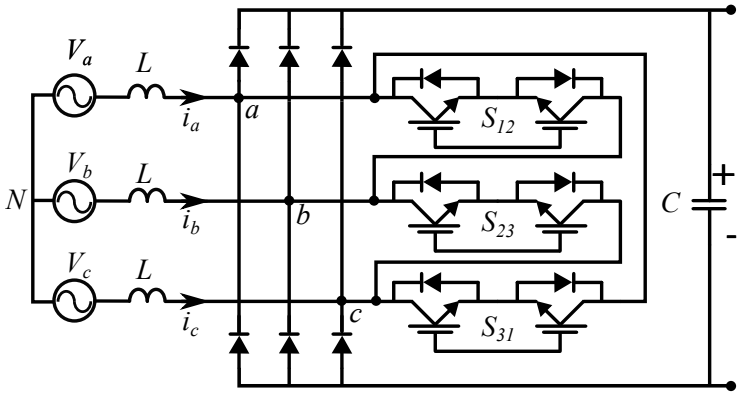

Figure 2.5: Diode bridge with delta-connected switches.

A modified version of the diode bridge rectifier is proposed in [32], which has bidirectional switches connected in Delta configuration. With the control proposed in [33], the converter is able to operate even with one phase loss. However, the diodes and the switches need to block the full dc-link voltage.

2.1.3 Three-Level Converters

In a three-level rectifier, the topology can generate three voltage levels at each of its ac terminals. This is done by connecting the ac terminals to either the positive voltage rail, the midpoint, or the negative voltage rail of the converter. When compared to the two-level converter, certain three-level converters can operate with twice the dc-link voltage using the same kind of switches. Consequently, they can process higher power.

For this application, several three-level converter topologies have been considered with the target of operating at high dc-link voltage, with high reliability and low overall size and weight.

2.1.3.1 Split DC Side Converter into Two Systems

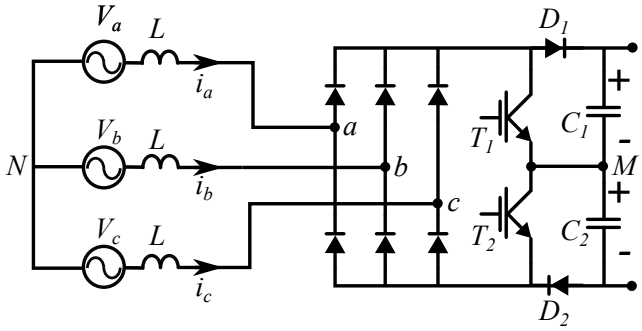

Figure 2.6: Split dc side converter into two simultaneously pulsed partial systems.

As reported in [34, 35], Fig. 2.6 illustrates an uncontrolled diode bridge rectifier followed by a dc-dc boost stage. This converter can regulate the dc output voltage using the active switches. Each switch in the configuration shown in Fig. 2.6 needs to block only half of the dc-link voltage. But the diodes need to block the full dc-link voltage. Application of this solution is limited, since the input current spectrum contains low frequency harmonics with high amplitudes. Hence, in the case of high power (high currents), the power semiconductor devices are under high stress, and the generated electromagnetic interference (EMI) is significant.

2.1.3.2 Diode-Clamped Converter

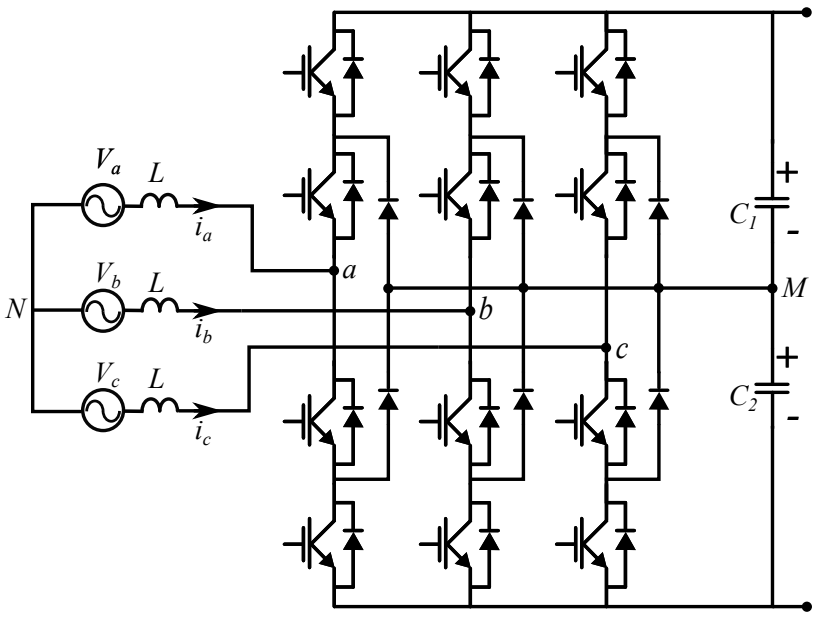

Figure 2.7: NPC converter.

The diode-clamped converter, also known as neutral-point-clamped (NPC) converter (Fig. 2.7), was introduced in 1981 by Nabae et al. [36], and it can transfer

power in both directions. It can produce three voltage levels. It is widely used nowadays by industry in high power applications. When compared to the two-level converter, the NPC has twice the number of transistors and additional diodes.

2.1.3.3 Forced Commutated Three-Level Boost Type Converter

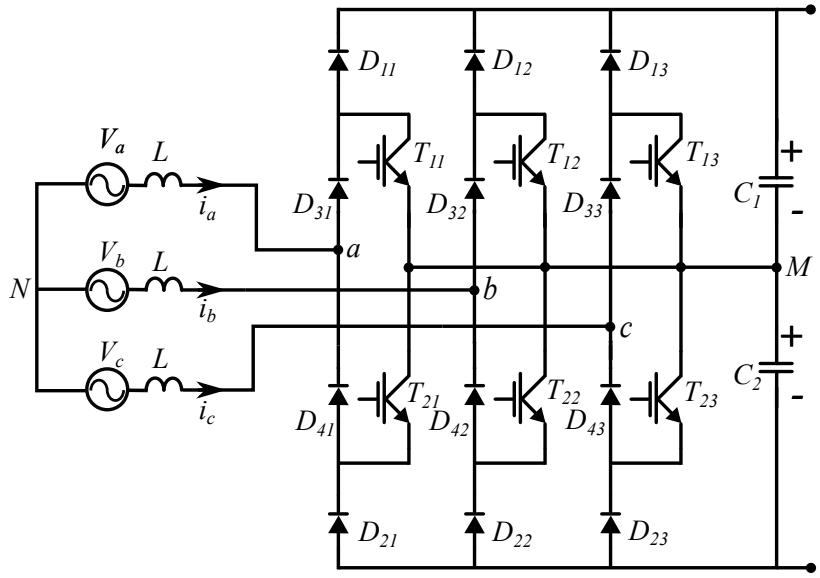

Figure 2.8: Special three-level rectifier.

As proposed in 1993 by Zhao et al. [37], all the power semiconductors of the topology shown in Fig. 2.8 need to block only half of the dc-link voltage. Also, the reliability is high due to its shoot-through free structure, as the rectification is done by diodes. As mentioned in [38] D_{3x} and D_{4x}, diodes (x = 1,2,3) switch at the fundamental frequency, while D_{1x} and D_{2x} diodes are free wheeling diodes in the boost stage. It has the ability to draw nearly sinusoidal currents from the grid, and it can either do this with unity power factor at the grid, or absorbing/injecting a certain amount of reactive power from/to the grid.

However, it has high conduction power loss as the current flows through series-connected diodes. In this converter, the bidirectional switch connecting to the neutral point is constructed using switches T_{1x} and T_{2x} in each phase. Also, as the rectification is based on a diode bridge rectifier, it has the limitation of unidirectional active power flow.

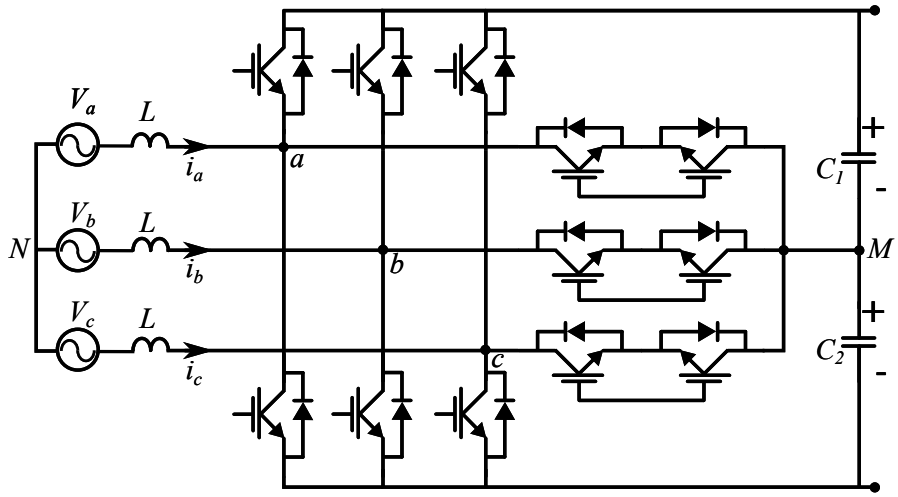

Figure 2.9: T-type converter.

2.1.3.4 T-Type Converter

The T-type converter [39,40], shown in Fig. 2.9, is a three-level converter. The dc output voltage can be regulated and the input current can be shaped to be sinusoidal. It can process active power in both directions. However, this topology requires 12 transistors (with antiparallel diodes), i.e., twice the number of transistors compared to the traditional two-level converter. Besides, the switches connected to the top and bottom of the dc bus terminals need to withstand the full dc-link voltage.

2.1.3.5 Vienna Rectifier

The original Vienna rectifier proposed in 1994 by Kolar et al. [34] had three switches, each switch with a full-bridge rectifier to make the connection to the neutral point bidirectional, as shown in Fig. 2.10(a). It had a hysteresis control of the input currents to shape them sinusoidal. Advantages include simple circuit structure with low active switch count, PWM operation, low harmonics in the grid currents, low blocking voltage stress on switches, and voltage boosting capability.

Subsequently, the Vienna rectifier was further improved (Fig. 2.10(b)) with two MOSFETs connected in anti-series configuration to create the bidirectional switch making the total switch count six. This topology has lower conduction loss compared to that in Fig. 2.10(a), as the current goes through two semiconductors instead of three when connecting to the neutral point.

The power flow is unidirectional (from ac to dc) because diodes are being used for the rectification. As the aerospace generator demands only two quadrant operation,

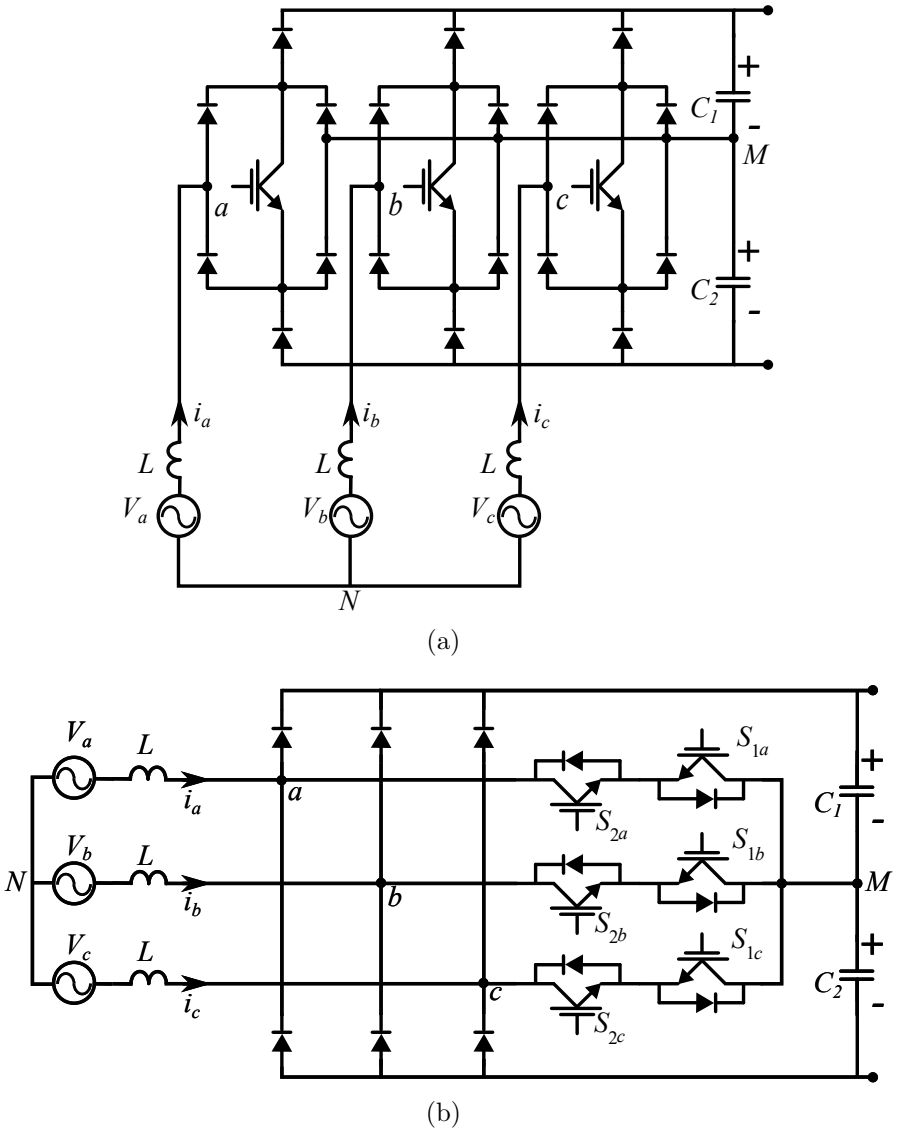

Figure 2.10: Vienna rectifier: (a) With three switches and (b) with six switches.

unidirectional power flow limitation is not a problem. One issue in this topology is the distortion that appears near the current zero crossings when there is a voltage-current displacement angle different than zero at the converter terminals. In each phase, when the switches that connect to the neutral-point are off, the current direction defines which diode conducts and thus the voltage polarity generated at the terminal of the converter. A more detailed analysis of this issue is presented in the next chapter.

The 12-pulse rectifier is compared with two- and three-level rectifiers in [30]. It is concluded that the three-level PWM rectifier is the most beneficial solution among them. A hybrid 12-pulse rectifier is introduced in [41], where the bulk power to the load is supplied by the 12-pulse rectifier and the input current shaping is done by a parallel-connected Vienna rectifier in order to reduce current harmonic distortion. It

shows that when the Vienna rectifier is contributing more to the power processing, the quality of the line currents improves. In [42], a comparison is done between a three-level buck rectifier, three-level boost rectifier and the Vienna rectifier. From the analysis, the authors conclude that the Vienna rectifier has the lowest volume and weight and highest efficiency among the others. The same results are confirmed in [43] and a volumetric power density of 15kW/dm3 is recorded for a 10-kW Vienna rectifier. As [44] discusses, due to the three-level characteristics of the bridge legs, the line inductance required is reduced by about 1/3 compared to the two-level converter for the same harmonic level of the input current and equal switching frequency. Moreover, as the transistors have to withstand only half of the dc-link voltage, the Vienna rectifier can be operated at relatively higher switching frequency to further increase the power density. In [45] several ac-to-dc converter topologies are compared for an electric vehicle charging station application and the Vienna rectifier achieves the highest power density. Hence, as stated in [30, 42, 46], the Vienna rectifier is suitable for aircraft applications. Although the two-level converter [33] is also suggested for aircraft applications, the Vienna rectifier is a very good alternative thanks to its three-level operation, high efficiency [47] and high power density.

Multilevel topologies with higher number of levels are not considered in this thesis since as the number of active switches increases, the converter reliability decreases, which is a paramount aspect to consider in aerospace applications. Furthermore, the voltage specification of the target application does not require to resort to converters that produce more than three voltage levels.

2.2 Two-Level Rectifier vs. Vienna Rectifier

The two-level converter is widely used in industry. Therefore, from the above mentioned topologies, the two-level converter is used to benchmark the Vienna rectifier for the MEA application. Aerospace converters have stringent requirements [48] compared to other transportation applications, like automotive and marine, as shown in Fig. 2.11. This is due to the strict regulations on safety criticality, reliability and mission profile attributes. Consequently, aerospace application is very conservative in adopting new technologies, and a particular technology would undergo various levels of testing before it ends up in an aircraft. Thermal management and power density are also vital for the aircraft converter design, however, has secondary importance

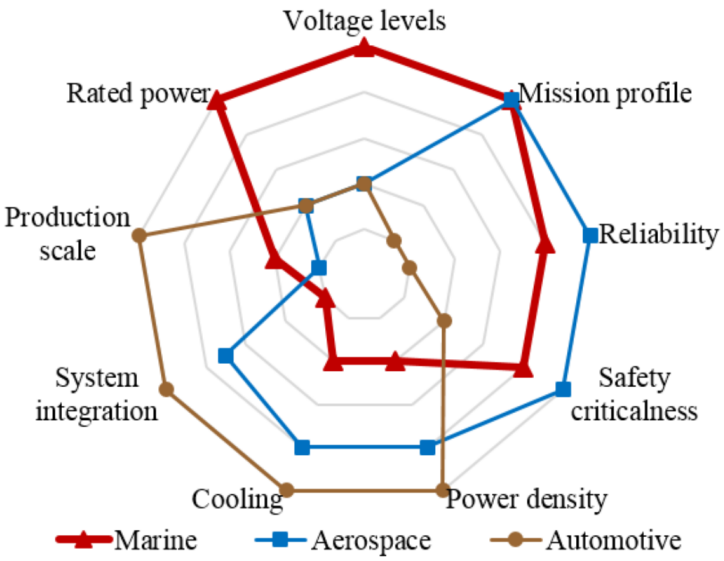

Figure 2.11: Design aspects of power electronic converter systems in electrified transportation [48].

compared to safety and reliability due to the nature of the application.

In this section, critical design aspects such as current waveform quality, voltage rating of the devices, power density of the converter, and efficiency are considered for comparison with the two-level converter. For the comparison, simulated converters with the parameters shown in Table 2.2 are used.

Table 2.2: Common Converter Parameters for Comparison

Parameters	Specifications
Line-to-line input voltage, V_{L-L}	400 V
DC-link output voltage, V_{dc}	700 V
Output power, P_{out}	1 kW
Output capacitor, C_{out}	220 uF
Fundamental frequency, f	50 Hz
Switching frequency, f_{sw}	50 kHz

2.2.1 Current THD at Various Operating Points

The current waveform quality is paramount in aircraft generator-fed rectifier applications, because a significant amount of losses in the machine (eddy currents in the permanent magnets and other conductive parts) will be contributed by the harmonics [49–51]. Furthermore, when the losses are reduced in the machine, there would be other benefits like extended lifetime due to less overheating.

Fig. 2.12 presents a comparison of the current waveform quality in a Vienna

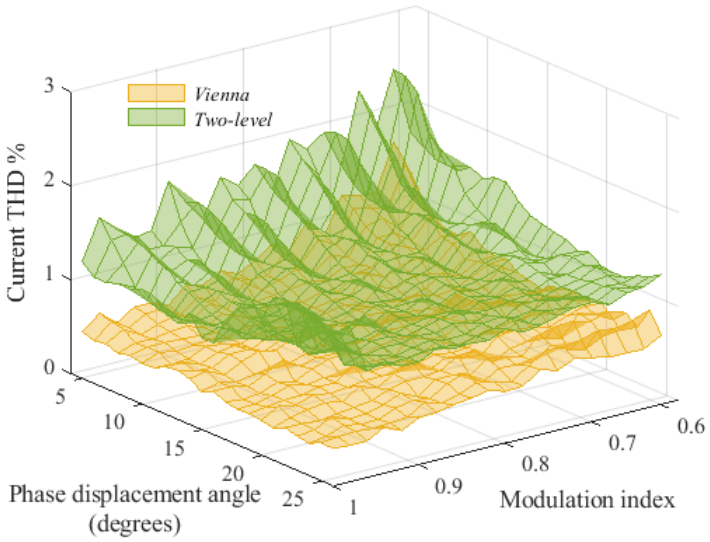

Figure 2.12: Current THD of the Vienna rectifier and the two-level converter at different operating conditions.

rectifier and a two-level converter, using the current THD, when the converters are operating with the system parameters shown in Table 2.2. The two converters were simulated using PLECS with the device thermal models provided by the device manufactures. The two rectifiers were simulated under various operating conditions to study the current waveforms.

The phase displacement angle is the phase between the input current and the reference voltage in the converter, measured in degrees. The modulation index is defined as,

$$m \triangleq \frac{\hat{E}}{v_{dc}/2} \tag{2.1}$$

where $\hat{E}$ is the phase voltage amplitude and v_{dc} is the dc-link voltage. Studying the impact on the current waveform quality in different operating conditions where the modulation index and the phase displacement angle vary, is important since this is a generator-fed application.

As expected, the Vienna rectifier has superior current waveform quality over the two-level converter, in all the operating points. The reason for this is the lesser current ripple in the Vienna rectifier compared to the two-level converter, for a given inductance, because of the three-level operation.

2.2.2 Voltage Rating of the devices

The switches of the two-level converter need to block the full dc-link voltage when they are not conducting. However, in the Vienna rectifier, the switches are used to connect to the midpoint of the dc-link, therefore they only have to block half of the dc-link voltage, when they are not conducting. Table 2.3 provides a summary of the voltage that each device needs to withstand.

When the electric field breakdown of the power semiconductor device increases, the specific on-resistance increases [52, 53], and this results in less efficient devices compared to the low voltage counterparts.

2.2.3 Converter Weight

For the weight analysis, three main parameters are considered; inductor, capacitor and heat sink, as they are significant contributors to the overall converter weight. The analysis is performed for the operating point mentioned in Table 2.2.

2.2.3.1 Inductor Weight

As the two-level converter can only connect to the top and bottom voltage levels, it produces larger transitions compared to the three-level Vienna rectifier. Therefore, the current ripple should be larger in a two-level converter, for a given inductor.

The inductances that would produce current ripple values 4%, 2%, and 1% are recorded in Table 2.4. The inductor weight calculations are based on a commercially available aviation-grade inductor which has a weight constant of $0.025\,\mathrm{kg\,mH^{-1}\,A^{-1}}$ [54]. Nevertheless, aerospace applications prefer higher impedance values, provided the weight penalty allows it, for limiting fault currents. Having higher fault currents would oversize the power converters and, particularly in aerospace application, it could raise reliability/safety concerns as the generator may become damaged due to overheating [55].

Table 2.3: Voltage Rating

	Blocking voltage	
Topology	Diode	Switch
Two-level converter	N/A	Vdc
Vienna rectifier	Vdc	Vdc/2

Table 2.4: Inductance Required

Inductance in each topology (mH)	Current ripple 4%	2%	1%
Two-level converter	0.42	0.82	1.54
Vienna rectifier	0.18	0.25	0.50

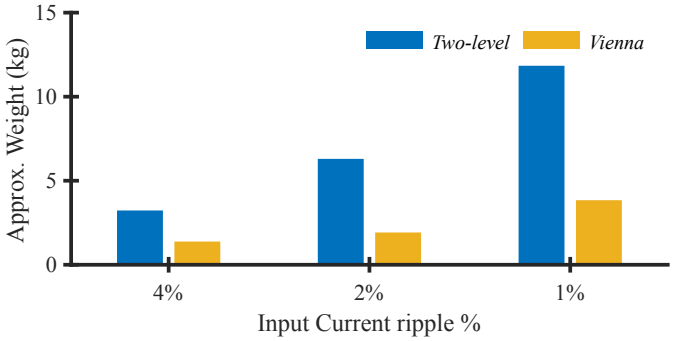

Figure 2.13: Inductor weight for different current ripples.

2.2.3.2 Capacitor Weight

The MIL-Std-704 standard specifies the voltage ripple amplitude for 270V dc bus should be less than 6V [56,57]. Since the dc-link voltage value considered in this thesis is for a future aerospace application, there are no governing standards. Nevertheless, it is assumed a conservative value of 2% as the maximum voltage ripple for the dc bus.

Having this value in mind, the required capacitance is shown in Table 2.5. (In the simulation, the Vienna rectifier capacitor consists of two 32 μF capacitors connected in series). For the voltage rating of the semiconductors, 50% margin is assumed. For the requirement in Table 2.5, film capacitor 947D191K112ACGSN (0.5kg) is selected for the two-level converter and two B25631B0207K600 connected in series (0.8kg) are selected for the Vienna rectifier.

Table 2.5: Minimum Capacitance Required

Topology	Capacitance total (μF)	Rated voltage (V)	Current rms (A)
Two-level converter	30	1050	17.2
Vienna rectifier	32+32=16	525	17

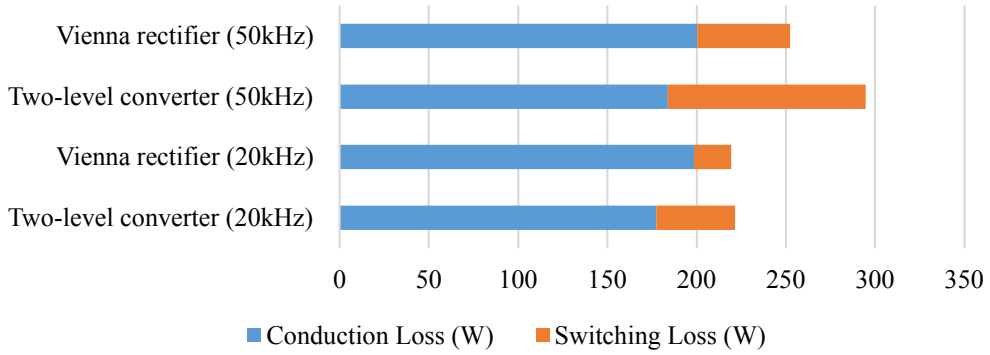

Figure 2.14: Loss comparison of the different rectifier topologies for the given operating point.

2.2.3.3 Cooling System Weight

For the entire cooling system including pumps, radiators, etc. 1kg/kW heat sink weight is assumed. The topology with more losses would require more cooling, impacting the converter weight. MATLAB PLECS tool box is used to simulate the two converters to check the power loss at the operating condition mentioned in Table 2.2. For the two-level converter, 1200V rated SiC (C2M0040120D) MOSFETs are chosen to match the 700V voltage level. In the case of the Vienna rectifier, 1200V rated SiC (C4D20120H) diodes and 650V rated SiC (C3M0045065D) MOSFETS are used for the efficiency analysis.

As Fig. 2.14 illustrates, both rectifiers show similar loss figures for 20kHz switching frequency. The Vienna rectifier has lower switching losses because the switches operate at half the dc-link voltage, and the two-level converter has lower conduction losses because it does not have the diodes. However, when the simulation is repeated at 50kHz, the Vienna rectifier outperforms the two-level converter. This trend agrees with the studies done in [58, 59]. In terms of switching ripple of both input current and dc-link voltage, operating at higher switching frequencies would make the required inductors and capacitors smaller. In a study done in [59], it is shown that the inductor losses will be reduced by 25% when moving from a two-level to a three-level converter topology.

These results agree with the study done in [60] where the three-level NPC topology is compared with the two-level converter, and the three-level converter demonstrated more power savings.

Multiple simulations are run for different operating points to study the power

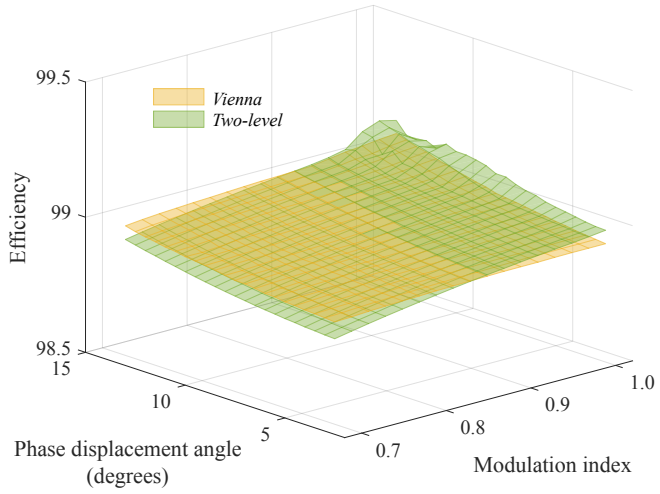

(a)

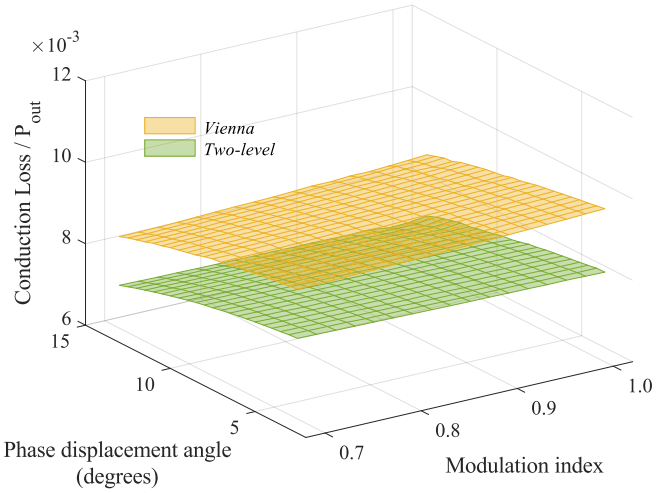

(b)

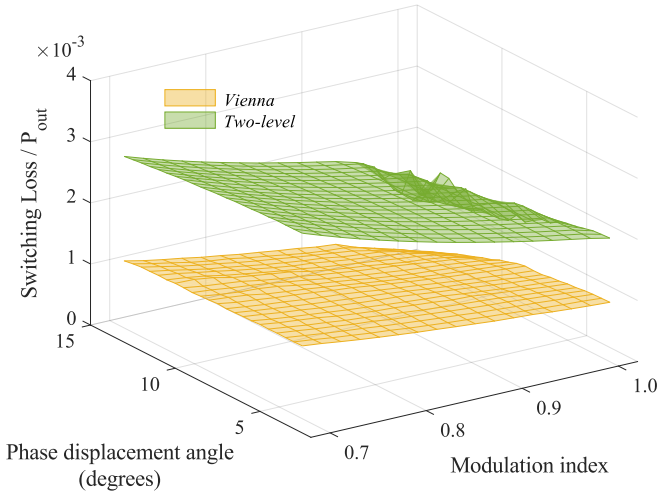

(c)

Figure 2.15: Loss analysis of the two-level converter and the Vienna rectifier in different operating conditions (simulated using PLECS): (a) Efficiency, (b) conduction loss and (c) switching loss.

loss variation, and the results are depicted in Fig. 2.15. The dominant conduction loss is seen in the Vienna rectifier, while it has better performance in switching loss. Throughout the operating regions the efficiencies of both converters remain close. Nevertheless, as Fig. 2.15(a) illustrates, for lower modulation indices, the Vienna rectifier efficiency is higher than in the two-level converter. This can be explained with Fig. 2.15(c). When the dc-link voltage increases, the switching loss component in the two-level converter increases much more than that of the Vienna rectifier, simply because in the two-level converter the MOSFETs switch between the full dc-link voltage, whereas they switch only between half the dc-link voltage in the Vienna rectifier.

Table 2.6 shows the steady state device junction temperatures in the two converters, and according to this, the Vienna rectifier switches would be cooler, compared to those in the two-level converter. Therefore, the life of the devices would be longer, when operated with lower junction temperatures [61].

2.2.4 Summary

A summary of the comparisons is given in Table 2.7 and Fig. 2.16. In this comparison, the two-level converter is used as the benchmark, and the design parameters for the Vienna rectifier are expressed with respect to this benchmark (the lower the better). Converter reliability is not included in the summary as further quantitative analysis is required.

Table 2.6: Active Switch Thermal Analysis

	T_j ^{0}C	
Topology	f_{sw} =20kHz	f_{sw} =50kHz
Two-level converter	104	113.8
Vienna rectifier	97.1	102.7

Table 2.7: Comparison Summary

Design parameter	Two-level converter	Vienna rectifier
Current waveform quality (THD)	1	0.52
Switch voltage rating	1	0.5
Weight	1	0.83
Cost	1	0.65
Loss	1	0.98

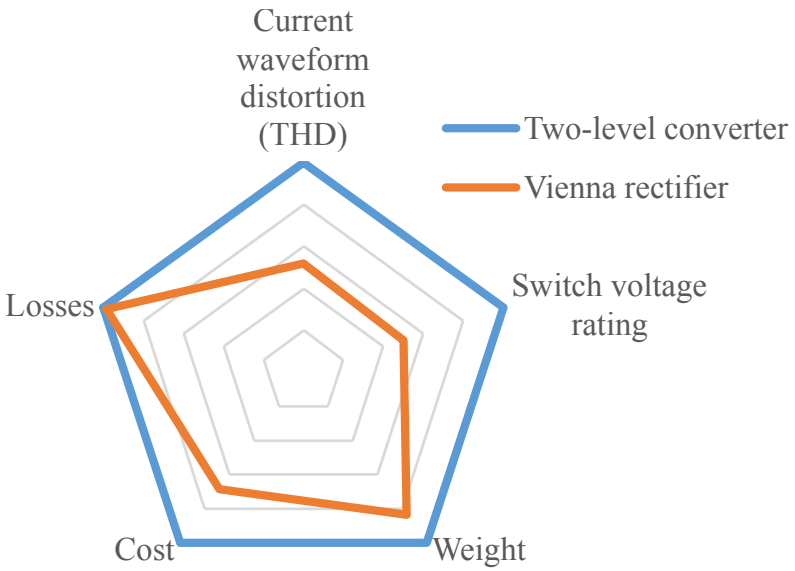

Figure 2.16: Summary of design parameter comparison for the two-level converter and the Vienna rectifier (lower is better).

With the study carried out thus far, the Vienna rectifier exhibits superior benefits compared to the two-level converter for the aerospace generator-rectifier application. The parameters discussed above are interrelated and finding the best combination would require multi objective optimization, which is out of the scope of the thesis. Based on the above analysis, the Vienna rectifier is selected and the subsequent chapter discussions are based on this topology.

2.3 Hardware Description

2.3.1 Vienna Rectifier System

Experimental verification of the proposed techniques in this research is performed using a three-phase power factor correction (PFC) Vienna rectifier, using the C2000 Texas Instruments (TI) board, which is shown in the Fig. 2.17. The digital signal processor (DSP) controller card-F28379D Delfino Experimenter Kit, is on a separate printed circuit board (PCB) and connects to the converter base board.

Fig. 2.18 shows a block diagram of the Vienna rectifier system, describing the main sections in the experimental setup. In this system, the phase voltage, input current, and dc-link voltage are measured, and the signals are fed to the DSP using the internal analog-to-digital converter (ADC). Three hall effect sensors LEM LTSR 6-NP are used to sense the currents and the TI AMC1301DWVR, which has isolation

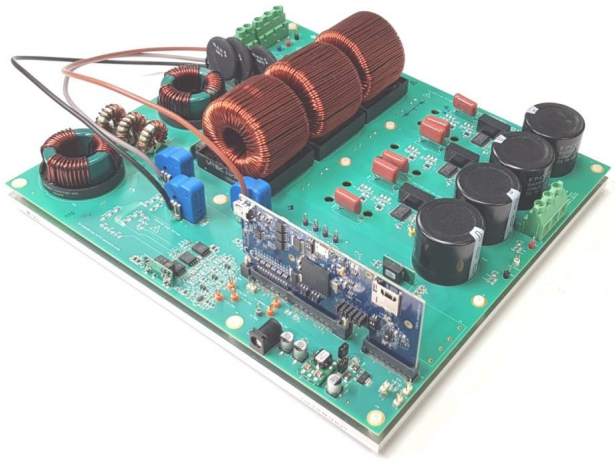

Figure 2.17: Texas Instrument Vienna rectifier reference design.

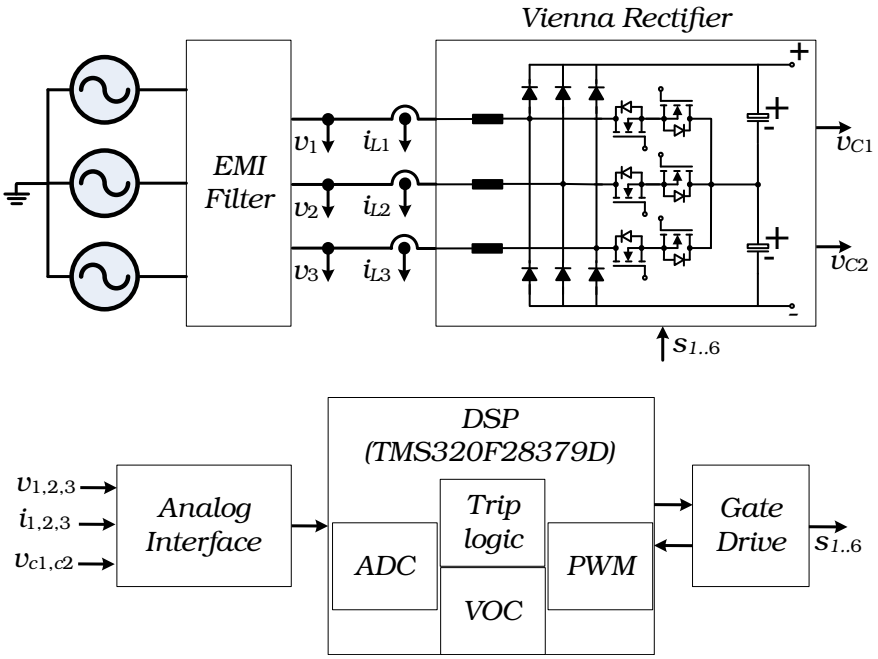

Figure 2.18: Vienna rectifier block diagram.

capacity, is used to sense the voltages. The current measured going into the converter is considered as positive direction of current. Though the TI board is designed for a grid-connected system, it could be easily modified to be connected to a generator.

The bidirectional switch that connects the phase leg to the neutral point is constructed by two 650V Infineon MOSFETs (IPP65R190C7) connected in common source configuration. The diodes used are CREE 1200V SiC C4D08120A. Since the neutral-point-clamp switches only see half of the dc-link voltage, the MOSFETs only need to withstand that voltage. However, the diodes should be rated at full dc-link voltage. The isolated dual channel gate driver UCC21520D, is used to drive each

neutral-point-clamp switch. It saves space on the PCB due to the isolation feature of the driver, which otherwise would require isolated transformers.

The WBG semiconductors, particularly SiC in this application, exhibit superior properties such as higher operating temperatures, higher blocking voltages, and faster switching compared to their Si-based counterparts. The use of WBG materials is not seen in aerospace power converters thus far, mainly because of reliability uncertainties. In order to increase the power density of the converters, designers tend to increase the switching frequency (to reduce the passive component sizes) by using WBG semiconductor devices. These devices have very short turn on and turn off times. This give rise to very high di/dt and dv/dt in the device related circuit traces. When parasitic inductances and capacitances are coupled with high di/dt and dv/dt there would be voltage spikes and ringing in circuits which may lead to erroneous pulses, device malfunction and unpredictable operation of the converter. Therefore, in high frequency designs, the parasitic inductances and capacitances should be taken into account throughout the design, including the layout of the circuit traces. Despite these issues, because of the benefits of WBG semiconductors, it is expected that the designers use WBG devices in future aircraft power converters.

The Vienna rectifier is connected to a programmable ac power source (California Instruments 4500Ls) and a resistive load bank is connected to the output of the Vienna rectifier, as shown in Fig. 2.19.

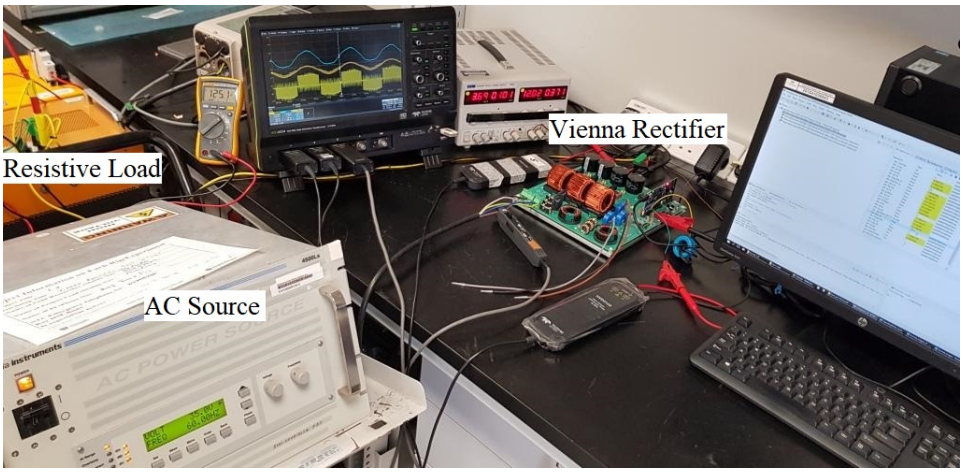

Figure 2.19: Experimental setup.

2.3.2 Digital Signal Controller

The Vienna rectifier is controlled with the TMS320F28379D, a 32-bit fixed point DSP, which has a dual core architecture with floating point unit (FPU) and a trigonometric math unit (TMU) that gives hardware support to accelerate code execution. This helps to have high bandwidth control loops, especially when dq and inverse dq transformations are used.

The ADC module of the TI C2000 TMS320F28379d DSP is coupled with the integrated comparator subsystem (CMPSS), providing fast overvoltage and overcurrent protection, as the internal trip circuitry works with minimal delay because it is hardware implemented. In the comparator subsystem, the analog channels could be configured with threshold values, which once exceeded would enable fast trip of the PWM module. Since external devices are not used for protection, this saves space and simplifies the layout of the PCB. Alternatively, this feature can be used as a redundent protection mechanism, if the designer chooses to keep the hardware trip in place. The ADC module is configured to have 12-bit resolution and the ADC clock runs at 50 MHz while the system clock is set at 200 MHz. The process of converting an analog voltage to a digital value is broken down into two parts as follows,

1. Sample and hold time t_{SH}
2. Conversion time t_{LAT}

For this DSP the t_{SH} and t_{LAT} is configured to have 21 and 43 system clock cycles, respectively. When these two latencies are added, the total time sums up to 320 ns. Therefore, the sampling rate at which the ADC is sampling the current and voltage is 3.125 MSPS.

The switching frequency of the rectifier is 50 kHz, which means the DSP code is interrupted every 20 μs. The voltage and current sensor measurements are read to the DSP through the ADC. Then, they are processed to calculate the required duty cycle value in each PWM period. Therefore, the ADC start of conversion (SOC) is triggered by the PWM carrier signal (PWM1 channel A). There are 8 sensor signals altogether (input side 3 phase voltage signals, 3 current signals and 2 output capacitor voltage signals as illustrated in Fig. 2.18) connected to the ADC through signal conditioning circuits.

The 12-bit digital-to-analog converter (DAC) is extremely useful when debugging

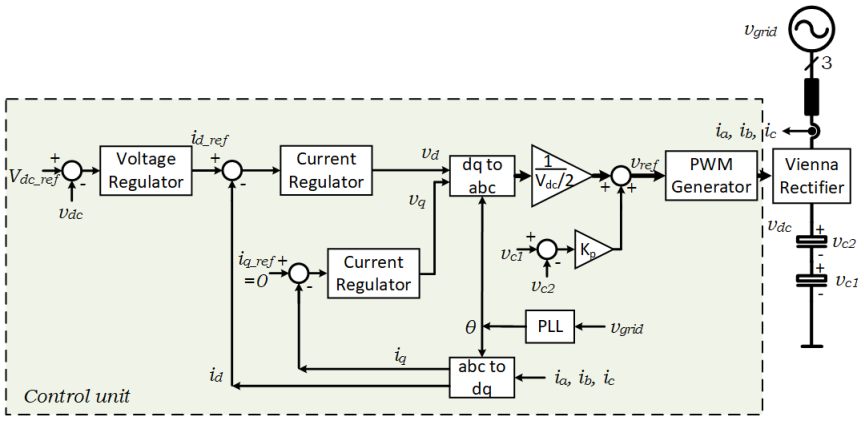

Figure 2.20: VOC diagram used in the Vienna rectifier.

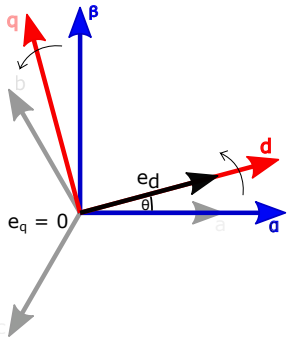

Figure 2.21: d-q axis synchronization.

the system, as it allows internal variables to be taken out and represented in an oscilloscope. The Code Composer Studio -the Integrated Development Environment (IDE) provided by TI- can be used for debugging the code, in real time, when connected via the XDS100 V2 emulator.

2.3.3 Control System Design

In the experiments, voltage oriented control (VOC) is used (Fig. 2.20). The modulation is implemented using CB-PWM, and the effects of changing the power factor of the converter will be tested.

As illustrated in Fig. 2.20, the inner loops control the ac currents and the outer loop regulates the dc-link voltage. The current loop has a bandwidth of 2kHz and the voltage loop bandwidth is 200Hz. Since the dc-link has a split capacitor, a balancing controller is used to balance the two capacitor voltages. The grid synchronization is done by a phase-locked loop (PLL), in such a way that the direct axis is aligned with the grid voltage vector and the quadrature axis is leading 90 degrees, as shown in Fig. 2.21. Consequently, i_d is responsible for the active power transfer, and i_q defines

the reactive power component.

2.4 Summary

After comparing different topologies to perform ac to dc conversion, the Vienna rectifier topology has been selected for aerospace applications. The Vienna rectifier is a three-level unidirectional power flow topology based on a diode bridge rectifier, but with advanced PWM features. Compared to the well-establish two-level converter, the Vienna rectifier offers significant benefits in aspects like current waveform quality, power density, reliability, etc. As the application does not require 4-quadrant operation, the Vienna rectifier offers lesser amount of failure points, with simple circuit structure and cost benefits compared to the other three-level topologies. One of the constraints of the Vienna rectifier is that it does not perform well under nonunity power factor operation due to current distortion near the zero crossings. The challenge of this research is to improve the performance of the Vienna rectifier under such operating conditions. Some solutions to that problem are discussed in the subsequent chapters. The hardware setup based on a Texas Instruments Vienna rectifier, which will be used to obtain experimental results, has also been introduced in this chapter.

Chapter 3

Extended Operation Mode in the Vienna Rectifier

The Vienna rectifier is a three-level three-phase converter which offers many advantages; however, it suffers from poor current waveform quality when there exists a phase displacement angle between the reference voltage and the current. Zero sequence voltage injection methods are popularly used to address the power quality issues. However, these methods restrict the range of modulation index because the resultant common mode voltage may cause the converter to operate in overmodulation in certain operating conditions.

Unlike the conventional methods, a new approach is introduced in this chapter that uses the reactive current injection under lower displacement power factors to extend the operating range of the Vienna rectifier. An algorithm is designed such that reactive current injection will be activated only during certain working conditions involving low power factor operation, where the zero sequence injection would produce overmodulation. A twin controller runs in parallel to the voltage oriented controller to assist the decision making for the algorithm. Additionally, a mathematical analysis is done for the reactive current calculation. The proposed method ensures the quality of ac current waveform, regardless of the operating conditions of the Vienna rectifier. The concept is verified by simulation and validated in a 1-kW Vienna rectifier experimental setup.

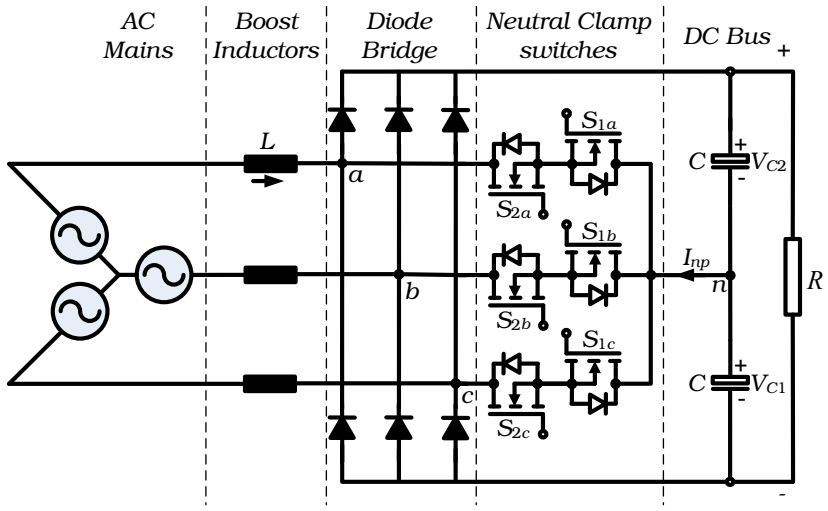

Figure 3.1: The Vienna rectifier topology.

3.1 Introduction

The Vienna rectifier shown in Fig. 3.1 includes a diode bridge rectifier and bidirectional switches that can connect each leg of the converter to the neutral point of the dc-link capacitors. It can generate three voltage levels in each of the nodes a, b, c and sinusoidal currents with unity power factor operation. The maximum voltage that the bidirectional switches have to withstand is half the dc-link voltage. The Vienna rectifier is similar to the T-type converter but with fewer active switches, thus a simplified topology. As a result, it can only transfer power in one direction, from the ac side to the dc side. Certain unidirectional active-front-end applications, which demand high power density and reliability, prefer the Vienna rectifier (Fig. 3.1) over other circuit topologies due to the advantages it offers like a simple circuit structure. Compared to the well established two-level converter, the Vienna rectifier produces lower current ripple for a given inductance, and better switches with lower blocking voltage can be used to have better efficiencies for a lower cost [34, 62], as discussed in the previous chapter.

The Vienna rectifier has an inherent problem of current zero-crossing distortion. Although the Vienna rectifier is a three-level converter, there is only full control of the midpoint connection. The top and bottom voltage levels are defined by the direction of the current that is flowing through the diodes. When there is no phase angle shift between the voltage reference and the input current, there is no low-frequency distortion. However, if there exists a displacement and no special action is taken, there would be low-frequency harmonics in the current frequency spectra [41, 63–71].

Switching methods based on space-vector modulation (SVM) for the Vienna rectifier was first proposed in [63] and then in [66,67]. The equivalence of SVM and carrier-based PWM (CB-PWM) on the Vienna rectifier is analyzed and a CB-PWM method is proposed in [72]. Switching-based on CB-PWM are discussed in [23, 46, 73, 74].

Clamping to the neutral point the leg that produces pulses with opposite sign was proposed in [63], [75]. It resulted in significant reduction in current distortion at the zero-crossing. The duration of the clamping periods depends on the displacement angle and may last for a few switching cycles. The clamping periods help to mitigate voltage and current distortion; however, they do not eliminate the low-frequency distortion completely and they have a negative effect on the voltage balancing of the dc-link capacitors. Therefore, the clamping periods should be minimized as much as possible. In [75], the authors used a fixed clamping angle, which was obtained experimentally. This would require a number of experiments for the different operation conditions. An analytical approach is discussed in [76] in which the clamping angle is calculated in an application where the Vienna rectifier is fed with a permanent magnet synchronous generator (PMSG). The current ripple due to the PWM is calculated and the maximum angular displacement of the current space vector in comparison to the fundamental voltage is used to find the required clamping angle.

Injecting a zero sequence into the reference signals to reduce the zero crossing distortion is discussed in [77]. A third harmonic is injected, which helps to make the duty cycles zero near the current zero crossings. But this does not solve the problem completely as still there would be some distortion due to the insufficient clamping time. The authors have extended the clamping time using redundant vectors in the space-vector PWM diagram.

Current distortion mitigation with discontinuous pulse width modulation (PWM) implemented with space vectors was presented in [67]. The method shows better performance at higher modulation indices. Moreover, changing between different modulation methods based on the converter operating point is proposed in [78]. However, such carrier-based discontinuous PWM operates well for a certain range of modulation indices [79, 80]. Even though the DPWM increases the efficiency, the current harmonic distortion also increases in the Vienna rectifier compared to continuous PWM.

The Vienna rectifier was introduced operating with a hysteresis current controller [34] with independent phase current controllers and a zero sequence component

balancing the capacitor voltages. It had the problem of variable switching frequency as the filter design process becomes complicated. In [73], a new control method, the one cycle control, is proposed for the Vienna rectifier. The switching frequency is constant while no ac voltage sensors are used, inductor current or average switch current can be used to implement the controller. The output voltage is integrated and compared with the inductor current measurement, and fed to the switches through flip/flops. The integrator and the flip/flops are reset at the switching frequency. However, as mentioned in [81], the utilization of the dc-link voltage is low. Also, it is an analog implementation and reactive power compensation is not possible. On the other hand, this method could be an option if the application does not permit a DSP. In another analog technique, the current controller is implemented without multipliers [82], in the abc-natural frame, which relies only on the input currents, and does not demand the input voltage measurements.

In a DSP-based implementation [74], proportional-integral (PI) controllers are used based on the average d-q model of the Vienna rectifier. Also the neutral point voltage balance of the dc-link capacitors is achieved through a zero sequence. A voltage sensor-less control is introduced in [68] where the grid voltages are estimated by an observer. A current oriented control, without the use of voltage sensors in the ac side, can mitigate the zero-crossing problem [83]. However, the converter may not operate as desired when the inductance is low or operating with light loading [38], where the current waveforms are expected to be highly distorted. Sensorless current control can address the current distortion, but additional circuits for overcurrent/short-circuit protection are needed [84].

A few methods based on carrier-based PWM implement special zero-sequence injection to remove the current distortion by connecting the ac terminals to the neutral point during certain intervals [23], [24]. However, these methods have constraints in the modulation index because the zero sequence introduces peaks to the reference voltages which may lead to overmodulation. Another similar method which combines the special zero sequence with reactive current injection is introduced in [25].

This chapter extends the idea proposed in [25] and includes more analysis and experimental results. The main contribution lies in proposing a method comprising of two operating modes for optimal operation of the Vienna rectifier. This allows the rectifier to operate without producing low order harmonics in the source currents without any constraints on the modulation index. In the first mode, a particular zero

sequence voltage is added to the reference voltages, which clamps a phase through the bidirectional switches to the midpoint whenever there exists a sign difference between the reference voltage and the grid current. As a result, the grid currents do not contain low-frequency distortion, but this technique has modulation index restriction. In the second mode, a calculated amount of reactive current (in real-time) is injected to achieve unity power factor (UPF) at the converter terminals, removing the constraint in the modulation index. Finally, an algorithm is proposed for smooth transition between the two operating modes. The proposed modulation and control scheme for the Vienna rectifier offers,

1. Wide power factor range of operation without compromising the quality of the grid currents. For the Vienna rectifier this is nontrivial as it has an inherent problem of current zero crossing distortion when operated with large phase displacement angles, which has limited its industry application.

2. A reactive current injection based method is proposed in combination with a zero sequence voltage injection method. An algorithm selects the best mode of operation for the Vienna rectifier depending on the operating point. The objective of the algorithm is to avoid overmodulation.

3. The zero sequence voltage injection method proposed in prior art has a restriction in the modulation index for high phase displacement angles. The proposed method operates with constraint-free modulation index.

4. Real-time reactive current calculation to obtain unity power factor (UPF) at the converter terminals, facilitating the control implementation in a DSP.

The chapter is structured as follows. In Section 3.2, the essential operation of the Vienna rectifier is presented explaining the issues associated with the zero-crossing distortion in the current waveform when operating with nonunity power factor. Section 3.3 presents selected existing distortion mitigation strategies. The reactive power compensation with transition between the two modes based on specific criteria is discussed in Section 3.4. Experimental results are presented in Section 3.5. Finally, Section 3.6 summarizes the main conclusions of the chapter.

3.2 Vienna Rectifier Operation

The three-level Vienna rectifier is popular among designers due to the various advantages such as simple circuit structure, unity power factor operation, low harmonics in the grid currents, and low blocking voltage stress on the bidirectional switches [34]. The Vienna rectifier is similar to the T-type converter but with fewer active switches, thus a simplified topology. As a result, it can only transfer power in one direction, from the ac side to the dc side.

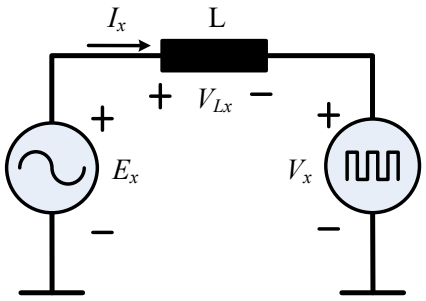

Figure 3.2: Simplified single-phase diagram of a grid-connected Vienna rectifier.

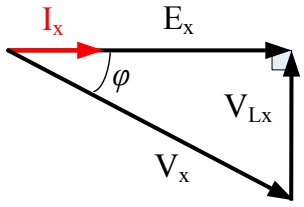

Figure 3.3: Phasor diagram operating with unity power factor at the grid side.

Although the Vienna rectifier is a three-level converter, only the neutral point connection is fully controlled through the bidirectional switches. The positive and negative voltage levels of the converter are decided by the current direction. If there is no phase displacement angle between the reference voltage and the input current, the desired voltage is generated at the input of the converter. However, if there is a certain phase displacement angle and no special action is taken, the voltage pulses generated by the converter will have opposite polarity during the intervals where the reference voltage and input current have different signs. This produces low-frequency voltage distortion, which deteriorates the quality of the grid currents. Even when operating at unity power factor at the grid side (Fig. 2.10(b)), the Vienna rectifier does not operate at unity power factor because of the filter inductors that cause a phase displacement angle between the current and voltage waveforms. Therefore, because of this displacement angle, current distortion will be appreciated around the

zero crossings [63–65]. Such a distortion in the grid currents is not desired because it may violate the grid codes.

In this analysis, the Vienna rectifier is connected to a fixed frequency ac source. The ultimate target is to connect it to an aerospace generator operating at variable frequency. Fig. 3.2 represents a simplified single-phase diagram of a grid-connected Vienna rectifier. The equivalent voltages are,

$$E_x = \omega L I_x + V_x \tag{3.1}$$

where E_x is the source voltage of phase $x \in \{\text{a,b,c}\}$, V_x is the converter terminal voltage, I_x is the input current and L is the line inductance.

Synchronization with the grid voltages is performed by measuring the grid voltages E_x in Fig. 3.2. The phasor diagram when operating with unity power factor at the grid side is represented in Fig. 3.3. In this chapter, the converter is fed from an ideal voltage source. In practical applications, the model of the voltage source will include some impedances, however they are usually very small compared with the impedance offered by the filter inductor L. For the Vienna rectifier under test, the voltage is measured at the source in Fig. 3.3. A PLL will extract the angle information from the voltage measurement. The converter uses this angle to regulate the currents and align them with the phase voltages, usually forcing the two variables to be in-phase at the source in the single-phase representation (unity power factor operation). The phase angle ϕ in Fig. 3.3 will depend on the filter inductance, the fundamental frequency, and the grid current magnitude.

Let a normalized set of three-phase voltages be defined as:

$$v_x = m \sin(\omega t + \delta_x) \tag{3.2}$$

with $x \in \{\text{a,b,c}\}$ where v_x is the normalized voltage of phase x, $\delta_{a,b,c} = \{0, 4\pi/3, 2\pi/3\}$ and m is the modulation index. Analogously, a three-phase set of currents with the polarity given in Fig. 3.1 is defined:

$$i_x = I \sin(\omega t + \delta_x + \phi) \tag{3.3}$$

where I is the amplitude of the current and ϕ is the phase difference between i_x and v_x with $x \in \{\text{a,b,c}\}$. The conventional method of controlling the switches in the Vienna

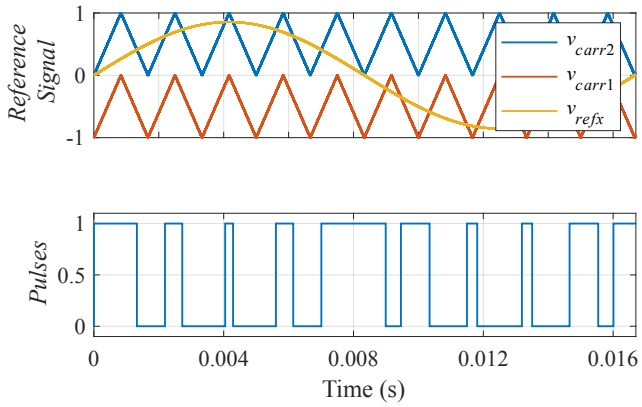

Figure 3.4: Control signals for switches controlled together with PD-PWM. Top: Reference signal with carriers. Bottom: Pulses applied to the switches.

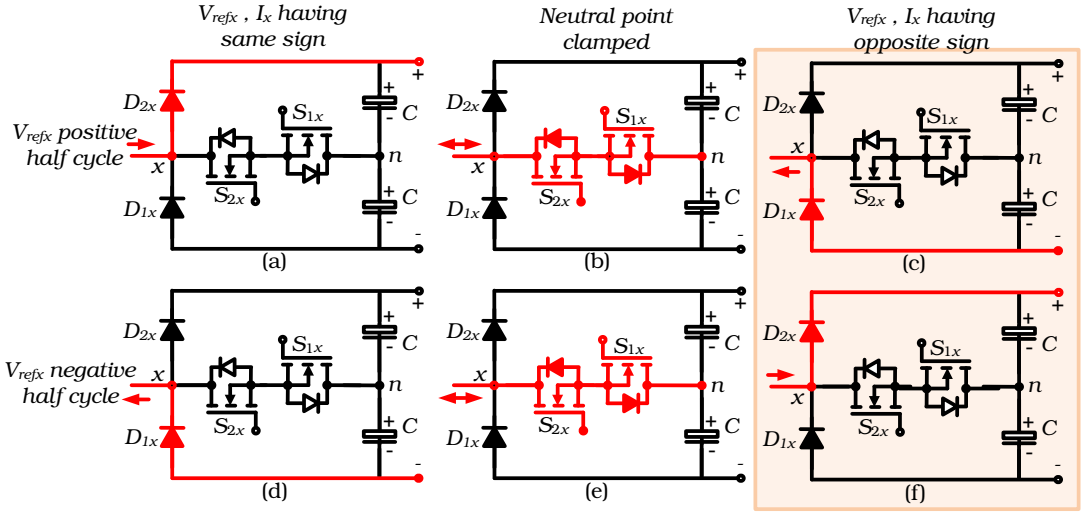

Figure 3.5: Various operating states of a phase-leg in the Vienna rectifier when the switches are controlled together. Positive half-cycle with: (a) Current in the positive direction, (b) clamping to the neutral point, and (c) current in the negative direction. Negative half-cycle with: (d) Current in the negative direction, (e) clamping to the neutral point, and (f) current in the positive direction.

rectifier is by using a common gate pulse on the bidirectional switch pair s_{1x}, s_{2x} as follows:

$$S_{1x} = S_{2x} = 1, \text{ if } v_{carr1} < v_{refx} \leq v_{carr2} \tag{3.4}$$

where $x = \{a, b, c\}$ are the phases of the rectifier. The lower and upper carrier signals are represented by v_{carr1} and v_{carr2}, respectively, while the modulating voltage reference is v_{refx}. Fig. 3.4 shows the waveforms of the generated pulses and the corresponding carrier and reference signals in a phase-disposition carrier-based PWM (PD-PWM) method [34].

Focusing on a phase-leg of the Vienna rectifier (phase-leg x), when the reference

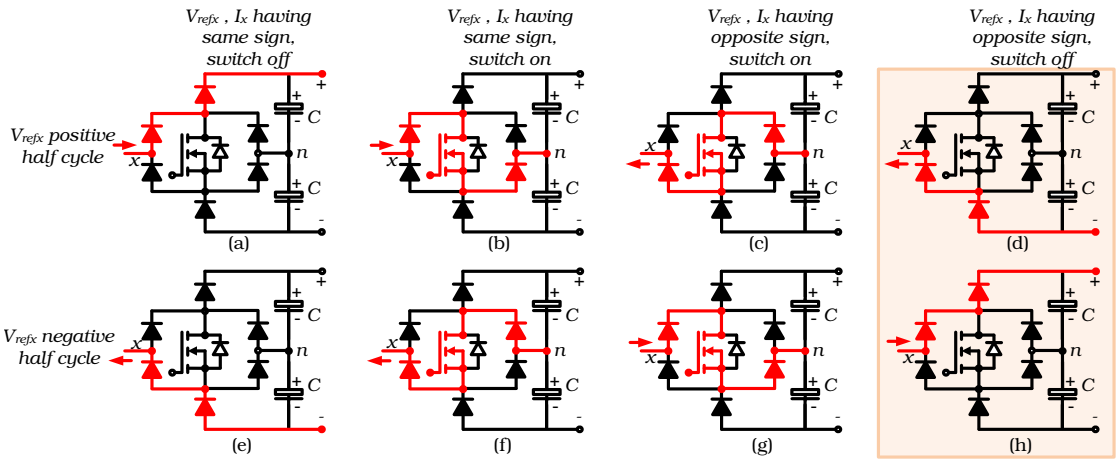

Figure 3.6: Various operating states of a phase-leg in the Vienna rectifier with a single switch. Positive half-cycle with: (a) Current in the positive direction with the switch off, (b) current in the positive direction with clamping to the neutral point, (c) current in the negative direction with clamping to the neutral point and (d) current in the negative direction with the switch off. Negative half-cycle with: (e) Current in the negative direction with the switch off, (f) current in the negative direction with clamping to the neutral point, (g) current in the positive direction with clamping to the neutral point and (h) current in the positive direction with the switch off.

voltage of the converter is in the positive half-cycle and the current flows in the positive direction (towards the rectifier from the source), if the switches are off, the top diode D_{2x} conducts forming a positive voltage pulse v_{xn} (Fig. 3.5(a)). If the switches are on, then the current flows through the switches to the neutral point (Fig. 3.5(b)). On the other hand, if there is a phase shift between the reference voltage and the current, there would be an interval in the positive half-cycle where the current is negative. In this interval, when the switches are off, the bottom diode D_{1x} conducts, as shown in Fig. 3.5(c), creating a negative voltage pulse in v_{xn}, which is undesired. This switching state creates distortion.

Likewise in the negative half-cycle, when both switches are off, the polarity of the voltage pulse is defined by the current direction. When the current is negative, a negative voltage pulse is created (Fig. 3.5(d)), but if the current is positive, a positive voltage pulse is created, which produces distortion (Fig. 3.5(f)). Therefore, the only voltage level that is fully controlled in the Vienna rectifier is the neutral point level. The top and bottom levels are decided by the current direction.

Similar to the Vienna rectifier when the switches are controlled together, the above problem exists in the Type I Vienna rectifier with single switch per phase as illustrated in Fig. 3.6.

Fig. 3.7 depicts the main waveforms and the source current frequency spectra

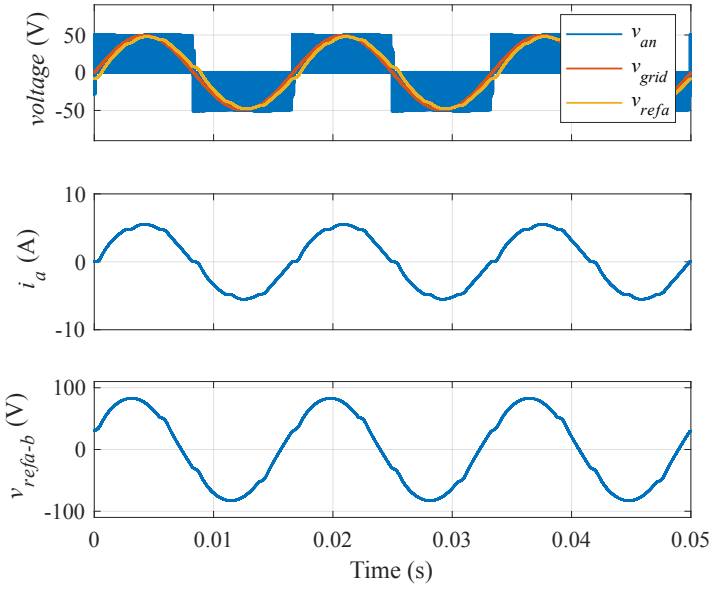

(a)

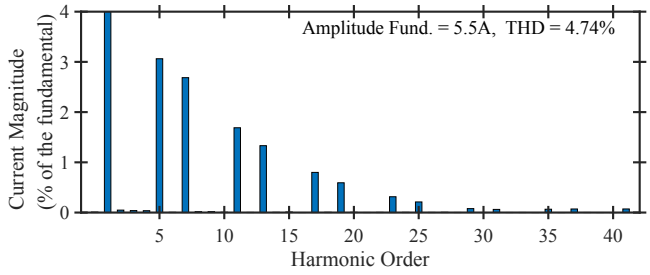

(b)

Figure 3.7: Switches controlled together with a single gate pulse: (a) Main waveforms and (b) frequency spectrum of the grid current.

when the above method is used, based on the parameters given in Table 3.1, simulated using Matlab Simscape Electrical Tool Box. The phase displacement angle in this test condition is 6.87 degrees. As it can be observed in Fig. 3.7(a), despite operating with unity power factor at the grid side, there is a phase angle displacement between the reference voltage and the current at the converters side. As a consequence, the

Table 3.1: Vienna Rectifier Parameters

Parameter	Value
Input inductor, L	3 mH
Output capacitors, C	220 μF
Line-to-line voltage rms, V_{l-l}	60.6 V
Output voltage, V_{dc}	99 V
Output power, P_{out}	416 W
Fundamental frequency, f	60 Hz
Switching frequency, f_{sw}	50 kHz

voltage at the converter terminals becomes distorted. This is due to the fact that the current direction will define the polarity of the voltage pulses when the neutral point connection is not activated, producing pulses with opposite polarity during some intervals near zero crossing of the current [25]. This results in zero-crossing distortion in the current waveforms and it is reflected as low order harmonics, which is undesirable. Fig. 3.7(b) shows the current spectra and it illustrates the low-frequency distortion as a result of such operation mode of the converter. The THD of the current under such condition is 4.74%.

3.3 Distortion Mitigation Methods

3.3.1 Switches Operating Independently

The bidirectional switch pairs in the Vienna rectifier are controlled independently by applying PD-PWM and are formulated as presented in Fig. 3.8 using the following control strategy:

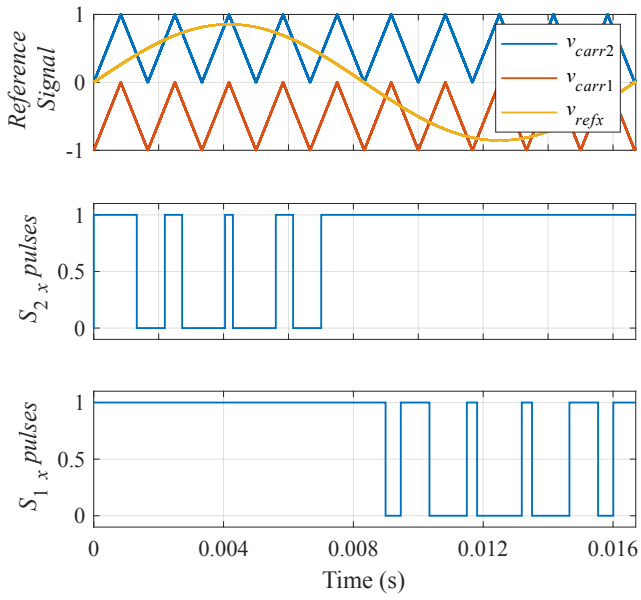

Figure 3.8: Independent control signal waveforms for the bidirectional switch pair with PD-PWM.

$$S_{2x} = \begin{cases} 0, & \text{if } v_{refx} > v_{carr1} \text{ and } v_{refx} > v_{carr2} \\ 1, & \text{otherwise} \end{cases} \tag{3.5}$$

$$S_{1x} = \begin{cases} 0, & \text{if } v_{refx} \leq v_{carr1} \text{ and } v_{refx} \leq v_{carr2} \\ 1, & \text{otherwise} \end{cases} \tag{3.6}$$

With this control technique, switch S_{2x} is switching while the other switch (S_{1x}) is continuously on during the positive half-cycle of the reference voltage. Likewise, switch S_{2x} is on in the negative half-cycle while S_{1x} is switching. The relevant operating states are illustrated in Fig. 3.9. Now the Vienna rectifier does not produce erroneous voltage pulses when the reference voltage and the current have opposite signs as the neutral point connection is activated during this time period.

Fig. 3.10(a) depicts the main waveforms when the bidirectional switch pairs are fed with pulses obtained using (3.5) and (3.6) and the frequency spectrum of the grid current is shown in Fig. 3.10(b). The line-to-line voltage distortion can be seen in Fig. 3.10(a) during the time interval where the clamping to the neutral point occurs.

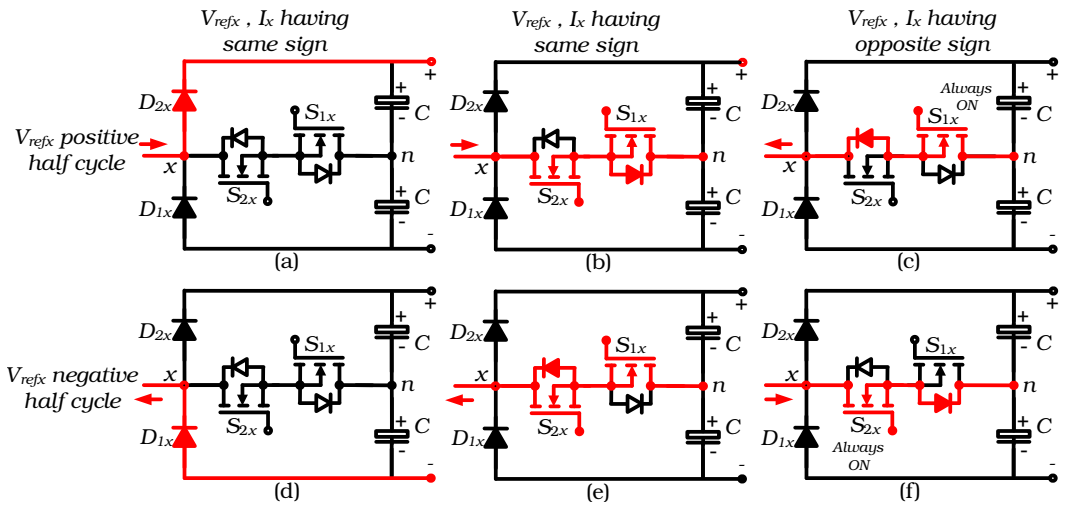

Figure 3.9: Various operating states of a phase-leg in the Vienna rectifier with independent control of the switches. Positive half-a-cycle: (a) Positive current and (b) negative current (S_{1x} on, S_{2x} off). Negative half-a-cycle: (c) negative current and (d) positive current (S_{1x} off, S_{2x} on).

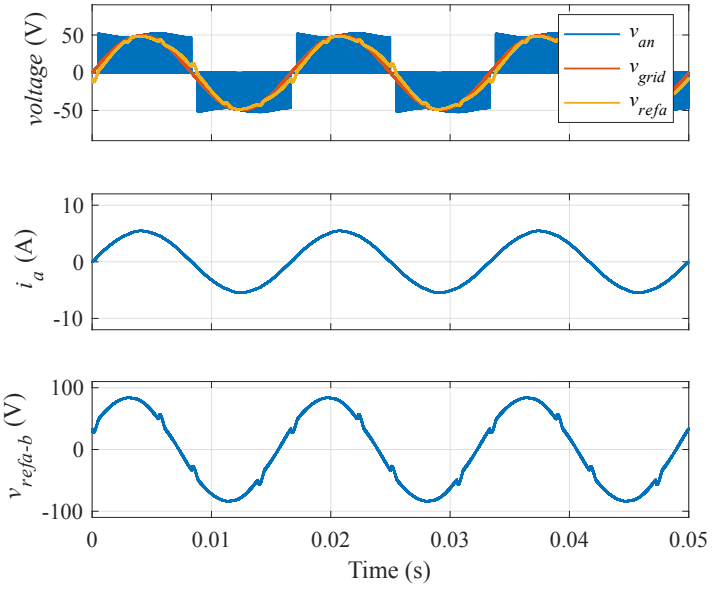

(a)

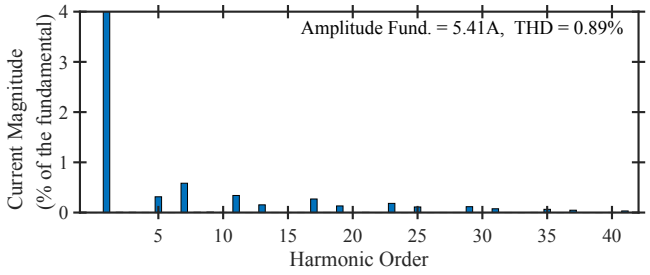

(b)

Figure 3.10: Switches controlled independently without any zero sequence voltage injected: (a) Main waveforms and (b) frequency spectrum of the grid current.

3.3.2 Zero Sequence Injection

Even though the voltage pulses with opposite polarity are eliminated with the previous control technique, the reference voltage is not followed at the ac terminal during some intervals, as it is clamped to the neutral point. While the reference voltage of a phase-leg is forced to be zero during those intervals, the same amount could be subtracted from the reference voltages of the other two phases, thus creating a zero sequence. As a consequence, the low-frequency distortion produced in the Vienna rectifier should disappear. A lookup table-based method can be used to calculate the zero sequence [23]. Fig. 3.11(a) shows another method with simpler implementation to calculate the common mode voltage based on the product of the reference voltage and the input current [24]. However, both of these methods have limitations on power factor variation and will have to restrict the modulation index

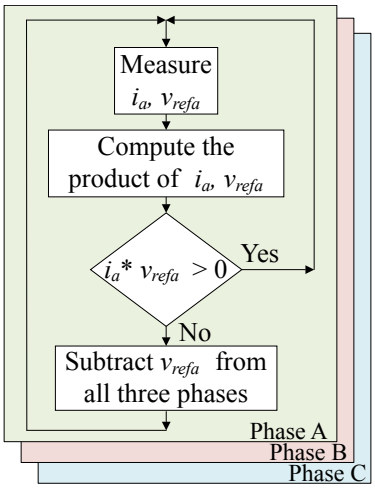

(a)

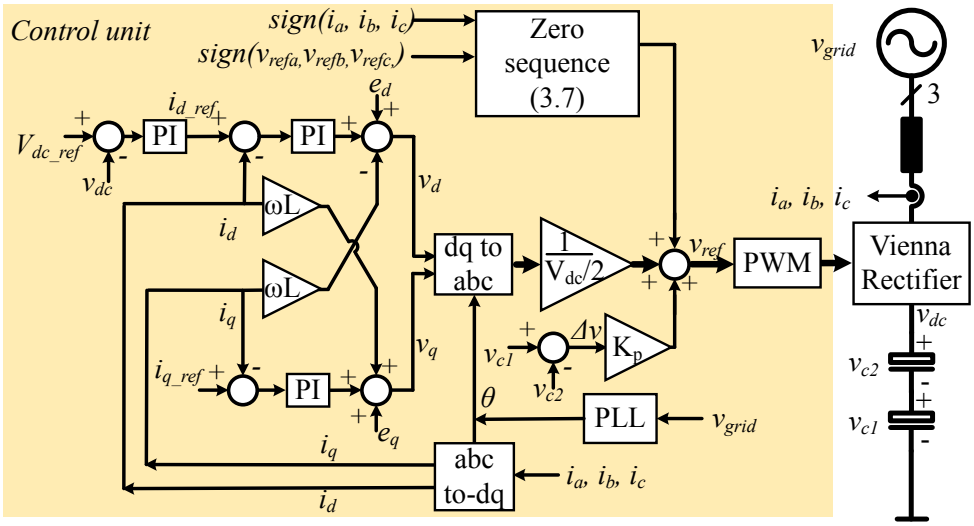

(b)

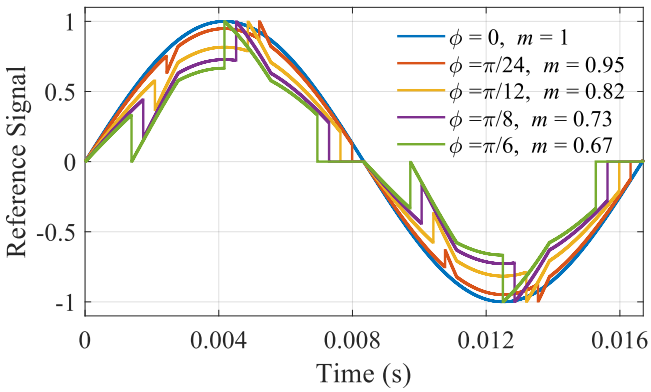

(c)

Figure 3.11: Vienna rectifier with the zero sequence voltage injection: (a) Flow chart of the zero sequence generation [24], (b) Voltage oriented control and (c) Modulation index restriction based on the phase difference between i_x and v_x.

when operating with high phase displacement angles, as described later in this section.

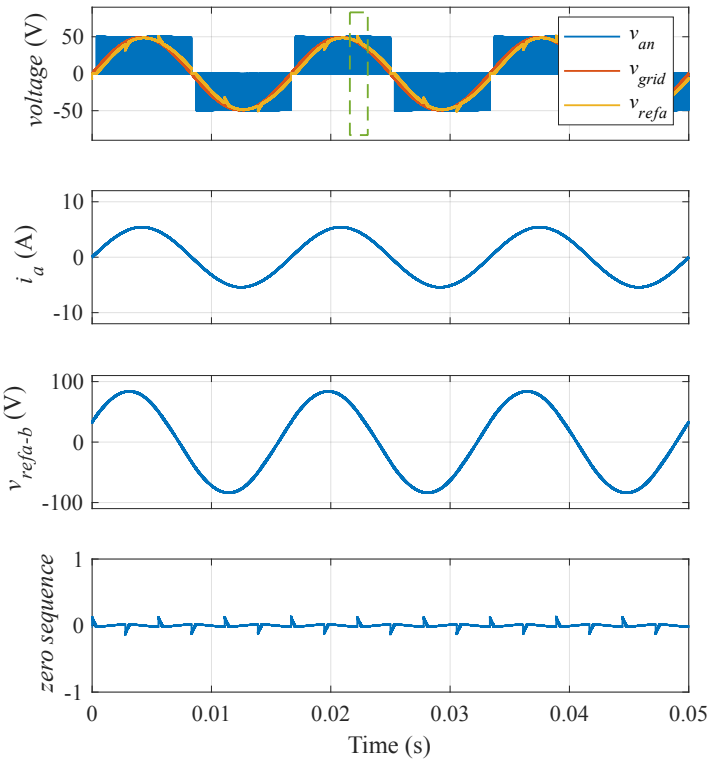

(a)

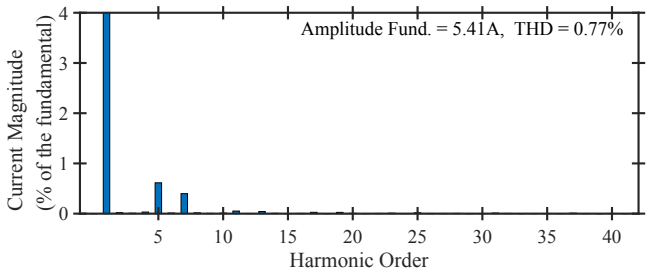

(b)

Figure 3.12: Zero sequence voltage injection: (a) Main waveforms and (b) frequency spectrum of the grid current.

Fig. 3.11(b) shows the zero sequence fed to a VOC, where the inner current loop regulates the sinusoidal current and the outer voltage loop regulates the dc-link voltage. The capacitor voltage balance block adds an offset to the reference voltages, as detailed in Fig. 3.11(b), in order to balance the capacitor voltages. As illustrated in Fig. 3.12, once the zero sequence is injected, the line-to-line voltage distortion is eliminated and the quality of the grid currents is improved.

Some peaks appear in the reference voltages with the injected zero sequence, as shown in Fig. 3.12(a), which may produce overmodulation, especially when operating with high modulation indices. As a result, the modulation index will have to

be limited. The highest modulation index that the converter can operate without producing overmodulation is determined by examining the maximum value of the reference voltage once the zero sequence is added. The generalized zero sequence can be expressed as a common mode voltage as follows,

$$v_{cm} = \begin{cases} -m\sin(\omega t), & k\pi \leq \omega t < k\pi + \phi \\ -m\sin(\omega t - \frac{2\pi}{3}), & \frac{(3k+2)\pi}{3} \leq \omega t < \frac{(3k+2)\pi}{3} + \phi \\ -m\sin(\omega t + \frac{2\pi}{3}), & \frac{(3k+1)\pi}{3} \leq \omega t < \frac{(3k+1)\pi}{3} + \phi \\ 0 & \text{otherwise} \end{cases} \tag{3.7}$$

where $k \in \mathbb{Z}$. The normalized reference voltage for phase a in the interval indicated by the green box in Fig. 3.12(a), is expressed as:

$$\frac{v_{refa}}{v_{dc}/2} = m[\sin(\omega t) - \sin(\omega t - \frac{2\pi}{3})] \tag{3.8}$$

The maximum value of (3.8), should not exceed one to avoid overmodulation, which leads to the following condition:

$$m \leq \frac{1}{\sqrt{3}\sin(\frac{\pi}{6} + \phi)} \tag{3.9}$$

For phase displacement angles up to 5.26 degrees, the zero sequence addition has no effect on the maximum modulation index reachable, as the peak of the notch created by the zero sequence is less than the peak of the reference sinewave. On the other hand, for phase displacement angles greater than this value, the modulation index will have to be restricted to avoid overmodulation. It should be highlighted though that even if overmodulation occurs, the distortion originated in the input currents would be significantly smaller than in the former cases where no zero sequence is injected. Fig. 3.11(c) presents the maximum modulation index to avoid overmodulation depending on the displacement angle. It is clear that when the modulation index is low, the converter can handle larger displacement angles, making this control technique more suitable for low modulation index operation. As the Vienna rectifier injects current into the neutral-point of the dc-link capacitors, capacitor voltage balance is required [81, 85] and it could effect the current waveform quality [86] if it is not properly balanced. Nevertheless, Fig. 3.12(a) v_{an} depicts the capacitor voltages are balanced, which means that the average neutral-point current is zero.

Table 3.2: Summary of Modulation and Control Methods for the Vienna Rectifier

Modulation and Control	Advantages	Disadvantages
Hysteresis control [34]	Simple controller implementation	Varying switching frequency, challenging filter design
Current oriented control [83]	Distortion in the current waveform eliminated	Synchronization problems at lower loads
CB-PWM together [34]	Simple implementation, less gate drivers	Current zero-crossing distortion
CB-PWM independent [24]	Current distortion reduced	Still some distortion exists in the line-to-line voltage
CB-PWM special zero sequence [23, 24]	Distortion completely removed	May create overmodulation for working conditions with high modulation index and phase displacement
Proposed method	No current distortion, no modulation index restriction	Reactive current usage leads to VA rating increase

Table 3.2 summarizes the methods for avoiding the current distortion in the Vienna rectifier.

3.4 Reactive Power Injection with Mode-Transition

An alternative method to eliminate the zero-crossing distortion without compromising the modulation index is the injection of precomputed reactive current. This helps in reducing the phase shift between the voltage reference and the current. With proper reactive current injection, the modulation index does not need to be restricted and the converter can operate with high modulation indices.

By solving the triangles in Fig. 3.13, the reactive current demand to obtain UPF at the converter terminals can be derived as follows:

$$\sin\alpha = \frac{V_{1L}}{E_d} = \frac{\omega L I_1}{E_d} = \frac{I_q}{I_1} \tag{3.10}$$

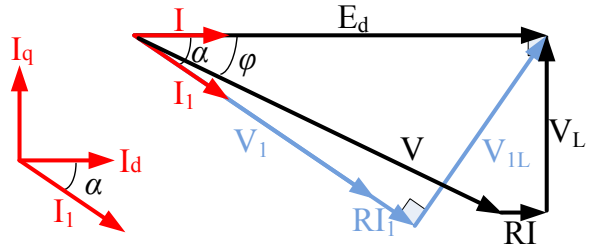

Figure 3.13: Simplified phasor diagram: UPF at the converter terminal (in blue) and UPF at the source (in black).

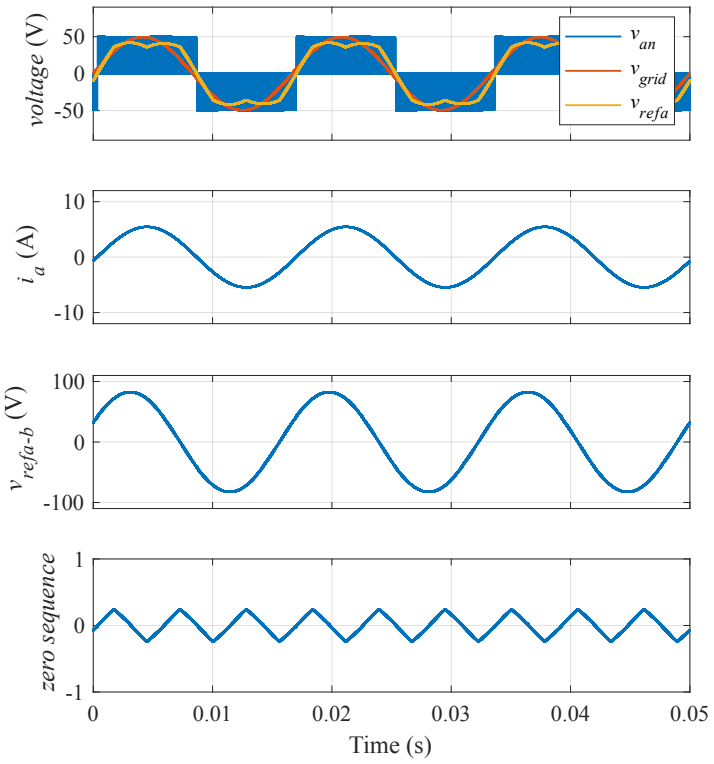

(a)

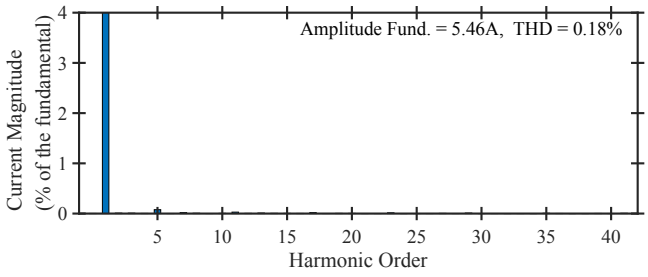

(b)

Figure 3.14: Mode-2 with reactive current injection: (a) Main waveforms and (b) frequency spectrum of the grid current.

where I_1 is:

$$I_1 = \sqrt{I_d^2 + I_q^2} \tag{3.11}$$

substituting I_1 in (3.10):

$$\omega L(I_d^2 + I_q^2) = I_q E_d \tag{3.12}$$

Solving (3.12) for I_q, the calculated reactive current for achieving UPF at the converter terminals is as follows,

$$I_q = -\frac{E_d}{2\omega L}\left[1 - \sqrt{1 - \left(\frac{2\omega L I_d}{E_d}\right)^2}\right] \tag{3.13}$$

The parameters used in (3.13) are readily available in the controller as instantaneous values and, therefore, knowledge of the load is unnecessary. Solving (3.13) with the system parameters given in Table 3.1, one obtains $I_q = 0.85A$ as the reference reactive current to be provided to the current controller. By adding the zero sequence $-(V_{max} + V_{min})/2$ the modulation range is extended by 15% in this operation mode.

Fig. 3.14(a) shows the main waveforms when the reactive current is injected. The current waveform and the reference voltage of the converter are in-phase, avoiding the current distortion. Fig. 3.14(b) illustrates the input current frequency spectrum. The current THD has improved by a significant amount to 0.18% in Mode-2 (reactive power compensation) compared to the previous methods; 0.77% in Mode-1 (zero sequence injection), 0.89% (when the switches were driven independently), and 4.74% (when the switches were operated together).

Therefore, Mode-1 can be used when operating with low modulation indices, since large modulation indices can produce overmodulation, while Mode-2 can be applied for any modulation index. However, it is usually not of interest to operate in Mode-2 with low modulation indices, since UPF is not achieved at the grid-side. Therefore, Mode-2 will be applied for large modulation indices only, i.e., when Mode-1 cannot be applied.

3.4.1 Effect of Parameter Variability

The inductance is varied by ± 10% to evaluate the effect on the reactive current (Fig. 3.15) calculation and on the current THD (Fig. 3.16), when the Vienna rectifier is operating in Mode-2. As shown in Fig. 3.16, there is no change in the current THD

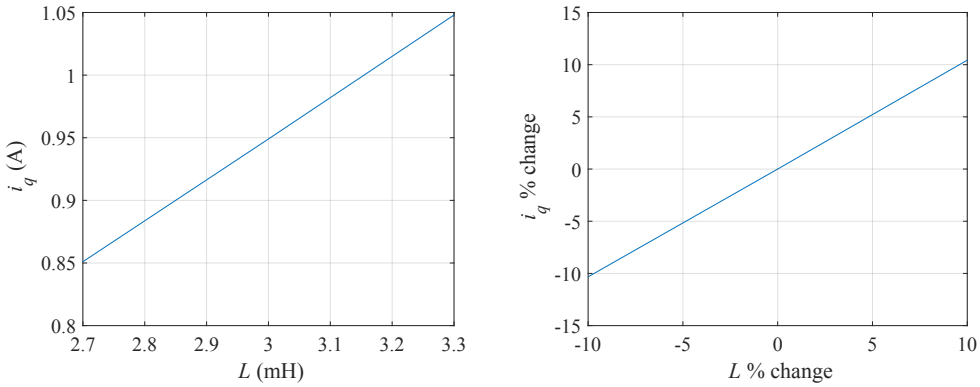

Figure 3.15: Deviation of i_q for an uncertainty of $\pm$ 10% of inductance solving (3.13): (a) Absolute values and (b) as a percentage.

with the $\pm$ 10% uncertainty in the inductance. The reactive currents and the current THD values for the inductance uncertainty are summarized in Table. 3.3.

3.4.2 Twin Controller

As discussed above, since the zero sequence injection and the reactive power compensation have their own limitations, transition between the modes is required. Fig. 3.17 illustrates the mode transition algorithm. The converter operates in Mode-1 by default, and Mode-2 is activated only when the peak of the reference voltage is more than 1 to avoid overmodulation. Because Mode-2 involves reactive current injection, the objective is to return to Mode-1 as soon as it is safe to do so. However, the transition from Mode-2 to Mode-1 is nontrivial as the peak of the reference voltages in Mode-1 is not known until the converter is operated in that mode. The peak of the reference voltages could be higher or lower than 1. In Mode-2, the converter is injecting reactive power such that grid currents and reference voltages at the converter terminals are in phase, which does not require any special zero sequence, i.e., the calculated zero sequence would be zero. To recreate the condition in Mode-1,

Table 3.3: Effects of Inductance Uncertainty

L uncertainty	$L-10\%$	L	$L+10\%$
Reactive current I_q (A)	0.851	0.9489	1.048
Current THD%	0.211	0.216	0.221

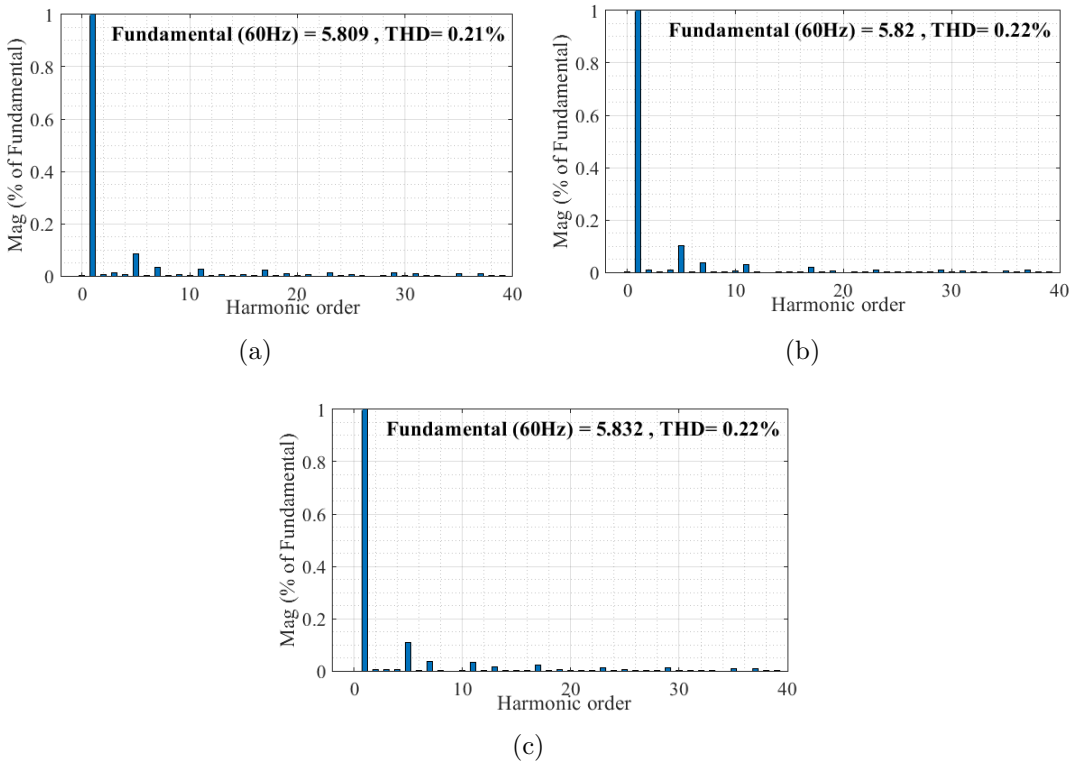

Figure 3.16: Impact on the current frequency spectrum simulated when the inductance is varied with an uncertainty of 10%: (a) Inductance reduced by 10%, (b) inductance nominal value and (c) inductance increased by 10%.

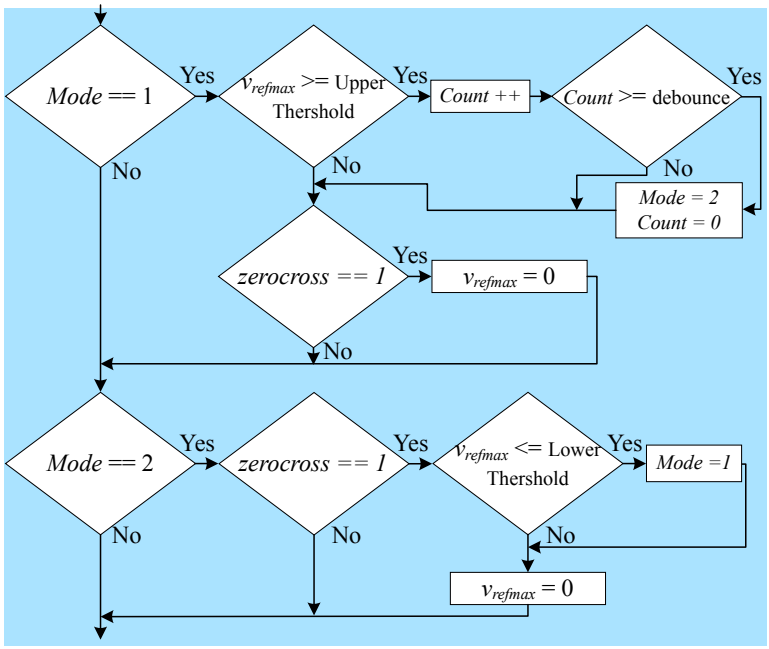

Figure 3.17: Mode transition algorithm.

a twin controller is introduced in Fig. 3.18, which calculates the maximum of the reference signals v_{refmax}, the converter would have if it was operating in Mode-1 with

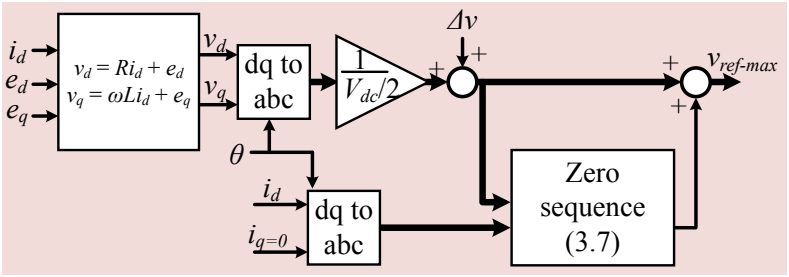

Figure 3.18: Twin controller for the Mode-1 reference voltage.

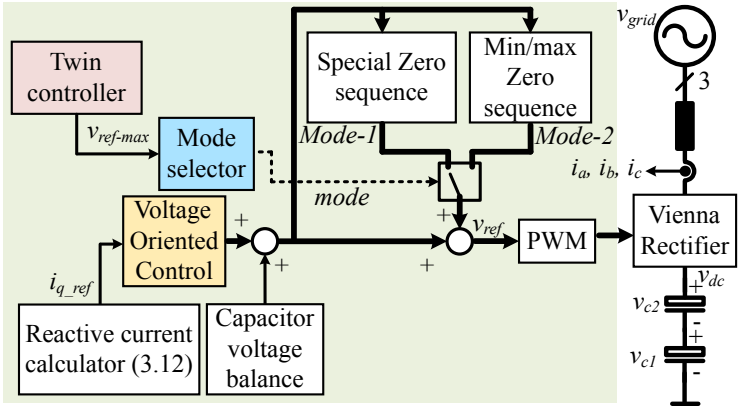

Figure 3.19: Block diagram of the proposed modulation and control scheme for the Vienna rectifier.

the corresponding zero sequence injected, i.e., if reactive power was not injected. It is calculated by using the steady-state values of the converter *d-q* voltage components (3.14) and (3.15) with $E_q = 0$. Imposing i_q as zero:

$$V_d = RI_d + E_d \tag{3.14}$$

$$V_q = \omega LI_d + E_q \tag{3.15}$$

This twin controller will run in parallel to the main controller, calculating the reference voltages in Mode-1 when the converter is operated in Mode-2. A hysteresis band from 1.0 (upper threshold) to 0.98 (lower threshold) exists for the v_{refmax} to avoid unintended mode transitions. If the v_{refmax} goes beyond the upper threshold value, the algorithm switches to Mode-2 from Mode-1 to avoid overmodulation produced by the peaks in the special zero sequence. If the v_{refmax} goes below the lower threshold value during half-a-cycle, the algorithm switches to Mode-1 from Mode-2 because Mode-1 would operate without overmodulation. Mode-2 should be applied only when Mode-1 produces overmodulation, since it involves injecting reactive cur-

rent and thus increases the VA rating of the converter. The phase displacement angle ϕ is given by:

$$\phi = \tan^{-1}(\frac{\omega LI}{E}) \tag{3.16}$$

The displacement angle given in (3.16) along with the modulation index will decide the operation mode of the converter.

Fig. 3.19 shows the proposed modulation and control scheme. The mode transition algorithm that runs in the mode selector would be choosing between the two zero sequences based on the v_{refmax} it receives from the twin controller. When the two modes are combined, the Vienna rectifier can operate within the full range of modulation index $[0, 2/\sqrt{3}]$ without any constraint.

Figs. 3.20(a) and 3.20(b) show the main waveforms of the converter for the transitions from Mode-1 to Mode-2 (operating point is shifted from A to B) and vice versa, respectively, when the operating conditions are changed according to Table 3.4. The simulation is done while maintaining the same loading conditions. The value of the estimated voltage reference in Mode-1 is obtained by the twin controller and its maximum is computed every half-cycle. When the maximum reference voltage (v_{refmax}) from the twin controller is above the threshold (one in this case), the algorithm changes from Mode-1 to Mode-2. The control signal that indicates the change of mode is latched until the next zero-crossing to avoid consecutive changes between the two modes.

In Fig. 3.20(a), the load resistor is reduced from 37.5Ω to 25Ω and the dc-link voltage is reduced from 125V to 99V (operating point changed from A to B in Fig. 3.22) at time $t = 0.017$s, thus increasing the modulation index, until v_{refmax} reaches 1. Then, the mode selector switches from Mode-1 to Mode-2. The converter would change back to Mode-1 if the v_{refmax} from the twin controller is below 0.98.

In the next experiment, the operating conditions are changed from B to A, at

Table 3.4: Operating Conditions for the Experiments

Operating Point	A	B	C	D	E
DC-link voltage, V_{dc} (V)	125	99	99	99	99
Load (Ω)	37.5	25	37.5	37.5	37.5
Modulation index	0.8	1	1	1	1
Fundamental frequency (Hz)	60	60	60	120	180
Phase displacement (deg)	7.2	7.2	4.5	9	13.3

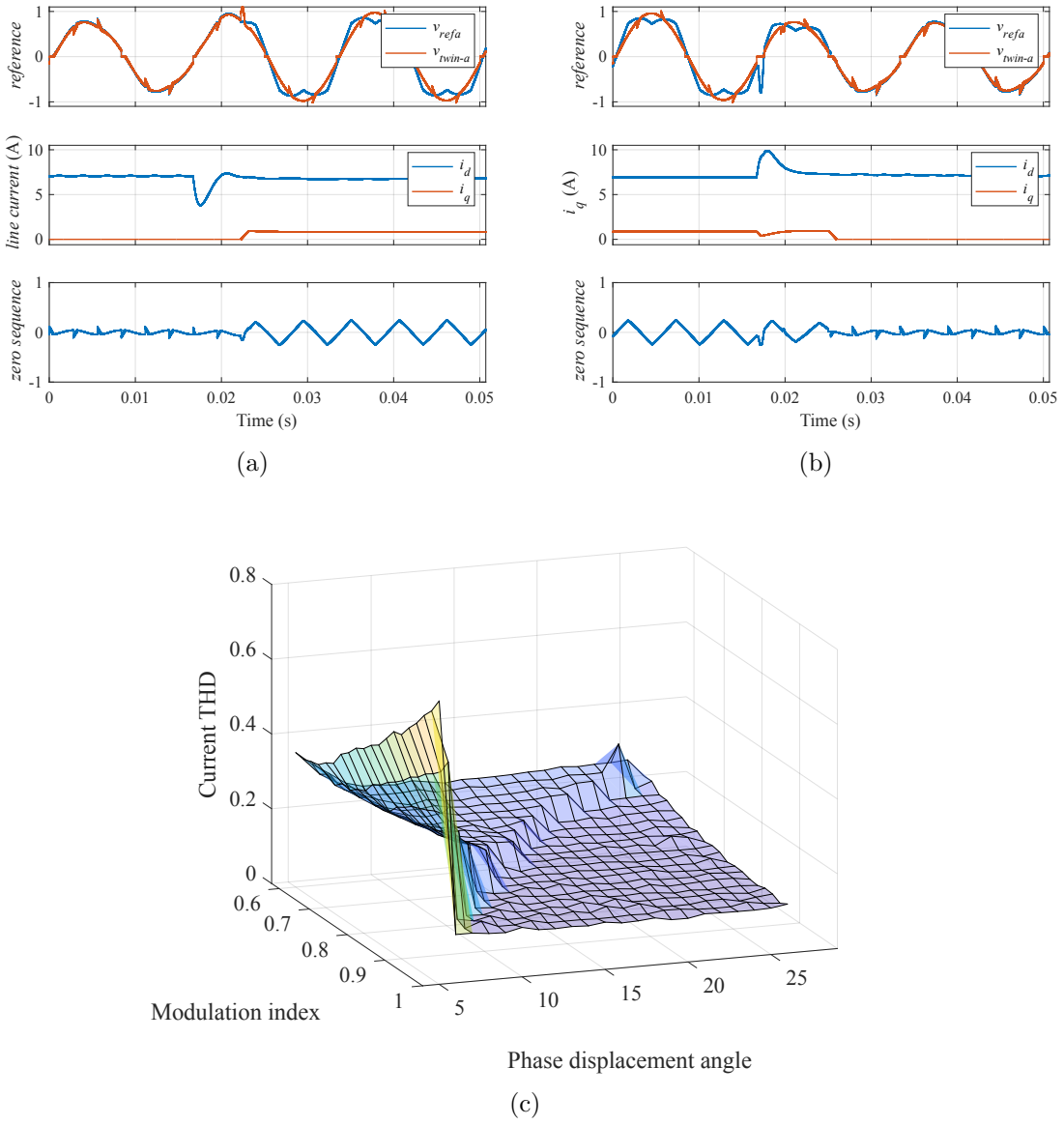

Figure 3.20: Transition of operating modes: (a) Mode-1 to Mode-2, (b) Mode-2 to Mode-1 and (c) current THD at different operating conditions.

time $t = 0.017$s as depicted in Fig. 3.20(b). The reference voltage from the twin controller indicates a value below 0.98 in the next half-cycle, and the converter switches from Mode-2 to Mode-1, which happens at $t = 0.025$s. Afterwards the experiment is repeated for multiple operating points, using the phase displacement angle and modulation index as the independent variables, while keeping $\mathbf{E_d}$, $\mathbf{I}$, and L constant. The current waveform quality varies as depicted in Fig. 3.20(c) and it clearly shows the boundary of the mode transition. For higher modulation indices with larger phase displacement angles the converter operates in Mode-2 to avoid overmodulation.

3.4.3 Efficiency Analysis

An efficiency analysis is performed using PLECS simulation, and the efficiencies at various operation conditions are obtained. Only power losses in the semiconductors are considered, i.e., conduction and the switching losses in the active switches and diodes (losses in the input filter stage are not considered) defined by;

$$\eta = \frac{v_{dc} i_{dc}}{v_{dc} i_{dc} + losses} \tag{3.17}$$

where the *losses* are the conduction and switching losses of the rectifier. 70° C ambient temperature (used as a guideline derived from the aerospace environmental conditions and test standard DO-160, and used as the most common value when the converter is operating) and 0.1° C/W case-to-ambient thermal resistance are assumed for the analysis. Mode-1 and independent switch control will have less switching loss compared to switches controlled together as they have a clamping period where the bidirectional switches are clamped to the mid-point. Depending on the reactive power injected, Mode-2 would have more losses, compared to the other methods. This has been validated using some operating points under the experimental results section.

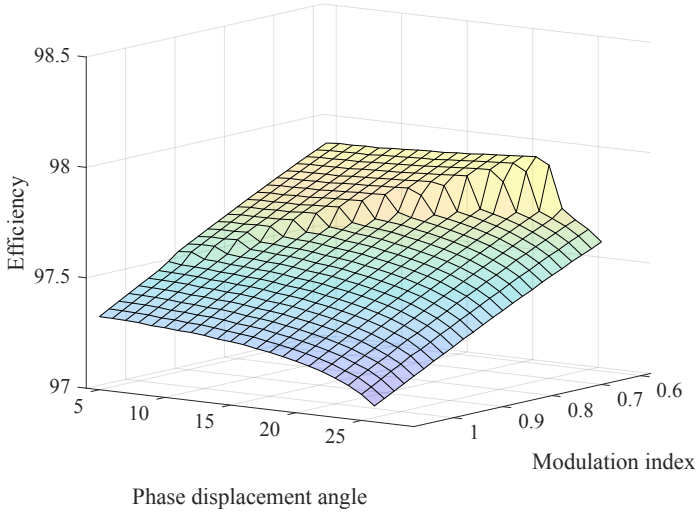

Figure 3.21: Efficiency variation for different operating points when the mode transition is used.

Fig. 3.21 illustrates the efficiency variation when the mode transition is used with the objective of improving the current waveform quality.

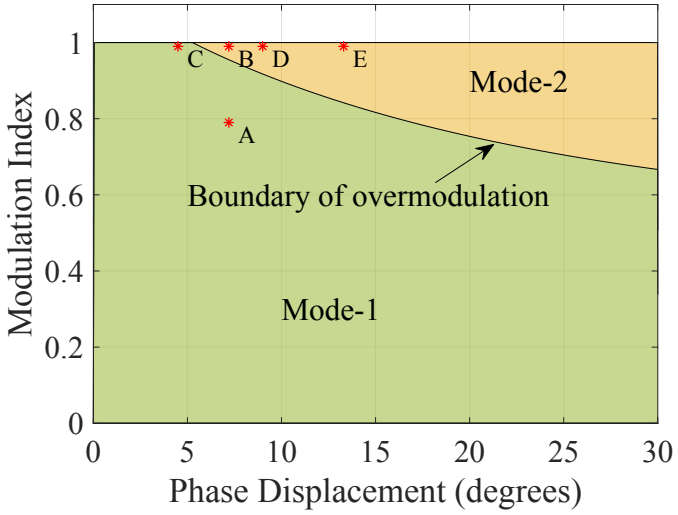

Figure 3.22: Operating modes.

3.5 Experimental Results

The steady state and the transient waveforms from the converter are verified and discussed in this section. Fig. 3.22 shows the different operating points in which the experiments are performed. The zero sequence calculation from the measurements in Mode-1, the reactive current calculation using the real-time values in Mode-2 and the twin controller running parallel to the VOC in both modes are executed within the 20μs time interval in the DSP to update the duty cycle values for the PWM switching. Selection of the voltage loop bandwidth in the VOC is important in this application, and it would be a trade-off between the current THD and the transient response. A 10-Hz voltage bandwidth is selected for the experiment.

Fig. 3.23(a) shows the main waveforms of the Vienna rectifier operating in Point B (Table 3.4), when both neutral-point-clamp switches are operating together and, as expected, the current waveform has significant low-frequency distortion. It can also be observed in its frequency spectrum shown in Fig. 3.23(e). The current waveform quality improves when the switches are controlled independently, as depicted in Figs. 3.23(b) and 3.23(f). This improvement is due to the fact that when the switches are driven together there are voltage pulses with opposite polarity near the zero-crossings and when the switches are driven independently, these erroneous pulses are clamped to the midpoint. This extended clamping period to the neutral can be seen when the V_{an} traces of Figs. 3.23(a) and 3.23(b) are compared. The phase displacement angle for this operating condition is 7.2 degrees.

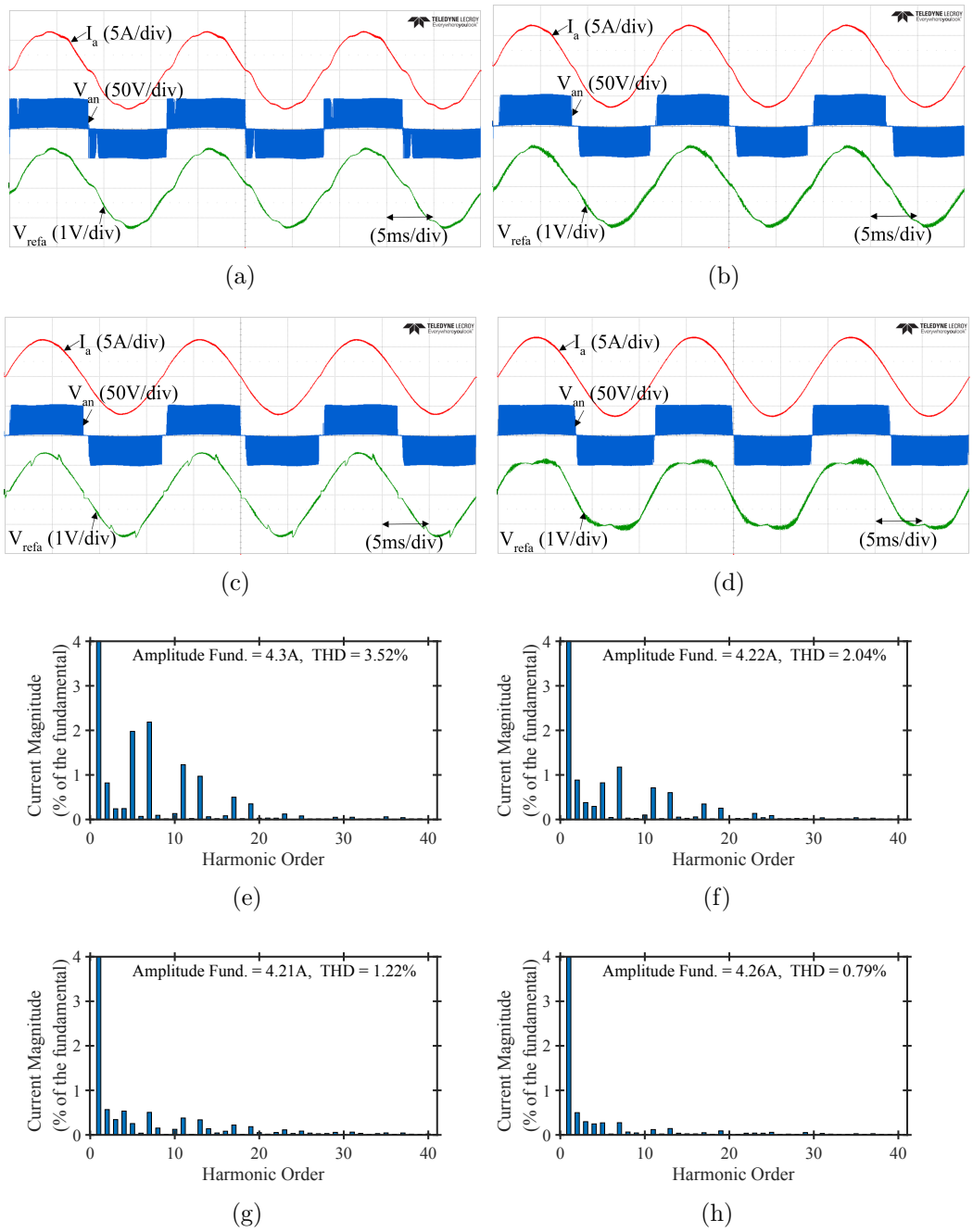

Figure 3.23: Experimental results with different modulation and control techniques: (a) Switches working together, (b) switches working with independent PWM, (c) Mode-1, (d) Mode-2, current frequency spectrum of (e) switches working together, (f) switches working with independent PWM, (g) Mode-1 and (h) Mode-2.

Figs. 3.23(c) and 3.23(g) show the main waveforms and current spectrum, respectively, when the Vienna rectifier works in Mode-1. The results are further improved when the reactive current is injected solving (3.13) using the real-time values such that the current and the reference voltage is aligned, as depicted in Figs. 3.23(d) and 3.23(h). The current THD values are recorded as 3.52% for switches working together, 2.04% for switches working independently, 1.22% for Mode-1 and 0.79%

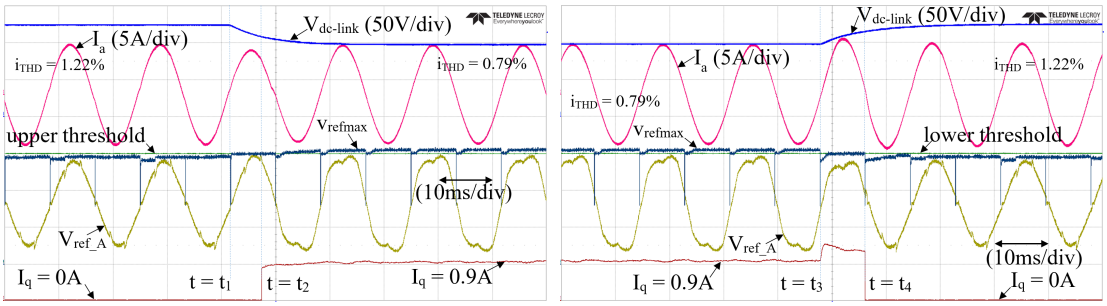

(a) (b)

Figure 3.24: Experimental results of the mode transitions: (a) Transition from Mode-1 to Mode-2, and (b) transition from Mode-2 to Mode-1.

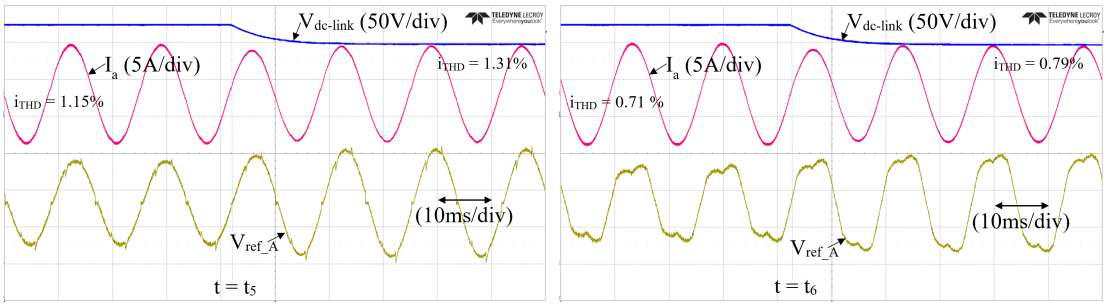

(a) (b)

Figure 3.25: Experimental results of the mode transition algorithm disabled: (a) Force Mode-1 with operating point changing from A to B, and (b) force Mode-2 with operating point changing from A to B.

for Mode-2. The improvement in the current waveform quality is evident from the reduced THD.

Fig. 3.24 shows a transition from Mode-1 to Mode-2 and vice versa by changing the operating point from A to B and back. In both operating points the same loading conditions are maintained as a result of the load step and the dc-link voltage step. As shown in Fig. 3.24(a), the operating point change happens at time $t = t_1$, and the transition from Mode-1 to Mode-2 happens instantaneously when v_{refmax} from the twin controller exceeds the upper threshold value, which occurs at time $t = t_2$. When the operating point is shifted from B to A at time $t = t_3$, as shown in Fig. 3.24(b), the transition from Mode-2 to Mode-1 waits until the next zero-crossing to verify that v_{refmax} from the twin controller drops below the lower threshold, and eventually goes to Mode-1 at time $t = t_4$. As shown in Fig. 3.24, v_{refmax} is reset at each zero-crossing of phase a to obtain the new maximum in the next half cycle. The zero sequence change is visible in the voltage reference signal V_{ref_A} with the mode transition.

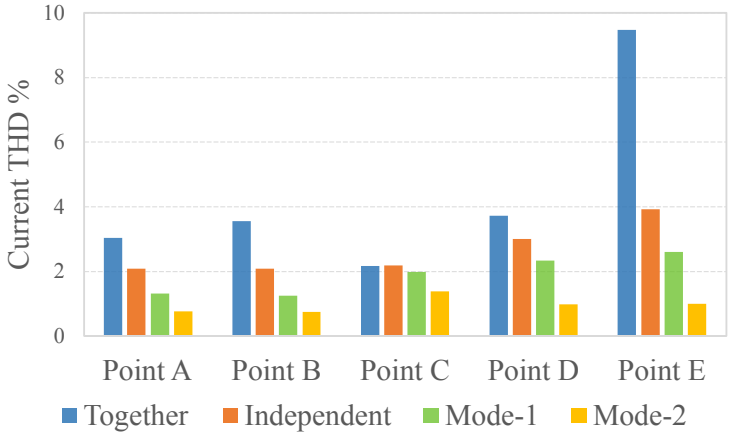

Figure 3.26: Current THD at different operating conditions.

Fig. 3.25 highlights the importance of the mode transition. In Fig. 3.25(a), the Mode transition algorithm is disabled and Mode-1 is forced throughout the operating point shift from Point A to B at time $t = t_5$. When the converter operates in Point B, Mode-1 produces overmodulation, as seen from the increased current THD. In Fig. 3.25(b), Mode-2 is forced when the Mode transition algorithm is disabled, while the operating point shifts from A to B at time $t = t_6$. As expected in this situation, there is no overmodulation but at the cost of reactive power injection. Therefore, Mode-2 is only used in operating conditions where Mode-1 produces overmodulation.

Fig. 3.26 summarizes the current waveform quality at different operating points, when the four methods are used. The current THD values are higher when the converter operates in Points B, D and E. This is because they lie in the overmodulation region shown in Fig. 3.22. Mode-2 has the best current waveform quality regardless of the operating point, but at the cost of injecting reactive current. In Point A, the modulation index is less than operating in Point B, but has the same phase displacement. A slight improvement in the current THD values is observed compared to Point B, as Point A lies beneath the boundary of overmodulation. When the converter operates in Point C, the phase displacement angle is the lowest. If the switches are controlled together, the time period of the erroneous voltage pulses is the lowest in Point C, with respect to the other operating points. This results in a better current waveform quality compared to the other operating points when the same method is used. As the phase angle increases (Points D and E) the overmodulation duration increases resulting in increased current distortion in methods other than Mode-2.

Efficiency values for the four modulation and control techniques, when operated in Points A and B, are summarized in Table 3.5. Due to the higher harmonic content

Table 3.5: Efficiency Comparison

Modulation	Together	Independent	Mode-1	Mode-2
A efficiency %	93.74	95.55	95.24	94.05
B efficiency %	92.72	94.12	93.94	93.25

when the switches are controlled together, there is an efficiency drop in this method compared to the other ones. Generally, when the operating point is shifted from A to B (where B is above the boundary of overmodulation) the efficiency drops for all the four methods. This is as a result of Point A having a higher dc-link voltage and Point B having increased harmonic content in the first three methods. However, this is not relevant to Mode-2. It has a slightly lower efficiency because it involves reactive current injection and the current would be higher compared to the other methods. Nevertheless, it avoids overmodulation and, therefore, produces grid currents without low-frequency distortion.

3.6 Conclusion

In this chapter, current distortion produced in the Vienna rectifier around zero current crossings has been analyzed and a modulation and control method comprising two modes has been presented to reduce such distortion. Mode-1 consists of adding a proper zero sequence to the reference signal while maintaining UPF at the grid-side. However, overmodulation may be produced when operating with high modulation indices and large phase displacement angles. This problem can be avoided by activating Mode-2 where reactive power (calculated in real-time) is injected to obtain UPF at the converter terminals. Since there is no phase angle displacement between the converter reference voltages and the grid currents, the zero-crossing current distortion is avoided. An algorithm for transiting from one method to another has been presented. It makes use of a twin controller, which runs in parallel with the main controller, to check the peak of the reference signals and determine the operation mode that needs to be applied to the converter at any time.

It is concluded that Mode-1 is more suitable for low modulation index operation, while for high modulation indices Mode-2 is more convenient. When the two methods are combined, full control of the converter can be achieved, as if it was a T-type converter (with top and bottom switches instead of only diodes). Effectiveness of the

proposed methods has been demonstrated and verified in a hardware prototype.

Mode-2 is implemented for operating points where Mode-1 produces overmodulation. In Mode-2 a certain amount of reactive current is injected to force UPF operation at the converter side. Although Mode-2 avoids overmodulation, the amount of reactive power injected is significant and could be reduced. The next chapter further improves the method discussed, to reduce the injected reactive current.

Chapter 4

Hybrid Modulation Strategy for the Vienna Rectifier

In this chapter, a hybrid modulation strategy is introduced where a calculated minimal amount of reactive current depending on the operating conditions is injected to avoid overmodulation. The reduction of reactive current required compared to the state-of-the-art solutions is up to 100% in certain operating conditions. With the proposed method, the Vienna rectifier can operate in a wide range of power factors without compromising the quality of the source currents.

4.1 Introduction

In this chapter, the method proposed in Chapter 3 is further improved by using the special zero sequence and reactive power compensation (RPC) to create a hybrid modulation scheme that extends the operating range of the Vienna rectifier. The proposed method injects the minimum reactive current required, just enough to avoid overmodulation caused by the notches generated by the special zero sequence. The reduction in reactive current achieved compared to operating in Mode-2 is significant. This means the hybrid modulation and control method would achieve good current waveform quality and efficiency at the same time. It also uses the min-max zero sequence, instead of the sinusoidal third harmonic injection used in [87]. The major advantages of the proposed hybrid modulation are,

1. Wide power factor range of operation without compromising the quality of

source currents.

2. Operation with constraint-free modulation index.

3. Seamless transition between operating points.

4. Simple real-time reactive current calculation suitable to be implemented in a DSP.

Fig. 4.1 shows the reactive current demand analysis with respect to the modulation index of the converter and the phase displacement angle. The simulation uses a fixed source voltage and constant power. Therefore, the active current component would be constant, and the phase displacement angle is varied by changing the fundamental frequency of the source.

The main limiting factors in the methods discussed thus far are as follows. The zero sequence injection method, with UPF at the source side, offers the benefit of reduced low-frequency current distortion but restricts the modulation index range. Having UPF at the converter side resolves this issue, but increases the component ratings as it involves significant reactive power injection.

The chapter is organized as follows. Section 4.2 introduces the proposed hybrid modulation technique with the derivation of reactive current required, and an analysis on current waveform quality and efficiency. Section 4.3 focuses on the benefits of the proposed method supported with experimental validation. Finally, Section 4.4 summarizes the main conclusions.

Equation (3.9) in Chapter 3, provided the maximum modulation index that the

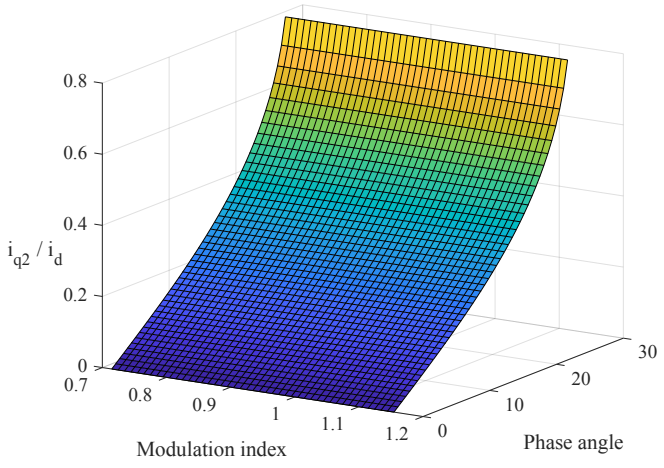

Figure 4.1: Reactive current injected to achieve UPF at the converter side.

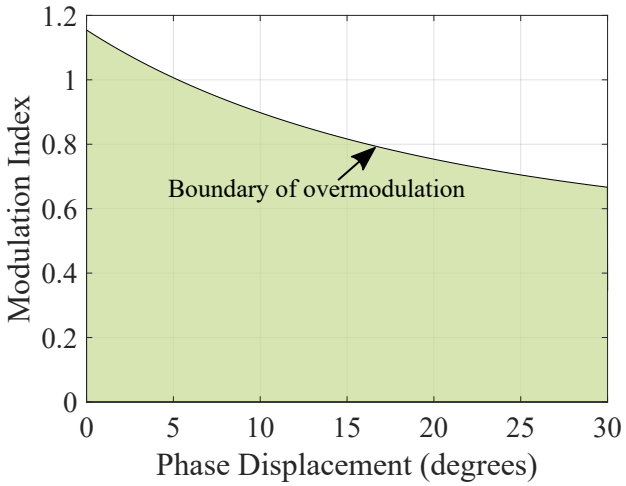

Figure 4.2: Modulation index restriction based on the phase displacement angle.

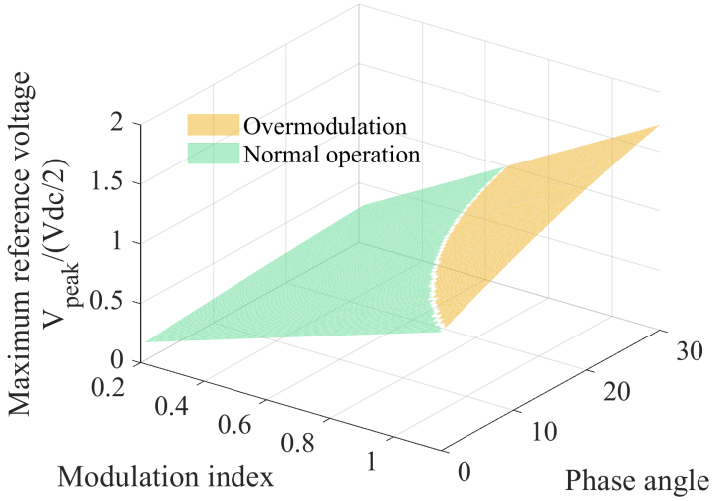

Figure 4.3: Maximum reference voltage when the zero sequence is injected without modulation index constrain.

Vienna rectifier can operate in Mode-1 without producing overmodulation and current distortion, as a function of the phase displacement angle between the voltage reference and the current. This condition is graphically illustrated in Fig. 4.2. If the condition is violated and the modulation index is unconstrained, as shown in Fig. 4.3, then the maximum reference voltage will exceed $v_{dc}/2$ and the converter will not be able to generate these voltages. If no action is taken, this will result in low-frequency distortion in the source currents. To avoid this problem, Mode-2 was introduced in Chapter 3, where a certain amount of reactive power is injected to force the converter to operate with UPF at the converter side.

4.2 Hybrid Modulation Strategy for the Vienna Rectifier

This Section introduces a combination of the above two methods, that uses only a fraction of the reactive current compared to the reactive power injection method (Mode-2), while avoiding overmodulation. If the converter is about to enter overmodulation due to the notches created by the special zero sequence, then a calculated minimum amount of reactive current depending on operating conditions will be injected to avoid overmodulation.

By considering the equality condition of (3.9), the angle just before overmodulation can be expressed as:

$$\sin(\frac{\pi}{6} + \phi_{lim}) = \frac{1}{\sqrt{3}m} \tag{4.1}$$

where ϕ_{lim} is defined as the critical phase displacement angle and can be obtained as follows.

By simplifying (4.1):

$$k \sec \phi_{lim} = 1 + \sqrt{3} \tan \phi_{lim} \tag{4.2}$$

where $k = \frac{2}{\sqrt{3}m}$, which leads to,

$$0 = 1 - k^2 + 2\sqrt{3} \tan \phi_{lim} + (3 - k^2) \tan^2 \phi_{lim} \tag{4.3}$$

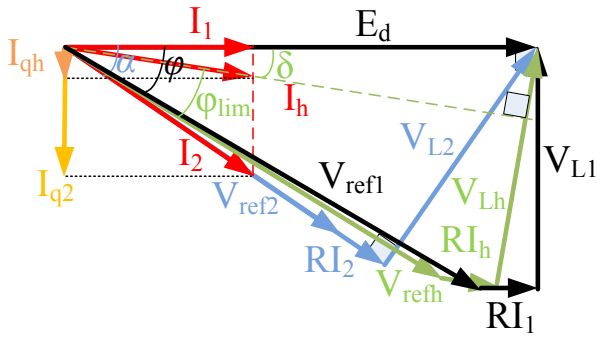

Figure 4.4: Phasor diagram for the Vienna rectifier when it is operating in different configurations: Black- UPF at the source, blue- UPF at the converter and green- UPF at the boundary of overmodulation.

By solving the quadratic equation and using the known $\phi_{lim} = 5.26$ degrees at $m = 1$:

$$\tan\phi_{lim} = \frac{-3\sqrt{3}m^2 + 2\sqrt{12m^2 - 4}}{9m^2 - 4} \tag{4.4}$$

Equation (4.4) provides the critical displacement angle as a function of the modulation index. The phase shift between the voltage at the converter terminals and the current should always be equal to or smaller than this critical displacement angle. Otherwise, the use of the special zero sequence voltage leads to overmodulation. The proposed hybrid modulation strategy injects the required fraction of reactive current so that the phase shift between voltage and current remains always below ϕ_{lim}. This operating condition is illustrated in Fig. 4.4. The hybrid current corresponds to I_h, and it has an angle ϕ_{lim} with the voltage at the converter terminals and δ with the source voltage. The steady state operation of this mode is represented by the polygon enclosed by the source voltage, voltage drop due to the series resistance in the inductor, converter reference voltage, voltage drop across inductor denoted by vectors $\mathbf{E_d}$, $\mathbf{RI_h}$, $\mathbf{V_{ref\text{-}h}}$ and $\mathbf{V_{L\text{-}h}}$, respectively. By making use of the properties of vector addition, the following equalities in the d and q axis are obtained:

$$E_d = v_{refh}\cos(\phi_{lim} + \delta) + RI_1 + \omega LI_{qh} \tag{4.5}$$

$$0 = v_{refh}\sin(\phi_{lim} + \delta) + RI_{qh} - \omega LI_1 \tag{4.6}$$

From (4.5)

$$v_{refh} = \frac{E_d - RI_1 - \omega LI_{qh}}{\cos(\phi_{lim} + \delta)} \tag{4.7}$$

and substituting v_{refh} in (4.6)

$$0 = \tan(\phi_{lim} + \delta)[E_d - RI_1 - \omega LI_{qh}] + RI_{qh} - \omega LI_1 \tag{4.8}$$

By using the sum identity for the tangent

$$\tan(\phi_{lim} + \delta) = \frac{\tan(\phi_{lim}) + \tan(\delta)}{1 - \tan(\phi_{lim})\tan(\delta)} \tag{4.9}$$

and considering

$$\tan(\delta) = \frac{I_{qh}}{I_1} \tag{4.10}$$

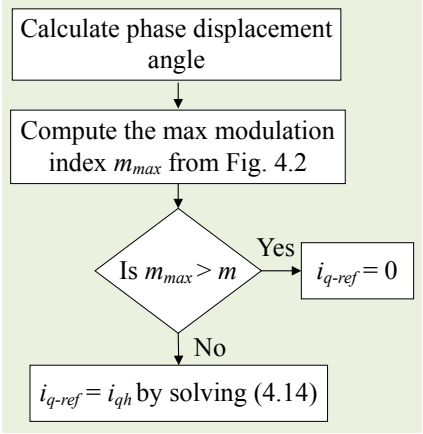

Figure 4.5: Flowchart of the reactive current reference (i_{q-ref}) calculator.

equation (4.9) can be simplified as

$$\tan(\phi_{lim} + \delta) = \frac{I_1 \tan(\phi_{lim}) + I_{qh}}{I_1 - I_{qh} \tan(\phi_{lim})}. \tag{4.11}$$

By substituting (4.11) in (4.8)

$$0 = [E_d - RI_1 - \omega L I_{qh}][I_1 \tan(\phi_{lim}) + I_{qh}] + [I_1 - I_{qh} \tan(\phi_{lim})][RI_{qh} - \omega L I_1] \tag{4.12}$$

which can be further simplified as

$$0 = (E_d - RI_1) I_1 \tan(\phi_{lim}) - \omega L I_1^2 + E_d I_{qh} - (R \tan(\phi_{lim}) + \omega L) I_{qh}^2 \tag{4.13}$$

Solving the resulting quadratic equation and neglecting the series resistance, the critical reactive current just enough to avoid overmodulation can be calculated as

$$I_{qh} = \frac{E_d}{2\omega L} \left[1 - \sqrt{1 - \left(\frac{2\omega L I_1}{E_d} \right)^2 + v_\beta} \right] \tag{4.14}$$

where $v_\beta = 4\omega L I_1 \tan(\phi_{lim})/E_d$. Note that the reactive current required to avoid overmodulation, which is given by (4.14), uses instantaneous variables that are readily available in the controller.

For lower phase displacement angles and lower modulation indices, the required reactive current is zero, since the zero sequence alone can handle the distortion compensation because there is no risk of overmodulation. The flow chart in Fig. 4.5 details the algorithm used for deciding when to use the reactive current. From the

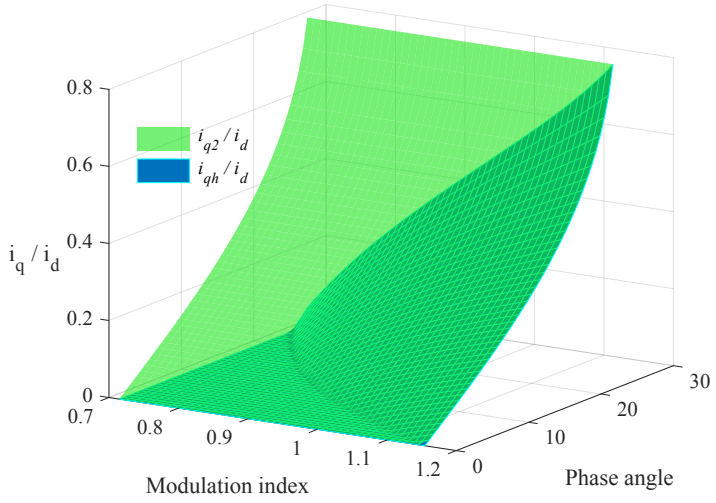

Figure 4.6: Comparison of reactive current injection with UPF at the converter side and the proposed hybrid modulation strategy.

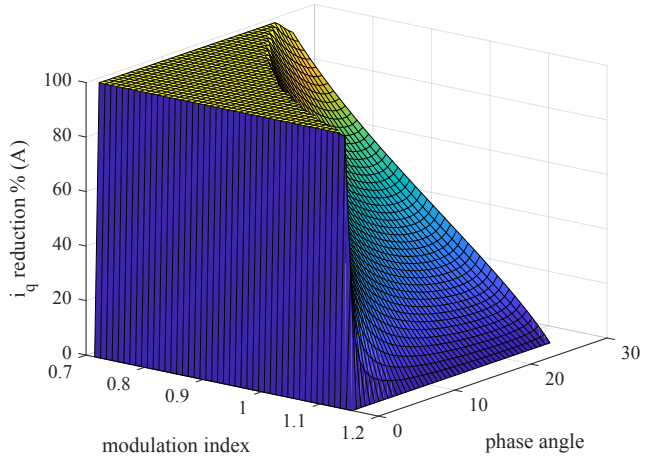

Figure 4.7: Reduction in the reactive current requirement to avoid overmodulation when the proposed method is used.

available measurements in the controller, the phase displacement angle and the corresponding maximum allowable modulation index (m_{max}) are calculated, as represented in Fig. 4.2. If m_{max} is greater than the modulation index, then there is no need for reactive power compensation as no distortion is caused by the zero sequence. However, if the modulation index of the converter is greater than m_{max}, then i_{qh} should be injected by solving (4.14) as the required reactive current. Fig. 4.6 depicts the reactive current requirement for the hybrid operation for different modulation indices and phase displacement angles. As expected, the converter needs more reactive cur-

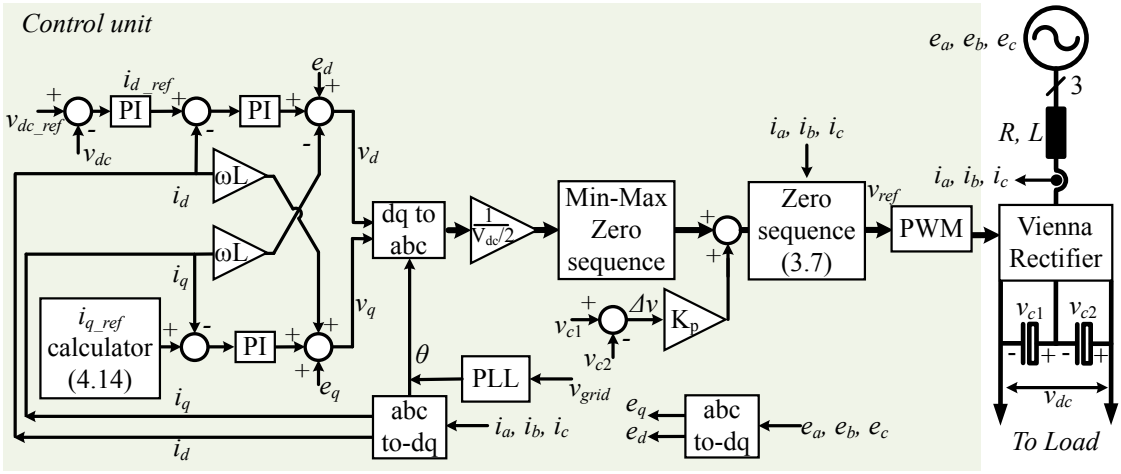

Figure 4.8: VOC with the zero sequence injection for the Vienna rectifier with the hybrid modulation.

rent when the phase displacement angle and modulation index increase, and follows the boundary line shown in Fig. 4.2. As Fig. 4.6 shows, the required reactive current is much less compared to Mode-2, as depicted in Fig. 4.1. The reduction in reactive current is shown in Fig. 4.7.

Fig. 4.8 illustrates the implementation of the proposed control for the Vienna rectifier. The reference voltage that comes out of the VOC, is injected with the zero sequence voltage provided by (3.7). The i_{q-ref} calculator block solves (4.14) and runs the algorithm in Fig. 4.5 giving the controller the magnitude of the reactive current reference and when to inject the reactive current.

Fig. 4.9 shows the main waveforms of the hybrid modulation method. It achieves similar current waveform quality as with Mode-2, but with only injecting a fraction of the reactive current. For the operating point given in Table 3.1, the reactive current requirement is reduced from 1.04A to 0.27A.

Fig. 4.10 illustrates the modulation index restriction removed by the proposed hybrid modulation and control scheme. Now the converter can operate with high phase displacement angles without current distortion, even at higher modulation indices. In the RPC region, the i_{q-ref} calculator determines the correct amount of reactive current just enough to avoid overmodulation. When these three modulation and control methods are used the current THD variation is illustrated in Fig. 4.11. As it shows, the first method produces higher distortion in the current waveform when the phase displacement increases.

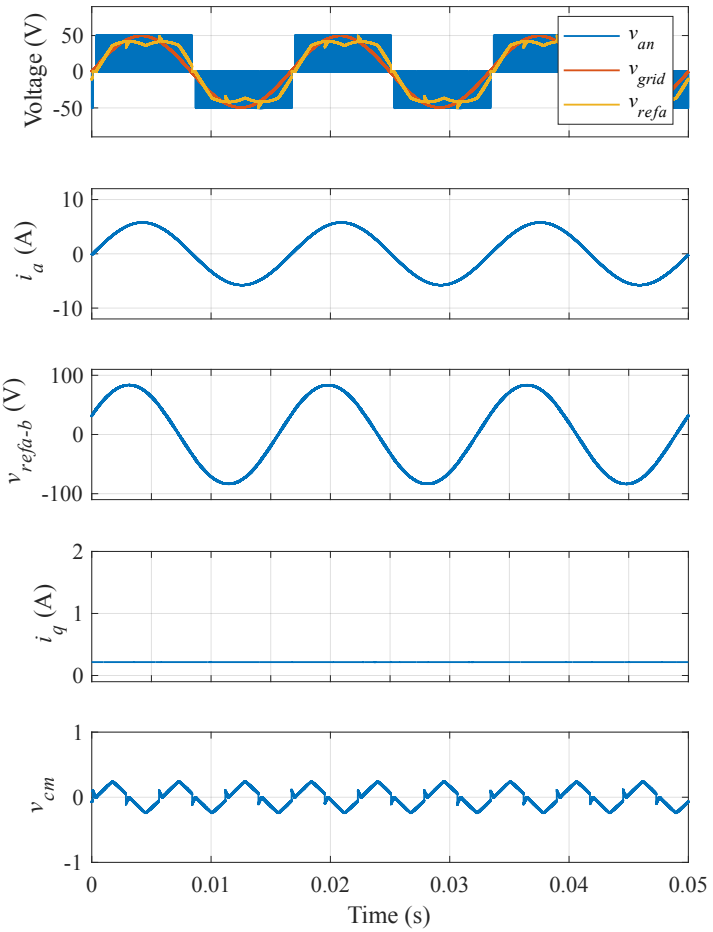

Figure 4.9: Main waveforms when the hybrid modulation is used in the Vienna rectifier.

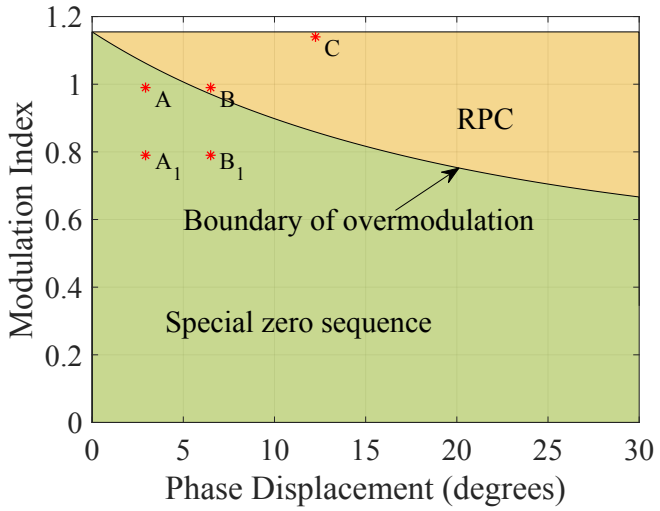

Figure 4.10: Modulation index restriction based on the phase displacement angle solved by the proposed modulation and control strategy.

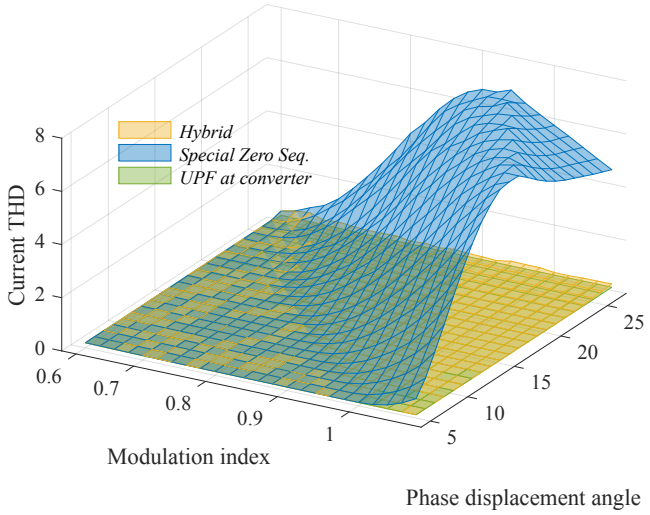

Figure 4.11: Current THD variation when different modulation and control methods are used in the Vienna rectifier.

The efficiency values are obtained using PLECS thermal models throughout the operating range of the Vienna rectifier when the hybrid modulation method is used as opposed to operating with Mode-2. 70° C ambient temperature and 0.1° C/W case to ambient thermal resistance are assumed for the analysis.

The conduction power loss normalized by the output power when the hybrid modulation method and Mode-2 are used, is illustrated in Fig. 4.12. As the modulation index reduces because the dc-side voltage increases, conduction loss reduces for both methods. However, in Mode-2, the reduction in loss is less compared to the hybrid modulation, as more reactive current is involved. As the phase displacement

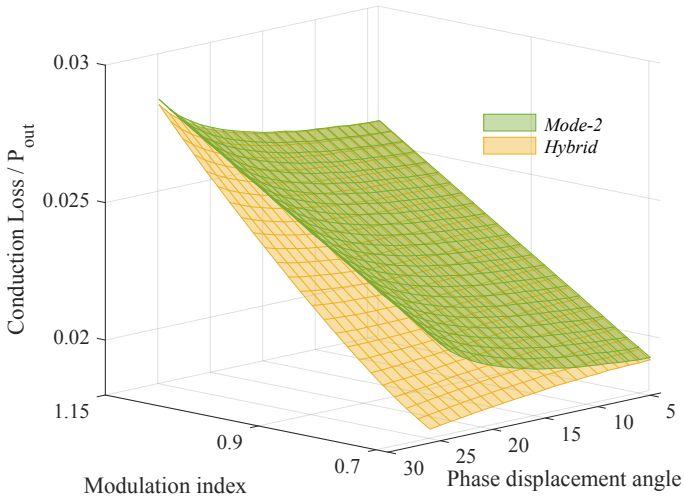

Figure 4.12: Conduction loss of the Vienna rectifier for different operating points.

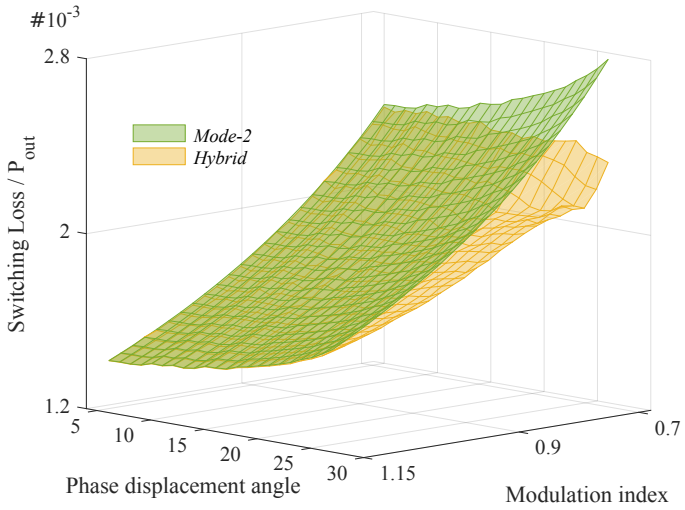

Figure 4.13: Switching loss of the Vienna rectifier for different operating points.

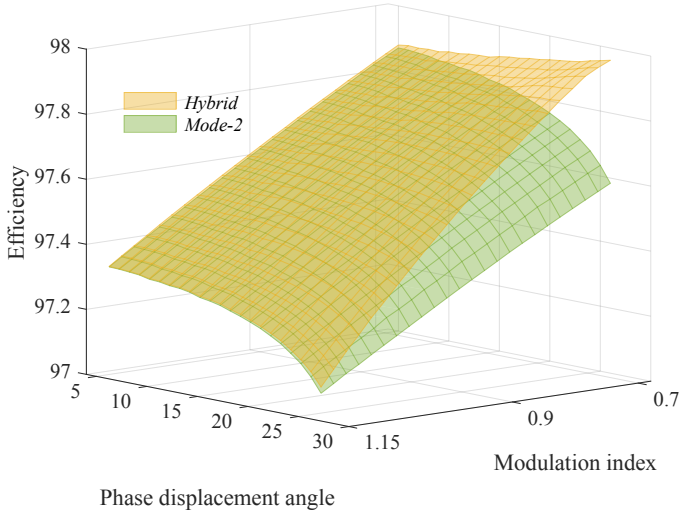

Figure 4.14: Efficiency at different operating conditions.

increases, the conduction loss increases in both cases, but more in Mode-2 for the aforementioned reason.

Fig. 4.13 depicts the switching loss representation. When the modulation index reduces as the dc-side voltage increases, in both cases the switching loss increases, but it is more significant in Mode-2 (as the current amplitude is more in Mode-2). At higher phase displacement angles, the current amplitude difference will be more in the two methods and it is reflected in the switching loss. Furthermore, as the neutral point clamping time increases, the number of switching transitions will be lower in the hybrid modulation compared to Mode-2, thus showing lower switching losses for larger phase displacement angles, more noticeably in low modulation indices.

As Fig. 4.14 illustrates, the proposed hybrid method has better efficiency throughout the operating region. When the modulation index is the maximum ($m = 1.15$), operating at UPF at the converter side and the hybrid method become identical, as both methods inject the same amount of reactive current. In summary, the hybrid method has better efficiency compared to Mode-2, particularly when the modulation index is lower. This is because the reactive current requirement is much lower in the hybrid method compared to Mode-2, as shown in Fig. 4.7.

4.3 Experimental Results

Five operating points designed as A, A_1, B, B_1 and C, as listed in Table 4.1 with their locations as marked in Fig. 4.10, have been considered for the experiment. The operating points represent both regions; the green region where overmodulation does not happen, and the orange region where the converter enters into overmodulation unless a special action is taken. The fundamental frequency of the voltage source is adjusted according to Table 4.1 in order to reach the different operating points. The corresponding waveforms when the Vienna rectifier is operating in these operating points are illustrated in Fig. 4.15 with the current spectrum in each case depicted in Fig. 4.16. The operating points are selected such that A, B, and C will be above the boundary of overmodulation (the orange zone in Fig. 4.10) where reactive current injection is needed to operate the converter without overmodulation. As Points A, A_1 and B_1 lie beneath the boundary of overmodulation (green zone in Fig. 4.10), the converter does not require any reactive power compensation because the notch created by the special zero sequence is less than half the dc-link voltage. The zero sequence calculation from the measurements and the reactive current calculation using the real-time values should be executed within the 20μs time interval in the DSP. With the DSP running at 200MHz clock frequency, the PWM interrupt service routine (ISR) that executes the proposed hybrid modulation only needs an execution time of 9.26μs, which is a marginal increase compared to the other two methods discussed. A summary of the ISR execution times is listed in Table 4.2.

Table 4.1: Operating Points in the Experiment

Operating point	A	A_1	B	B_1	C
Load Resistor (Ω)	44	44	21	44	21
Fundamental frequency (Hz)	60	30	60	60	120
Phase displacement (degrees)	2.9	2.9	6.2	6.2	12.25
Modulation index	1.14	0.79	1.14	0.79	1.14

Table 4.2: Execution Times with Different Control Techniques

Modulation	Mode-1	Mode-2	Hybrid
ISR execution time (μs)	8	8.85	9.26

4.3.1 Wider Range of Operation with Less Reactive Current

When the Vienna rectifier is operating with Mode-1, the current harmonic distortion is generally higher compared to the other two methods. This is illustrated in Figs. 4.15(a), (d), (g), (j) and (m) corresponding to Points A, A_1, B, B_1 and C, respectively. When the rectifier is operating in the orange zone, as the phase displacement angle between the current and the reference voltage increases, the current distortion is higher in this method due to the increase of overmodulation period. This is reflected in V_{an} in Fig. 4.15(m), corresponding to Point C, which has the highest phase displacement with maximum modulation index and it has the worst current quality in the study. When the Vienna rectifier operates with UPF at its terminals with the help of calculated reactive current, the current waveform quality improves, but at the cost of higher current rating. This is due to the additional reactive current component. This operating mode is illustrated in Figs. 4.15(b), (e), (h), (k) and (n) corresponding to Points A, A_1, B, B_1 and C, respectively.

The main waveforms from the proposed hybrid modulation method are depicted in Figs. 4.15(c), (f), (i), (l) and (o) corresponding to Points A, A_1, B, B_1 and C, respectively. The hybrid method shows similar performance to the UPF at the source with zero sequence method for operating points which are under the boundary of overmodulation (Points A, A_1 and B_1). This is because there is no overmodulation at these points, hence no reactive current is required. However, for the operating points above the boundary of overmodulation (B and C), the proposed hybrid modulation has superior current waveform quality (Fig. 4.16) when compared with UPF at the source with the special zero sequence, and the results are consistent throughout the

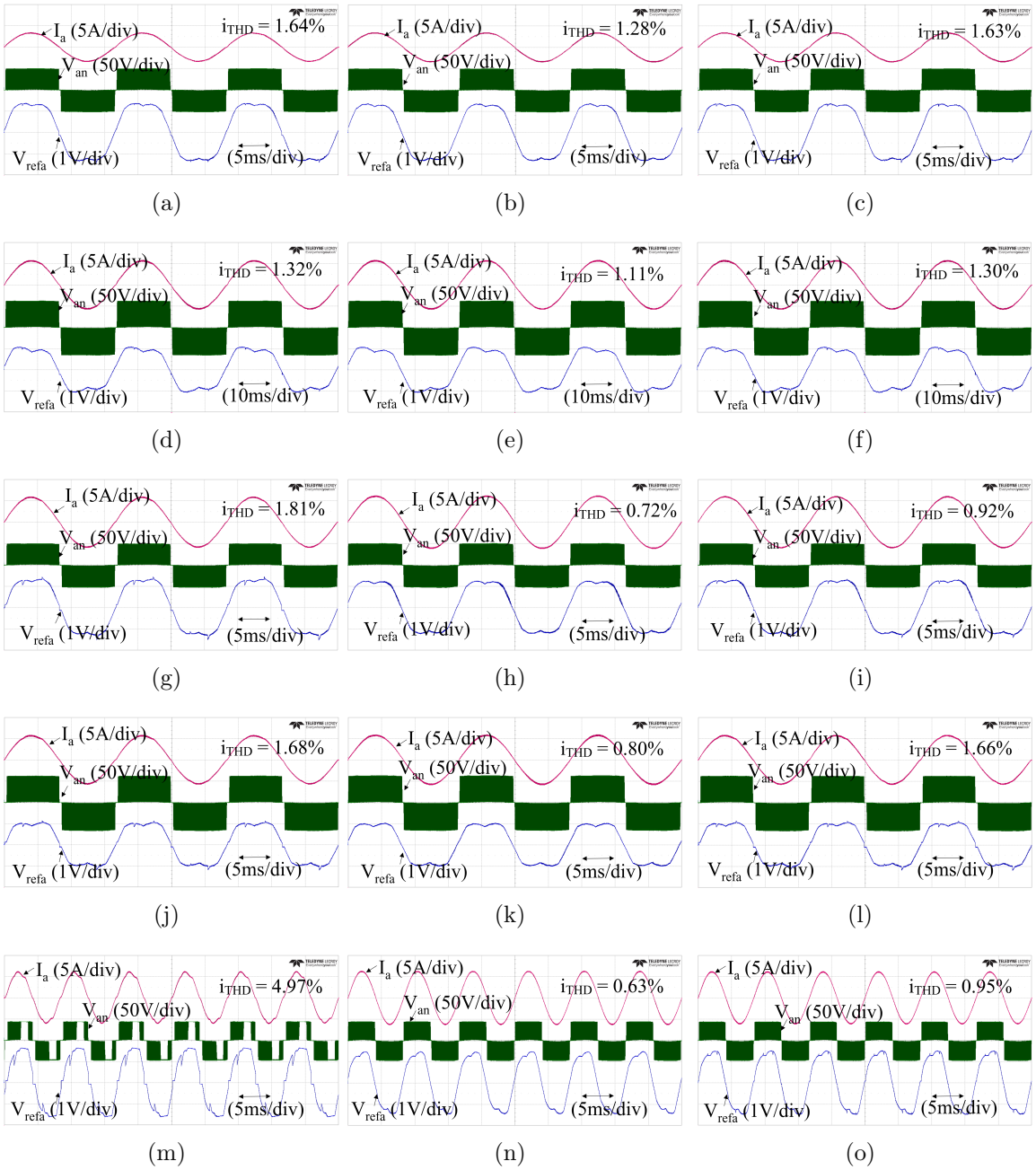

Figure 4.15: Experimental results with different modulation and control techniques, operating Point A (60Hz): (a) Mode-1, (b) Mode-2 and (c) hybrid modulation. Operating Point A_1 (30Hz): (d) Mode-1, (e) Mode-2 and (f) hybrid modulation. Operating Point B (60Hz): (g) Mode-1, (h) Mode-2 and (i) hybrid modulation. Operating Point B_1 (60Hz): (j) Mode-1, (k) Mode-2 and (l) hybrid modulation. Operating Point C (120Hz): (m) Mode-1, (n) Mode-2 and (o) hybrid modulation.

operating points. This can be achieved by a fraction of the reactive current required in the second method where the UPF is kept at the converter terminals. The reduction in reactive current for the five operating points in the experiment are summarized in Table 4.3.

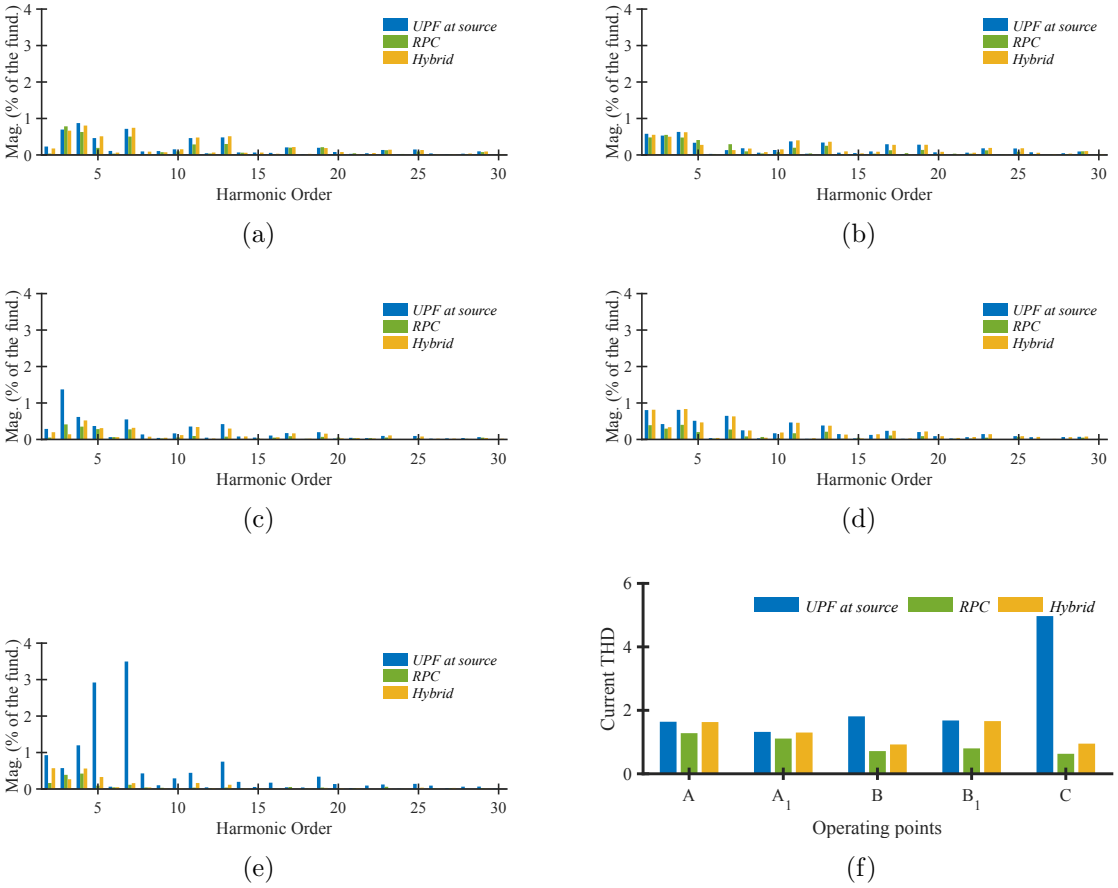

Figure 4.16: Experimental current spectrum from different operating points: (a) Point A, (b) Point A_1, (c) Point B, (d) Point B_1, (e) Point C and (f) summary of current THD.

Table 4.3: Reduction in Reactive Current when the Proposed Hybrid Modulation is Used Replacing Mode-2

Operating Point	i_{q2} (A)	i_{qh} (A)	% reduction in i_q
A	0.26	0	100
A_1	0.26	0	100
B	0.95	0.22	77
B_1	1.42	0	100
C	1.42	1.24	13

When the rectifier is operating at Point B with Mode-1, it will work in overmodulation. This is reflected in the increased current THD, as shown in Fig. 4.16(f). The improvement in the current waveform quality is evident from the reduced current THD, in UPF at converter and hybrid schemes. Regarding the efficiency, the hybrid modulation exhibits the best one. This makes sense as compared with the second method, since it uses less reactive current. The slight reduction of the efficiency observed for the first method is due to the higher harmonic content that produces extra

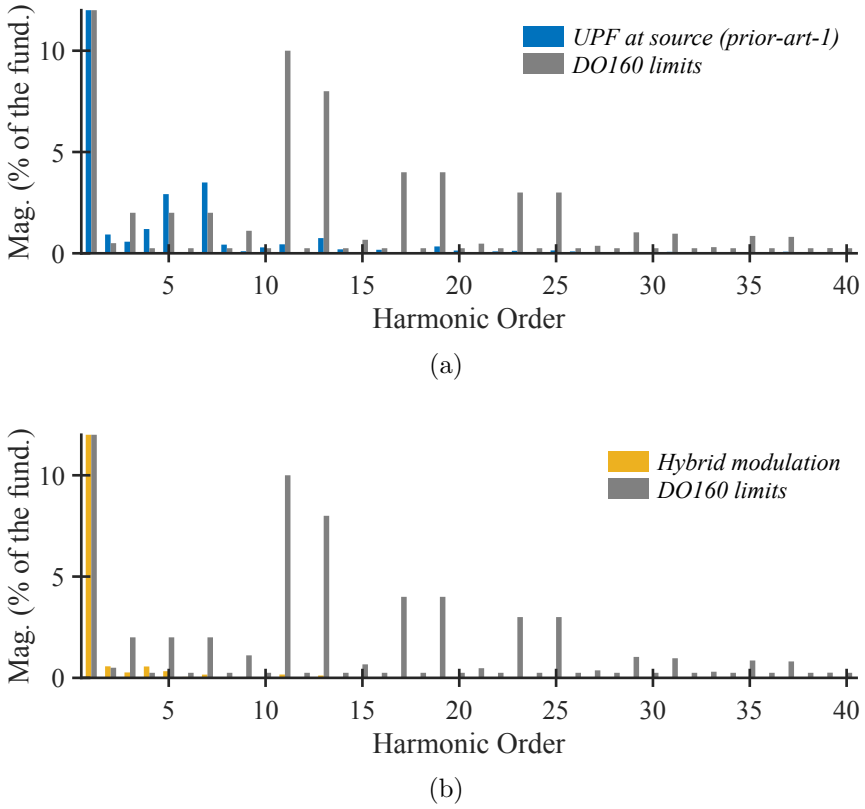

Figure 4.17: Vienna rectifier tested to comply with DO160 Aerospace Standard at Point C: (a) With Mode-1 and (b) with hybrid modulation.

losses. Therefore, these results show that the hybrid modulation scheme produces low current THD values and exhibits the best efficiency among the methods discussed.

Generator-connected rectifier in more electric aircraft is a potential application for the Vienna rectifier. The converters used in aerospace applications should guarantee current waveform quality specified by DO-160 standard, throughout its operating range, as discussed in Chapter 2. If Mode-1 is applied to the Vienna rectifier and proper action is not taken in certain operating points, overmodulation would occur deteriorating the current waveform quality.

Fig. 4.17(a) illustrates a comparison of harmonics against the DO-160 standard limits when the Vienna rectifier is operating in Point C, with UPF at the source side injecting the zero sequence to clamp the switches and without any reactive current (Mode-1). As the figure shows, there is a clear violation of the standard for the 5^{th} and 7^{th} harmonics when operated with this method. On the other hand, when the proposed hybrid modulation method is applied for the same operating point, as illustrated in Fig. 4.17(b), the converter operates with improved current waveform

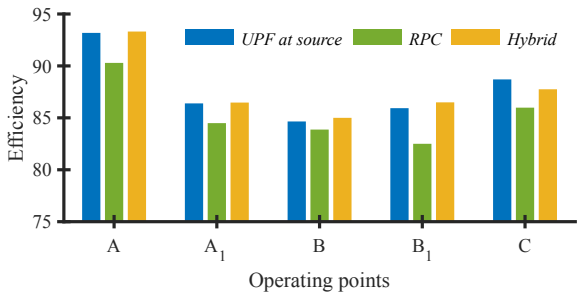

Figure 4.18: Efficiency of the Vienna rectifier setup at different operating points.

quality and within the regulation limits.

Therefore, these results demonstrate that the hybrid modulation scheme produces low current THD values and exhibits the best current waveform quality among the methods discussed, using the minimum reactive current.

4.3.2 Efficiency Analysis

Fig. 4.18 illustrates an efficiency analysis performed for the Vienna rectifier with the three methods discussed, using the experimental setup for the operating points listed in Fig. 4.10.

In the experiment, the points A, A_1, B_1 will have similar losses for the hybrid method and operating with UPF at the source side, i.e., Mode-1. In these points, the hybrid method does not use any reactive power as the points are below the boundary of overmodulation.

On the other hand, Point B is above the boundary of overmodulation, which means if the Vienna rectifier is controlled by Mode-1, it would create overmodulation. This is reflected in the increased current THD, as shown in Fig. 4.16(f). In this case, when the converter operates in Mode-1 the phase displacement between the current and the reference voltage would be 6.2 degrees. When the hybrid modulation is used, the angle will be reduced to 5.26 degrees, which is the critical angle for Point B (calculated by solving (4.4)). This is done by injecting 0.22A of reactive current. The experimental results show that the hybrid modulation has better performance compared to Mode-1 even though it injects the above reactive current. This is because when Mode-1 is used, the converter operates in overmodulation and the higher harmonic content produces extra losses. However, when Mode-2 is used, this phase displacement angle is made zero by injecting 0.95A of reactive current, and hence it has the lowest

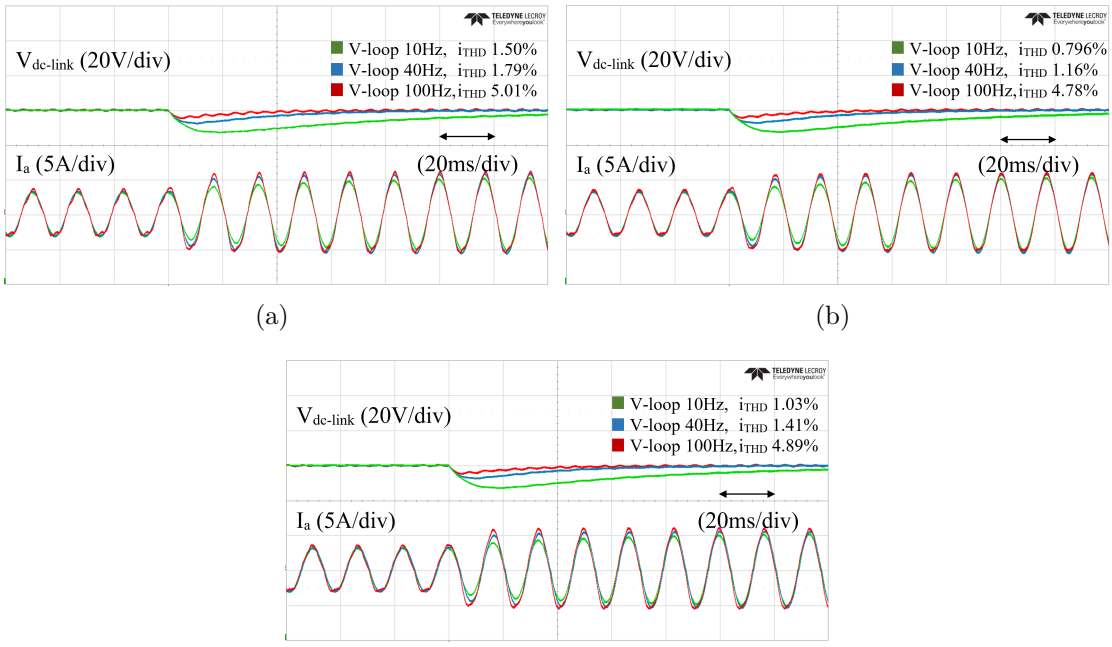

Figure 4.19: Effect of the voltage loop bandwidth on the current waveform quality under different modulation and control techniques: (a) Mode-1 [24], (b) Mode-2 and (c) hybrid modulation scheme.

efficiency for Point B.

Since Point C operates with a modulation index $m = 1.14$, when the converter operates with the hybrid modulation, the reactive current injected is 1.24A, which is lower than the reactive current used in Mode-2 (1.42A). Therefore, when the converter is operating at Point C, the hybrid modulation shows higher efficiency, compared to Mode-2. However, in this operating point, Mode-1 would perform better even with overmodulation because the reactive currents in the other two methods are significant. Overall, the hybrid modulation has better efficiency than Mode-2, and equal or less efficiency compared to Mode-1, depending on the operating point.

4.3.3 Transient Response

Selection of the voltage loop bandwidth in the VOC is important in this application, and it would be a trade-off between the current THD and the transient response. For the experiments illustrated in Fig. 4.15, a 10Hz voltage control loop bandwidth is selected. The experiment is repeated with different voltage loop bandwidths in the VOC under the three different modulation and control methods discussed in this chapter, which are summarized in Fig. 4.19. In all three methods, slower voltage

loop yields better line current quality. The improvement in current waveform quality is better when the converter operates with Mode-2, however at the cost of increased component rating. The proposed hybrid method generates good current waveform quality, with less reactive current requirement.

4.3.4 Seamless Transition

The proposed hybrid modulation does not inject any reactive current unless there is overmodulation, caused by the special zero sequence. If reactive current is required, (4.14) provides the exact reactive current value and the transition between operating points would be seamless, unlike the solution that forces the converter to operate with UPF at the converter terminals (Mode-2).

Fig. 4.20 depicts the main waveforms when the operating point is shifted from Point A to B. According to Fig. 4.20(a), when the converter operates in Point A, Mode-1 does not create any overmodulation. However, when the operating point is shifted to Point B, if no special action is taken, the current waveform will be distorted due to overmodulation. This is evident when the current THD values (operating Point

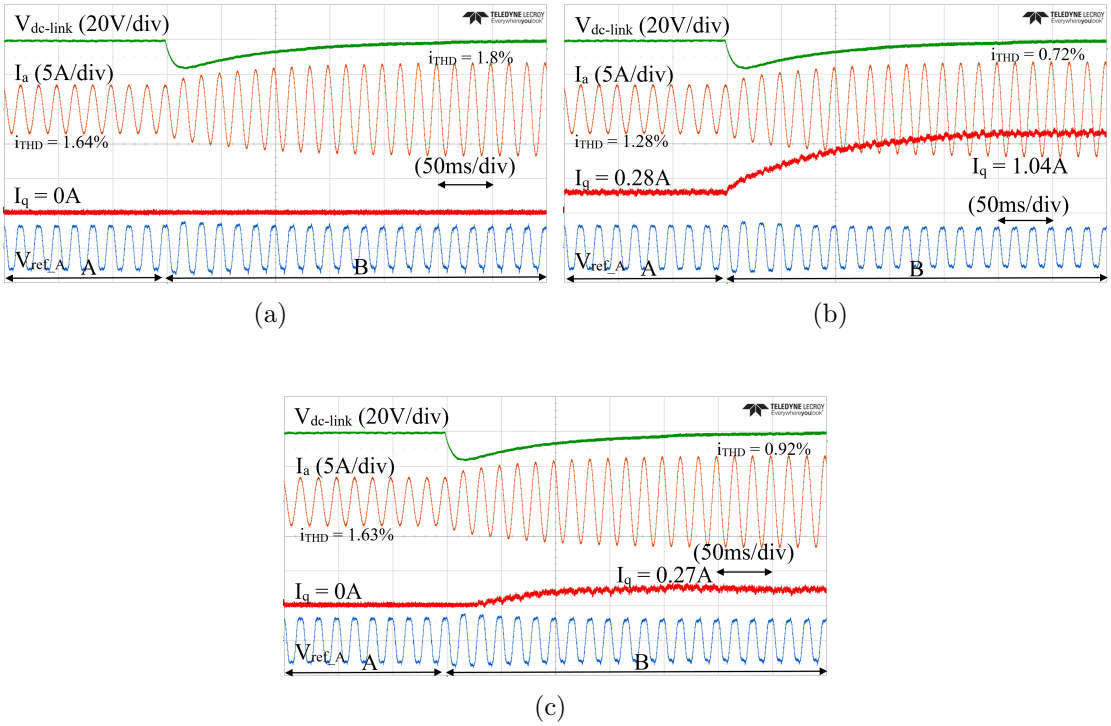

Figure 4.20: Seamless transition between operating points: (a) Mode-1, (b) Mode-2 and (c) with the hybrid modulation.

B) in Fig. 4.20(a) are compared with those in Fig. 4.20(b), the latter being corrected with Mode-2. In Fig. 4.20(c), the step change in the reactive current is less when hybrid modulation is used, compared to Mode-2 (Fig. 4.20(b)) and the transition happens smoothly.

4.4 Conclusion

In this chapter, the current distortion produced in the Vienna rectifier around zero current crossings has been analyzed, and a hybrid modulation method has been presented to reduce such distortion. The method consists of adding a special zero sequence to the reference signal while maintaining UPF at the source-side. However, overmodulation may be produced when operating with high modulation indices and large phase displacement angles. This problem can be avoided by injecting a calculated amount of reactive current in real-time just to avoid the overmodulation created by the notches introduced by the special zero sequence. By using the proposed method, low-frequency distortion due to the current zero crossings can be avoided without restricting the modulation index and with a minimal amount of reactive current. The study on efficiency shows clear improvements agreeing with the reactive current savings achieved by the hybrid modulation and control. Furthermore, the effect of the voltage control loop bandwidth that regulates the dc-link on the current waveform quality is demonstrated. When the operating point is shifted, the transients are smooth as the reactive current step is small.

When the proposed hybrid modulation is used, full control of the converter can be achieved, as if it was a T-type converter (with top and bottom switches instead of only diodes). The proposed method can also be used for variable source voltages such as those generated from a variable-speed permanent magnet synchronous generator. Effectiveness of the proposed methods has been demonstrated and verified by a hardware prototype.

Chapter 5

Generator-Fed Vienna Rectifier

In this chapter, the Vienna rectifier is connected to a generator, and various challenges associated with this application are discussed, including the operation with variable frequency. Also, some types of generators are compared for future MEA, and the permanent magnet synchronous generator (PMSG) is selected for the experiments, considering its advantages (high efficiency and power density). The target is to adapt the modulation and control strategies described in Chapters 3 and 4 to the case of the generator instead of a strong grid with fixed frequency.

5.1 Introduction

The benefits of the Vienna rectifier make it a suitable candidate for front-end rectification in transportation electrification applications. Permanent magnet synchronous generators (PMSGs) are becoming popular due to the high power density and high efficiency they offer over wound-rotor synchronous, induction and switched reluctance machines. PMSGs are becoming widely used in transportation applications, including aircraft applications [5].

5.1.1 A Comparison of MEA Generators

A review on aerospace electrical power generation is done in [5, 88]. For the MEA, electrical machines with brushes or commutators are not considered as they require frequent maintenance and have reliability issues [88]. Currently, three-stage wound-rotor generators [5, 89] and PMSGs are used in aircraft operating with variable fre-

quency. However, PMSGs are favored over the wound-rotor synchronous generators due to their higher power density [5]. For different reasons, the feasible candidates for future MEA power generators are the PMSG, induction generator (IG) and switched reluctance generator (SRG) [5, 88].

IGs are popular due to their low cost, high reliability, minimum maintenance, and ruggedness in harsh operating conditions. The disadvantages are low power density, large size and low efficiency. In [90], the Vienna rectifier is driven by an IG in a wind energy conversion system. It shows that the Vienna rectifier is more efficient than the classical two-level converter, when they are connected to an IG. An LC filter is connected between the IG and the converter, as the Vienna rectifier cannot supply enough reactive power to the machine, and the IG is self-excited using the delta connected capacitor. Since a single capacitance level cannot guarantee the angle constraint for the entire speed range, a switched capacitor bank is proposed.

The advantages of the SRG are robustness, intrinsic fault tolerance, and potential use in harsh environments. The thermal and mechanical properties are superior to the other two types of generators discussed in this section as it is capable of withstanding high mechanical and thermal stress. This is due to the absence of winding or permanent magnet (PM) in the rotor. But it suffers from lower power density, high torque ripple, loud noise and low efficiency.

PMSGs can be broadly classified into two types based on the rotor construction; surface mounted PM (SPM) and interior PM (IPM). In the IPM generators, the reluctance along the d-axis is higher than in the q-axis resulting in $L_d < L_q$, due to the saliency. On the other hand, SPM machines have similar values for L_d and L_q. The main advantages of PMSGs are high power density and efficiency, which are both very important for aircraft applications. But it has the disadvantages of demagnetization at high temperatures and higher cost due to the use of rare earth materials for the PMs. In [66], the Vienna rectifier is interfaced to a PMSG using direct torque control (DTC). A predictive control approach is implemented in a Vienna rectifier application interacting with a PMSG in [91, 92].

The performance criteria comparison among the three generator types is summarized in Table 5.1 [88].

Table 5.1: Comparison of Generator Types

Performance criteria	IG	SRG	PMSG
Fault tolerance	Low	High	High
Power density	Moderate	Moderate	High
Robustness	Yes	Yes	No
Efficiency	Moderate	High	High
Cost	Low	Low	High
Acoustic noise	No	Moderate	Low

Table 5.2: Generator Parameters

Description	Specification
Stator Inductance (uH)	30, 45, 60
Back EMF constant (V_{peak}l-l/krpm)	108.87
Pole pairs	8
Nominal rms current (A)	500
Fault current (p.u.)	2.50, 1.67, 1.25

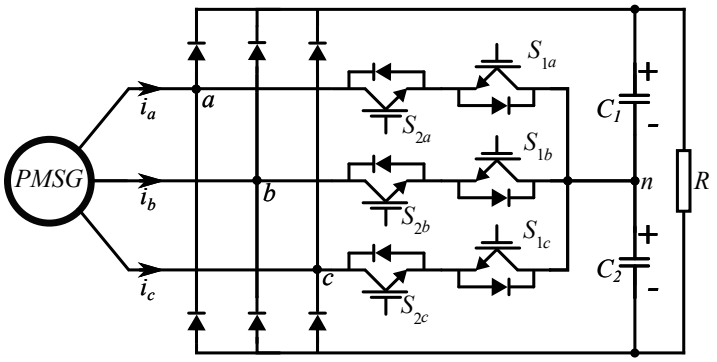

Figure 5.1: PMSG-fed Vienna rectifier.

5.1.2 Challenges in Generator-fed Vienna Rectifier

Fig. 5.1 illustrates a PMSG-fed Vienna rectifier where the stator windings perform as boosting inductors [93], and no additional inductors are used in this generator-connected application. Three candidate surface PMSGs are considered with the machine parameters listed in Table 5.2 for the analysis. The difference among the three generators is their stator inductance. With increased fundamental frequency (as high as 800Hz in aerospace applications), the phase displacement angle would increase creating more distortion in input currents at high engine speeds. Apart from that, with the variable speed of the generator shaft, the back electromotive force (EMF) is a function of the rotor speed. To increase the speed range of the generator, flux weakening is an option, which is performed by reactive power injection to the stator

circuit [89], given the fact that the Vienna rectifier is a two-quadrant converter and it could operate within the $\{-\frac{\pi}{6} +\frac{\pi}{6}\}$ phase region. With a careful design, the generator can operate at high speeds while the Vienna rectifier draws sinusoidal currents and provides a constant voltage dc-link that feeds critical loads.

As discussed earlier, when the Vienna rectifier is operating with a certain phase displacement angle, it creates distortion at the current zero crossings. This will be a problem in variable speed applications, as shown later using simulations, and it is addressed by using the hybrid modulation discussed in Chapter 4. Nevertheless, the phase displacement should be less than $\pi/6$ as it is a topological limit in the Vienna rectifier.

When the rectifier was connected to the grid, the grid voltages were measured to extract the voltage vector angle by a PLL in order to synchronize the rectifier with the grid. However, when the rectifier is connected to a generator, because the machine stator winding is used as boost inductances in this particular application, measuring the source voltage (back EMF) would not be possible. Using the converter terminal voltages is problematic because it contains PWM switching waveforms. Instead, the generator rotor angle could be measured and used for the estimation of the back EMF voltages. The next section discusses additional challenges when the rectifier is connected to the generator;

1. In the previous chapters, VOC method was used, with the controller parameters of the PI loops tuned to a specific operating point. However, in the generator-fed Vienna rectifier application, the frequency would change as a result of the engine speed changing depending on the phase of the flight. For this thesis, it is assumed that the engine speed can vary in the range 3000 rpm - 6000 rpm, and the fundamental frequency of the stator back EMF will be within the interval 400-800Hz. Thus, the controller should be able to work with this varying fundamental frequency.

2. Despite being a two-quadrant converter, as the Vienna rectifier has the phase angle restriction of $\{-\frac{\pi}{6} +\frac{\pi}{6}\}$, it would be convenient to operate with lower inductances such that even at higher fundamental frequencies the rectifier would operate without having any restrictions. However, the inductance values depend on the generator design. Besides, if low inductances could be achieved, this would result in high fault currents, and aerospace applications require lower fault currents.

3. With the variable speed of the generator shaft, frequency and back EMF are a

function of the rotor speed. Consequently, the EMI filter should be designed to work with a range of fundamental frequencies, instead of a fixed frequency. However, this is not discussed in this chapter as it is beyond the scope of this thesis.

5.2 Application of Hybrid Modulation and Control to the Generator-fed Vienna Rectifier

5.2.1 PMSG-fed Vienna Rectifier Modeling

Fig. 5.2 depicts a single-phase equivalent circuit of a PMSG and its phasor diagram when the generator is connected to a Vienna rectifier system with a resistive load. The armature reaction effects and the self-inductance in the generator are represented by the series reactance X_s. The winding resistance R_s is neglected for simplicity (since $X_s \gg R_s$). E_x and V_x are the internally generated voltage (back EMF) and the generator terminal voltage, respectively. The angle between E_x and V_x is the torque angle δ.

In this dissertation, the grid-connected system had i_d associated with active current and i_q with reactive current, as the direct axis (d-axis) was aligned with the voltage vector. However, in generator-connected systems the d-axis is usually aligned with the rotor flux position, hence the d-axis accounts for the reactive component and quadrature axis (q-axis) for the active component. By using the aforementioned convention for the PMSG and the amplitude conservative dq transform, the following

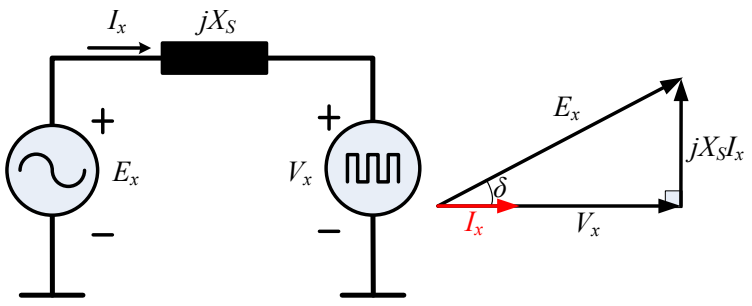

Figure 5.2: Simplified single phase circuit of PMSG-fed Vienna rectifier and phasor diagram at unity power factor operation.

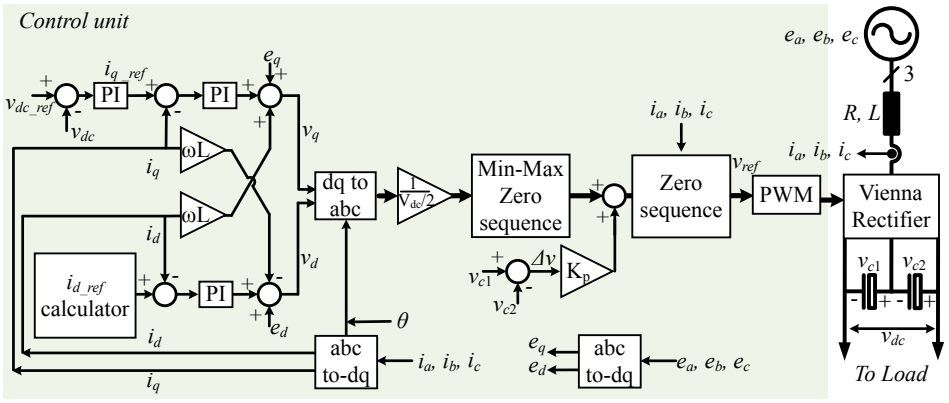

Figure 5.3: Field-oriented control of the generator-fed Vienna rectifier with hybrid modulation.

can be obtained [66, 89]:

$$v_d = R_s i_d + L_d \frac{di_d}{dt} - \omega_{re} L_q i_q \tag{5.1}$$

$$v_q = R_s i_q + L_q \frac{di_q}{dt} + \omega_{re} L_d i_d + \omega_{re} \psi_r \tag{5.2}$$

where v_d, v_q, i_d, and i_q, are the d-axis and q-axis components of the PMSG output voltage and current components, R_s, L_d and L_q are the stator resistance and dq transformed stator inductances, ω_r is the mechanical speed, ω_{re} is the electrical rotor speed ($\omega_{re} = p\omega_r$), ψ_r is the PM flux and p is the number of pole pairs. Here, the active current component is i_q, which is related to the torque, while i_d is related to the flux. Fig. 5.3 depicts the field-oriented control (FOC) implemented using (5.1) and (5.2). The control loops provide decoupled dq control with PI controllers. The main difference of the FOC compared to the VOC used in the previous grid-connected system is the alignment of the d-axis. Also, the PLL is not needed as the angle is measured from an encoder. In this chapter, the PI controller gains are selected such that the current and voltage bandwidth are 5kHz and 500Hz, respectively, with the fundamental frequency chosen as 800Hz (tuned to the highest frequency in the range). The rectifier switches at 50kHz.

5.2.2 Flux Weakening Control

As a result of variable frequency operation, the generator produces voltages with variable amplitude and frequency. In the wound rotor generator, the output voltages

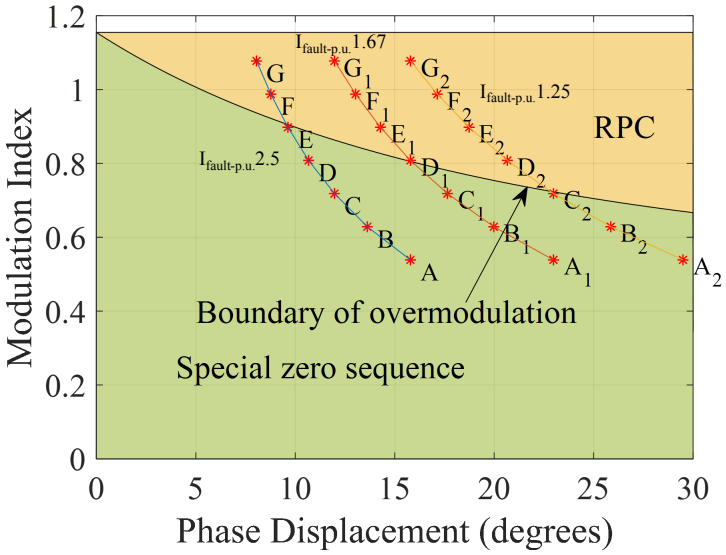

Figure 5.4: Operation of the generator-fed Vienna rectifier at different speeds.

are controlled by the GCU by controlling the field current. In PMSG, this is done by reactive power injection to the stator circuit [89, 94, 95], and it is known as flux weakening control. When the generator shaft is above a certain speed, in order to limit the generator output voltages, the machine flux is gradually decreased. This is achieved by regulating i_d (flux current component) to create an opposite flux to the PM flux and hence reduce the machine back EMF. With this, the generator can operate at high speeds while maintaining the magnitude of the generator output voltages. There are many flux weakening control strategies presented in the literature. In [96], flux weakening is used for an interior PM starter generator. In the motoring mode, maximum torque per ampere (MTPA) control is used to set the torque and,

Table 5.3: Operating Points in the Vienna Rectifier for Constant Power Load at Different Generator Speeds

Operating point	Speed (rpm)	Freq. (Hz)	Back EMF (V)	Phase displacement (deg) Gen1	Gen2	Gen3	Modulation index, m
A	3000	400	133.3	15.79	22.98	29.49	0.54
B	3500	466.7	155.6	13.62	19.98	25.86	0.63
C	4000	533.3	177.8	11.97	17.65	22.98	0.72
D	4500	600	200	10.67	15.79	20.66	0.81
E	5000	666.7	222.2	9.63	14.28	18.74	0.90
F	5500	733.3	244.4	8.77	13.03	17.14	0.99
G	6000	800	266.7	8.05	11.97	15.79	1.08

in the generator mode, the dc-link voltage is regulated. This enables the generator to operate at constant power. The instantaneous modulation index is used to determine whether flux weakening is required or not. In an aircraft with variable frequency generator (VFG), the fundamental frequency changes from 360Hz to 800Hz during landing and take off, but 80-90% of the time the frequency will be constant [5]. As shown in the next section, the hybrid modulation and control uses reactive current, nevertheless it employs the minimum amount of reactive current as possible, just to avoid overmodulation.

5.2.3 Hybrid Modulation and Control

This section analyzes a PMSG-fed Vienna rectifier system and adapts the carrier-based modulation and control strategies described in Chapter 4 to the case of the generator instead of the grid. Fig. 5.4 illustrates the different trajectories when the speed is varied from 3000 rpm to 6000 rpm, while operating with the hybrid modulation and control for three generators with different parameters. The operating points are obtained analytically, as summarized in Table 5.3, when the rectifier output is connected with a 620 μF dc-link capacitance and regulated at 700 V output voltage. The generators Gen1, Gen2 and Gen3 represent the PMSGs having 30 μH, 45 μH and 60 μH stator winding inductance and per-unit fault currents 2.50, 1.67 and 1.25, respectively. As the dc-link voltage is regulated at 700 V and the load is unchanged, the traces in Fig. 5.4 represent constant power (200 kW). When the generator speed is low, the back EMF is low, which means for the same power the rectifier will draw higher current.

Fig. 5.5 illustrates the main waveforms when the Gen1 configuration is connected to the Vienna rectifier with the hybrid modulation and control at various speeds. As expected, at Point G when the speed is the highest, the hybrid controller injects reactive current, to avoid overmodulation. Fig. 5.6 shows the current spectra at different speeds with their respective THD values. The current waveform quality is better at lower speeds as the current amplitude increases.

Fig. 5.7 compares the current spectra when the Gen-1 is connected to the Vienna rectifier and operating at 800Hz with Mode-1 and with hybrid modulation. As this operating point lies above the boundary of overmodulation Mode-1 produces distorted current waveforms with low frequency harmonics.

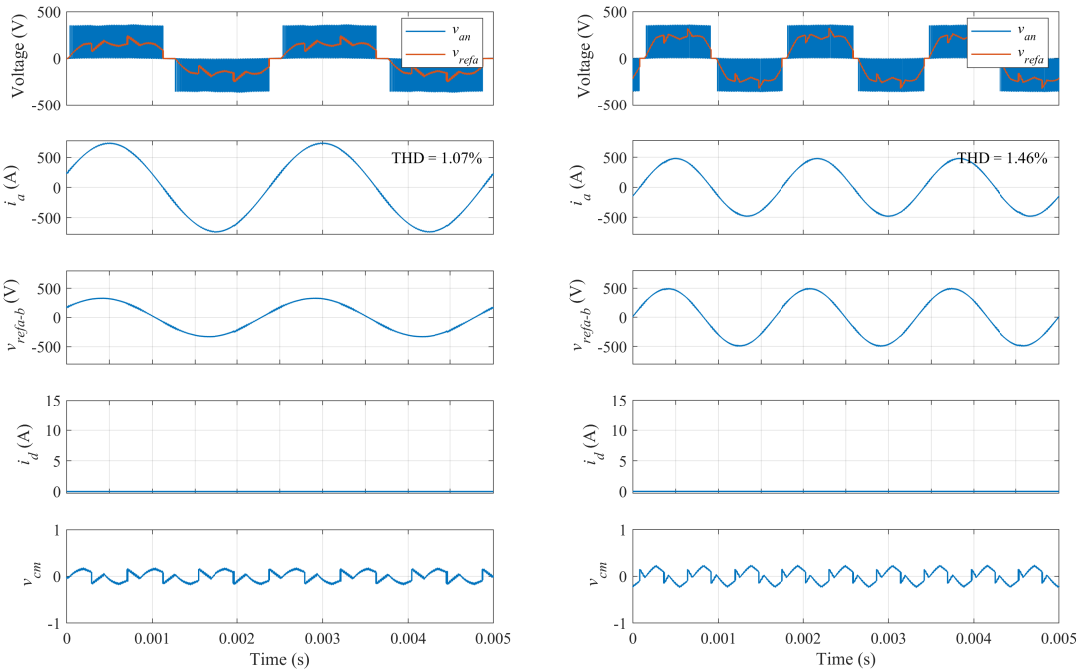

(a)

(b)

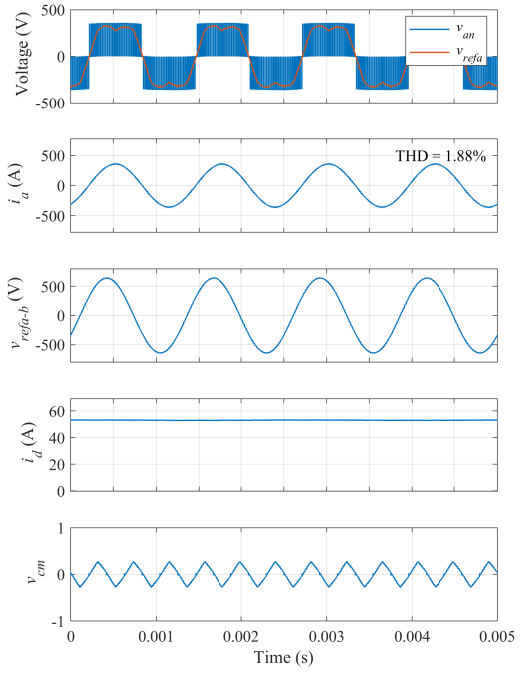

(c)

Figure 5.5: Main waveforms from the Gen1 generator-fed Vienna rectifier at different speeds when the proposed hybrid modulation is used: (a) Point A, (b) Point D and (c) Point G.

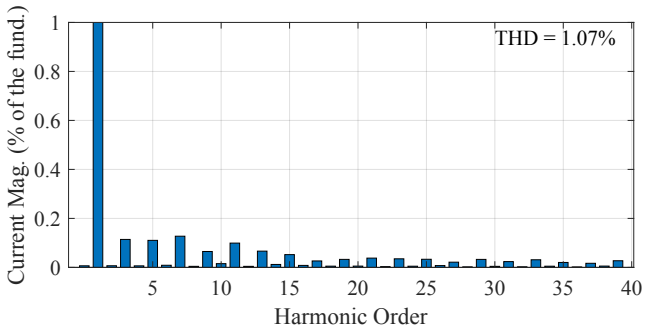

(a)

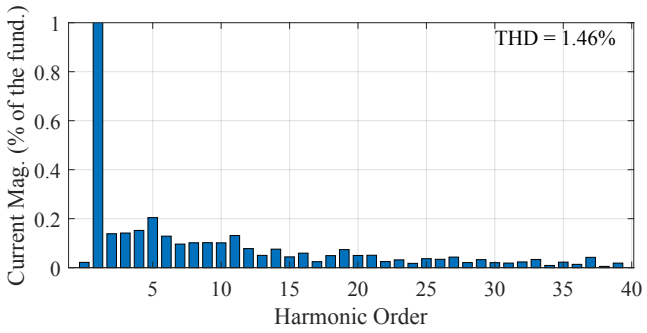

(b)

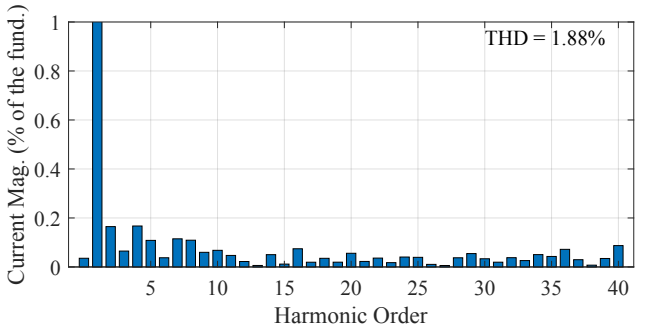

(c)

Figure 5.6: Input current spectra from the Gen1 generator-fed Vienna rectifier at different speeds when the proposed hybrid modulation is used: (a) Point A, (b) Point D and (c) Point G.

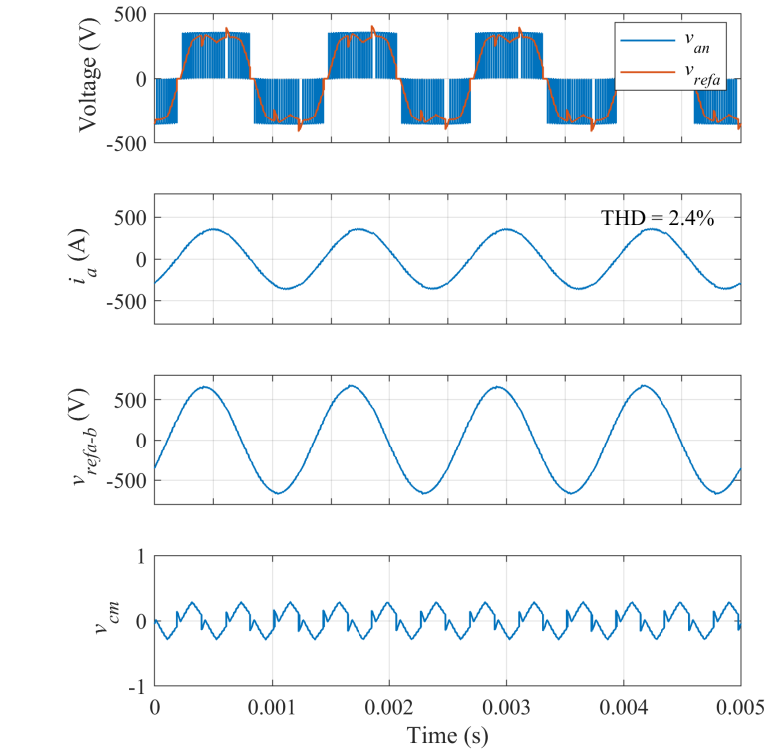

(a)

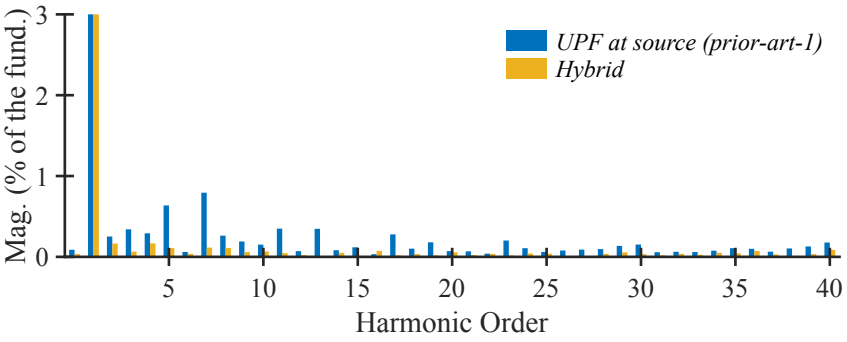

(b)

Figure 5.7: Operation of the Gen1 generator-fed Vienna rectifier at 800Hz: (a) Main waveforms of Mode-1 and (b) with and without the hybrid modulation.

Fig. 5.8 illustrates the main waveforms when the Gen2 generator is connected to the Vienna rectifier. Similar to the previous case, at Points D_1 and G_1, the hybrid controller injects reactive current to avoid overmodulation. Fig. 5.9 shows the current spectra at different speeds with their respective THD values.

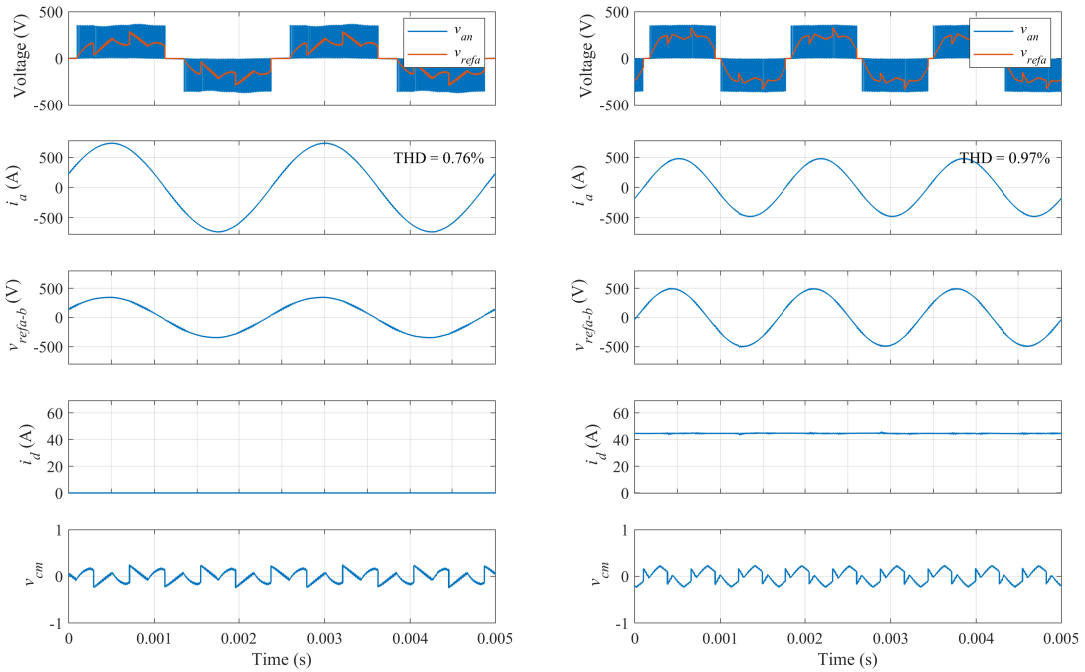

(a)

(b)

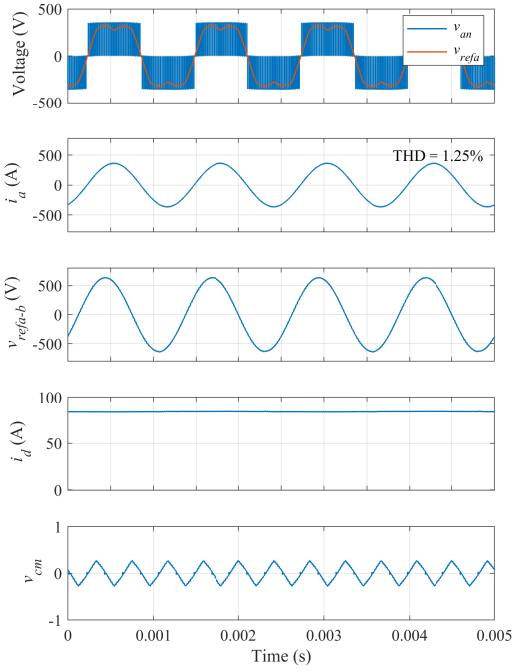

(c)

Figure 5.8: Main waveforms from the Gen2 generator-fed Vienna rectifier at different speeds when the proposed hybrid modulation is used: (a) Point A_1, (b) Point D_1 and (c) Point G_1.

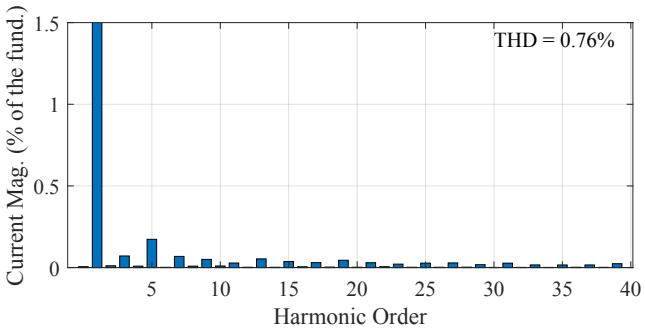

(a)

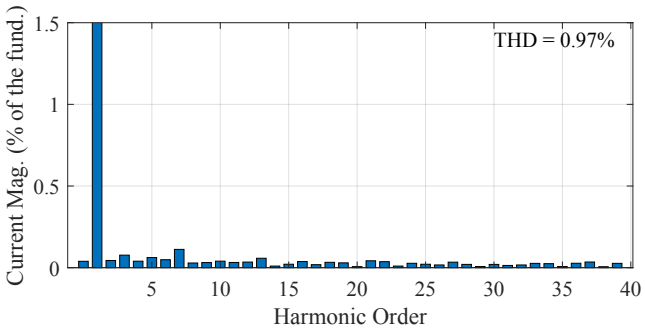

(b)

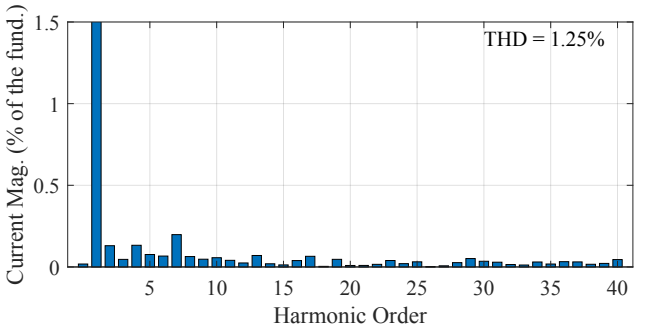

(c)

Figure 5.9: Input current spectra from the Gen2 generator-fed Vienna rectifier at different speeds when the proposed hybrid modulation is used: (a) Point A_1, (b) Point D_1 and (c) Point G_1.

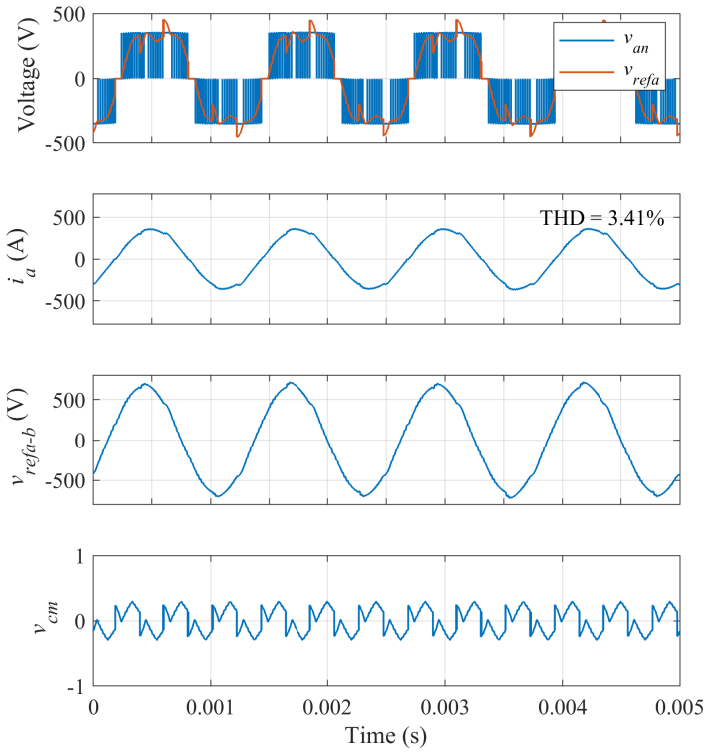

(a)

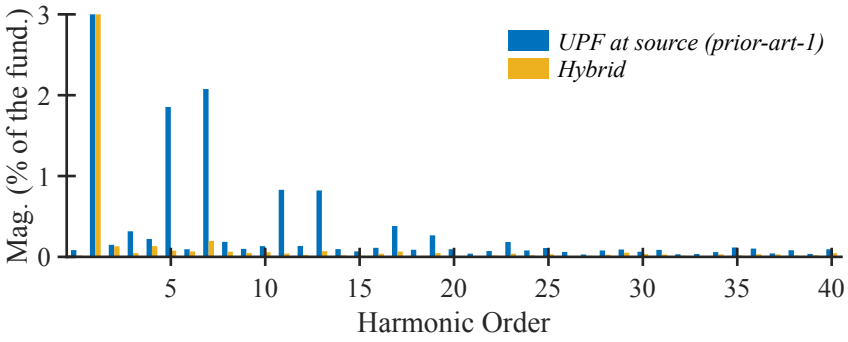

(b)

Figure 5.10: Operation of the Gen2 generator-fed Vienna rectifier at 800Hz: (a) Main waveforms of Mode-1 and (b) with and without the hybrid modulation.

Fig. 5.10 compares the current spectra of the Gen-2 connected Vienna rectifier operating at 800Hz with Mode-1 and with hybrid modulation. As this operating point lies above the boundary, Mode-1 produces overmodulation.

Fig. 5.11 illustrates the main waveforms when the Gen3 generator, which is having the highest stator inductance, is operated with the Vienna rectifier. Similar to the previous case, at Points D_1 and G_1, the hybrid controller injects reactive current to avoid overmodulation.

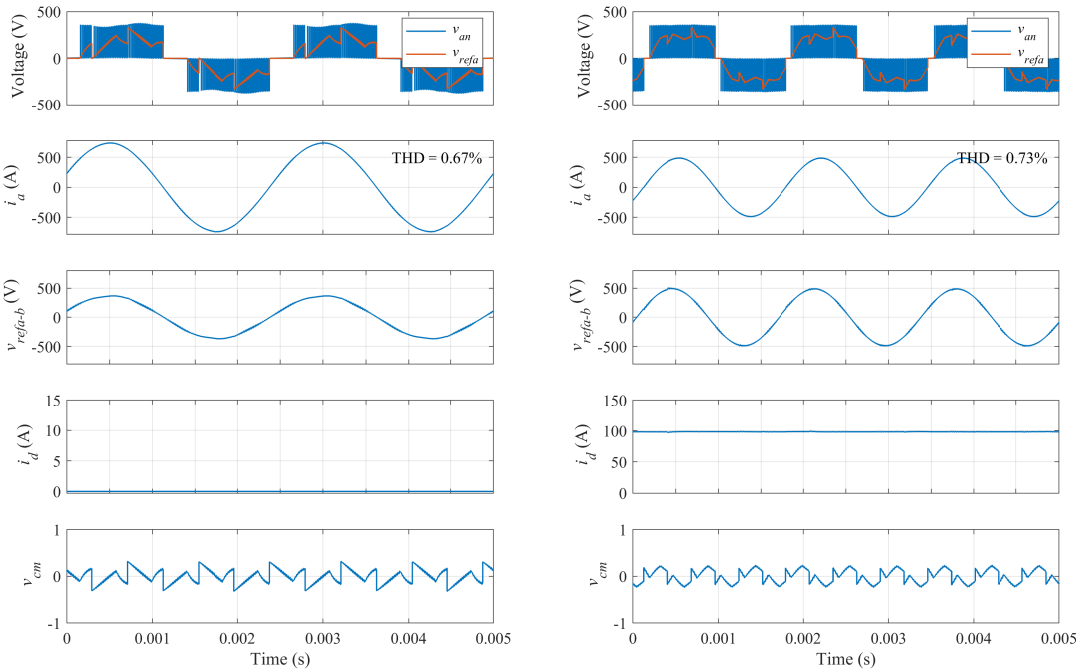

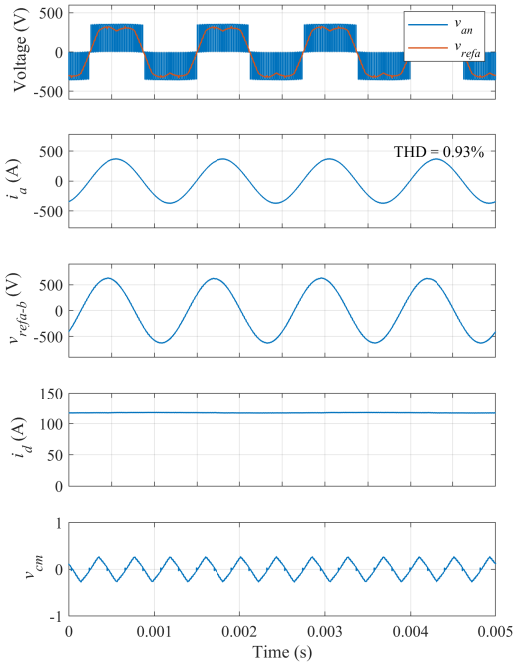

Figure 5.11: Main waveforms from the Gen3 generator-fed Vienna rectifier at different speeds when the proposed hybrid modulation is used: (a) Point A_2, (b) Point D_2 and (c) Point G_2.

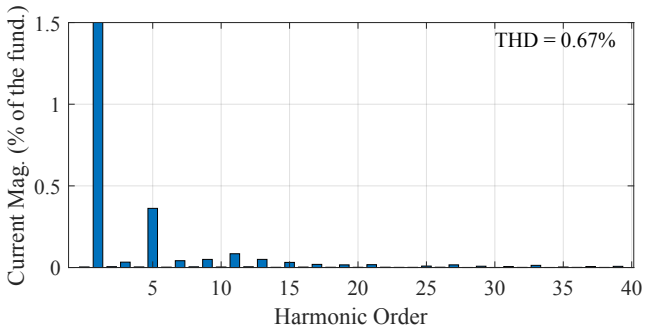

(a)

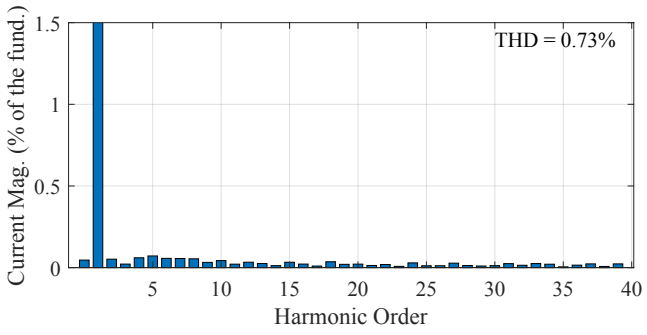

(b)

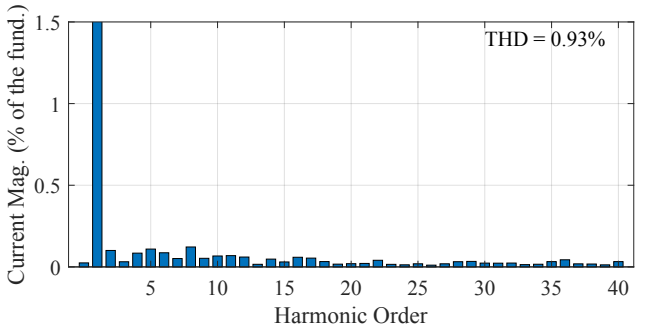

(c)

Figure 5.12: Input current spectra from the Gen3 generator-fed Vienna rectifier at different generator speeds when the proposed hybrid modulation is used: (a) Point A_2, (b) Point D_2 and (c) Point G_2.

Fig. 5.12 shows the current spectra at different speeds with their respective THD values. Figs. 5.13 and 5.14 compare the current spectra of the Gen-2 connected Vienna rectifier operating at 800Hz with Mode-1 and with hybrid modulation. As Fig. 5.14 shows at 800Hz the current distortion is significant, unless the hybrid modulation is used.

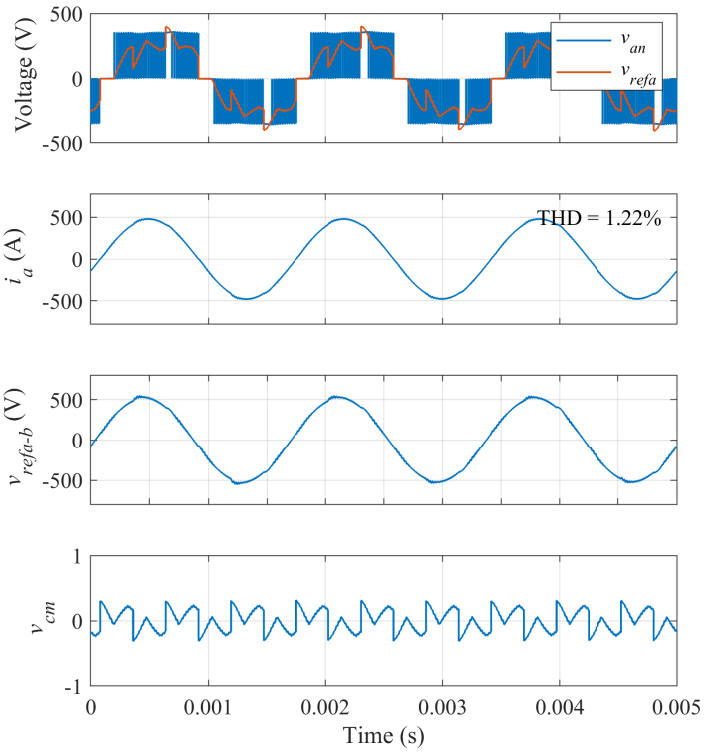

(a)

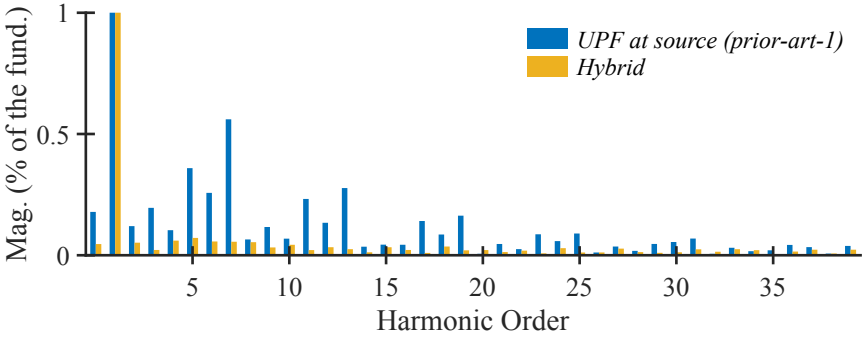

(b)

Figure 5.13: Operation of the Gen3 generator-fed Vienna rectifier at 600Hz: (a) Main waveforms of Mode-1 and (b) with and without the hybrid modulation.

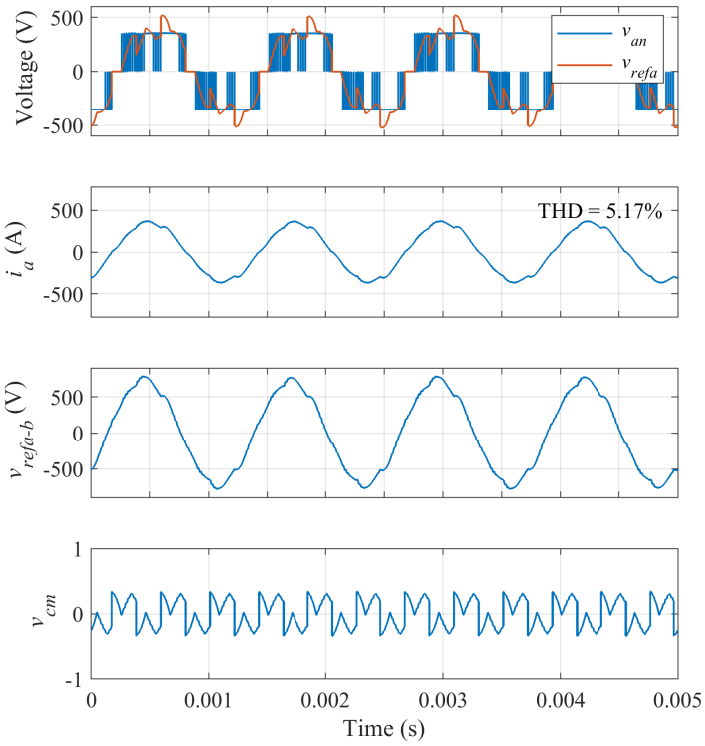

(a)

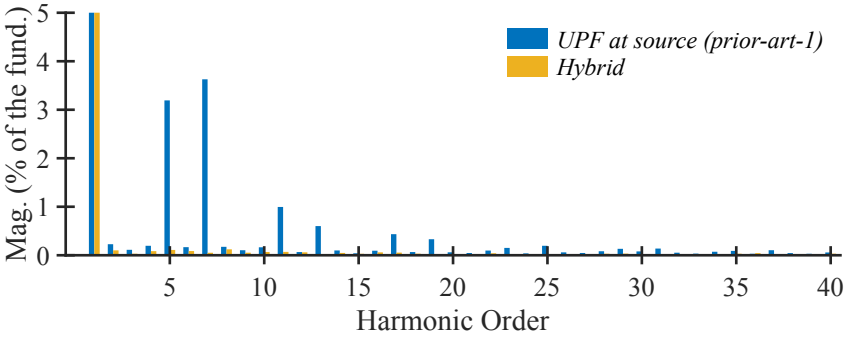

(b)

Figure 5.14: Operation of the Gen3 generator-fed Vienna rectifier at 800Hz: (a) Main waveforms of Mode-1 and (b) with and without the hybrid modulation.

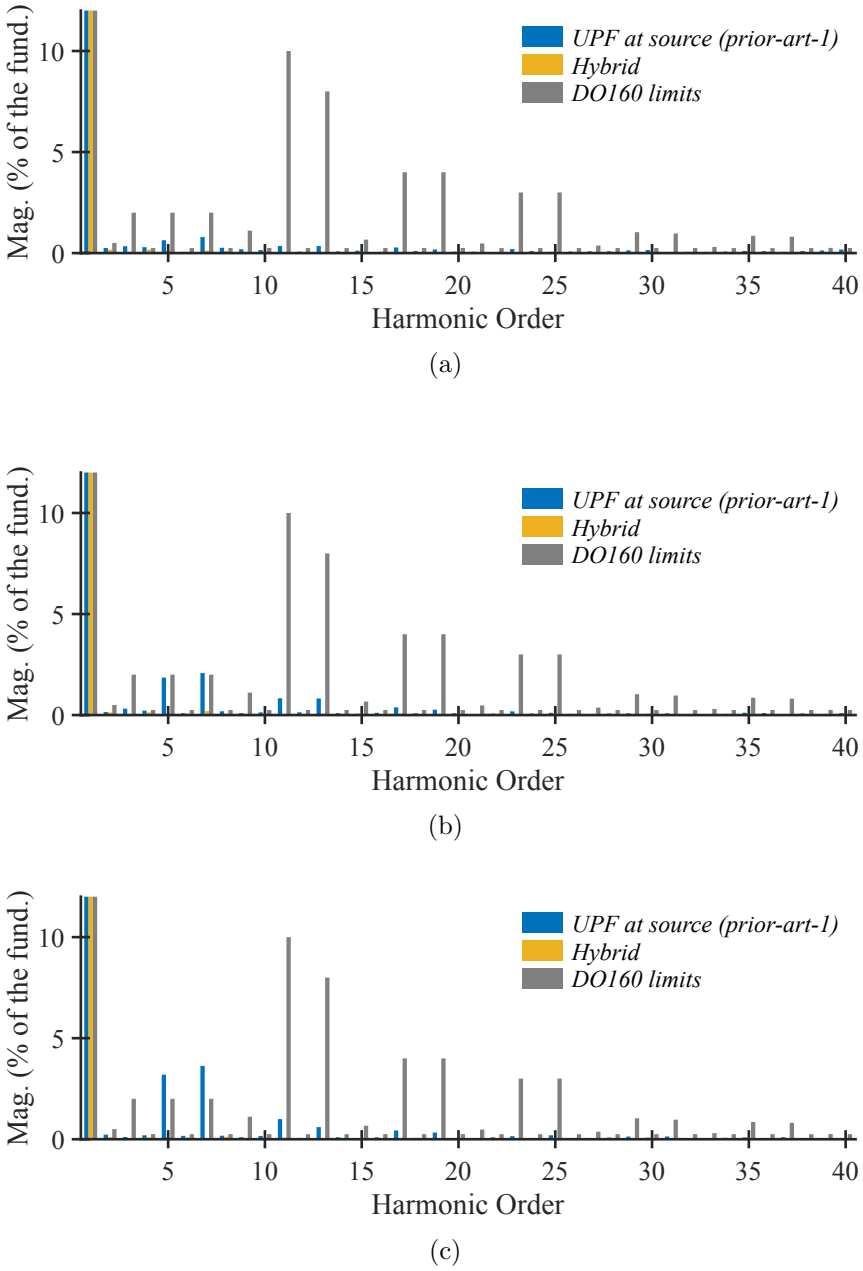

Figure 5.15: Input current DO-160 compliance of different generator configurations for the generator-fed Vienna rectifier operating at 800 Hz fundamental frequency, when the proposed hybrid modulation is used: (a) Gen1, (b) Gen2 and (c) Gen3 generator-fed Vienna rectifier.

Fig. 5.15 shows the input current spectra when the generator configurations are operating at 800 Hz fundamental frequency. The generator configuration Gen1, having the lowest stator winding inductance, does not violate the harmonic limits imposed by the DO-160 standard, even when the traditional modulation strategies are used. However, in generator configurations Gen2 and Gen3, the harmonics limits

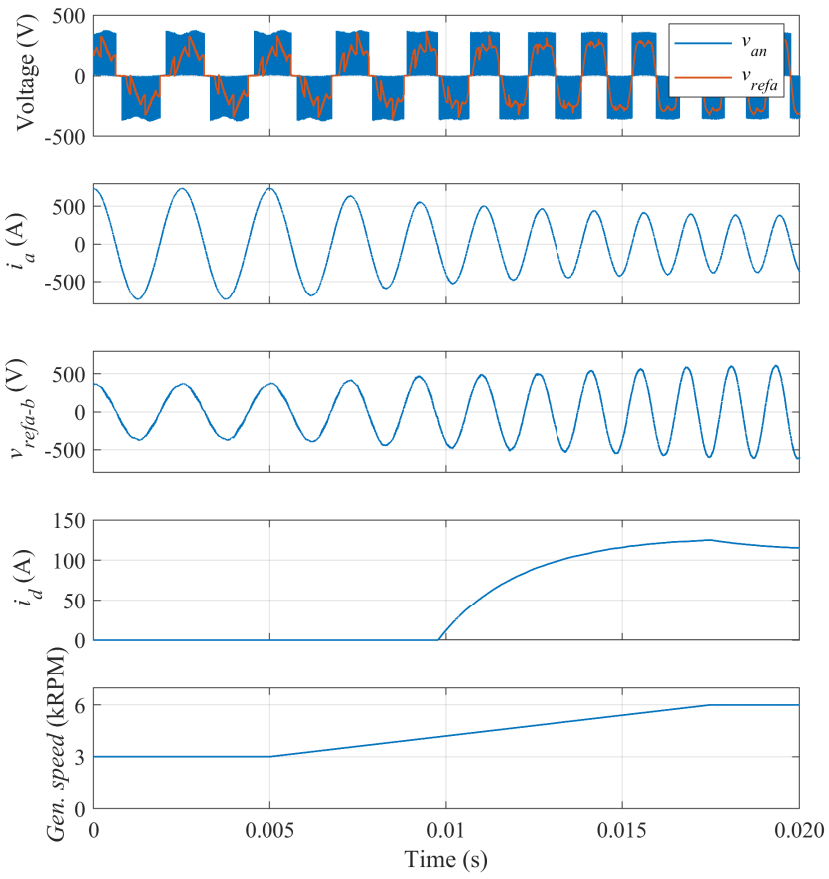

Figure 5.16: Dynamic simulation of the Vienna rectifier operating with hybrid modulation when Gen3 frequency changes from 400Hz to 800Hz.

are exceeded when the traditional modulations are used. When the proposed hybrid modulation method is applied, the current harmonics are well below the standard limits, guaranteeing the DO-160 standard compliance. Since aerospace applications prefer machines with higher stator winding inductance (in order to limit the fault current), the hybrid modulation will be very useful if a Vienna rectifier is used for the ac-to-dc converter.

Fig. 5.16 depicts the transient simulation where the Vienna rectifier is connected to the Gen3 generator configuration and the fundamental frequency changes from 400Hz to 800Hz (engine speed changes from 3000rpm to 6000rpm) starting at 5ms. When the frequency increases, the hybrid controller starts injecting reactive current to avoid overmodulation, as seen from the i_d trace, which increases from 0A to 11.5A.

5.3 Summary

In this chapter, the hybrid modulation is applied to a generator-connected Vienna rectifier to improve the current waveform quality, and tested in various operating conditions. Three PMSG configurations having different stator winding inductances are being considered to analyze the operation of the Vienna rectifier. In all generator configurations, for higher speeds, reactive current is required to avoid overmodulation. With the hybrid modulation and control, the generator-fed Vienna rectifier has superior current waveform quality throughout the required speed range, compared to the traditional method.

Chapter 6

Conclusion and Future Work

This chapter summarizes the main conclusions of this research and points out some future work that can be developed from the studies performed in this PhD dissertation.

6.1 Conclusions

Transportation electrification is a global trend towards a sustainable future. Different countries in the world have aggressive plans to achieve net-zero emissions. In aviation, extensive research is being done for electrification to improve the overall performance of the aircraft, and make air transportation more sustainable. The rectifier, which connects the aircraft generator to the dc-bus, is a main component in the MEA. After comparing different topologies to perform the ac to dc conversion, the Vienna rectifier topology has been selected for this aerospace application. The Vienna rectifier is a three-level unidirectional power flow topology based on a diode bridge rectifier, but with advanced PWM features. Compared to the well-established two-level converter, the Vienna rectifier offers significant benefits in aspects like current waveform quality, power density, reliability, etc. Since the application does not require 4-quadrant operation, the Vienna rectifier offers fewer failure points (only needs 6 gate drivers for the active switches), with simple circuit structure and cost benefits compared to the other three-level topologies. This thesis has discussed the state of the art of the Vienna rectifier and addressed its current zero crossing distortion issue, while allowing it to operate in a wide modulation index range, even with high phase displacement angle, which makes it an ideal candidate for the variable speed generator connected application. The main conclusions are summarized below.

The Vienna rectifier does not perform well under non-unity power factor operation due to current distortion near the zero crossings. The challenge of this research is to improve the performance of the Vienna rectifier under such operating conditions.

First, the current distortion produced in the Vienna rectifier around zero current crossings has been analyzed and then, a modulation and control method comprising of two modes has been presented to reduce such distortion. Mode-1 consists of adding a proper zero sequence to the reference signals while maintaining UPF at the grid-side. However, overmodulation may be produced when operating with high modulation indices and large phase displacement angles. This problem can be avoided by activating Mode-2 where reactive power (calculated in real-time) is injected to obtain UPF at the converter terminals. Since there is no phase angle displacement between the converter reference voltages and the grid currents, the zero-crossing current distortion is avoided. An algorithm for transiting from one method to another makes use of a twin controller that runs in parallel with the main controller, to check the peak of the reference signals, and determine the operation mode that needs to be applied to the converter. Mode-1 is more suitable for low modulation index operation, while for high modulation indices Mode-2 is more convenient. When the two methods are combined, full control of the converter can be achieved, within the $\{-\frac{\pi}{6} \ +\frac{\pi}{6}\}$ region. UPF at the converter terminals is used as a distortion mitigation technique in this context. However, it increases the VA rating of the converter, therefore the algorithm selects Mode-1 over Mode-2 if possible. The algorithm only switches to Mode-2 when needed to avoid low-frequency current distortion.

In order to further improve the performance of the Vienna rectifier, the injected reactive current is reduced such that it is just enough to avoid the overmodulation created by the notches introduced by the special zero sequence. With the proposed hybrid modulation and control, low-frequency distortion due to the current zero crossings can be avoided without restricting the modulation index, and with a minimal amount of reactive current. The study on efficiency shows clear improvements agreeing with the reactive current savings achieved by the hybrid modulation and control. Furthermore, the effect of the voltage control loop bandwidth that regulates the dc-link on the current waveform quality is demonstrated. When the operating point is shifted, the transients are smooth as reactive current steps are avoided. Finally, the solutions are tested with the generator-fed Vienna rectifier system.

6.2 Future Work

6.2.1 Sensorless Control with Source Unbalance

As mentioned in the previous chapter, eliminating the speed sensor will increase the reliability of the system. However, due to the mission critical nature of the application, if the sensor is removed, the converter should still function well even in the event of source imbalance. In aircraft applications, the generator is allowed to have 3V rms voltage imbalance and phase imbalance of $\pm$ 4 degrees [57], in traditional 115V ac systems.

From symmetrical components, balanced systems have only a positive sequence, and the negative sequence is zero all the time. However, in unbalanced systems, there are positive and negative sequences. This can be represented by defining two reference frames (double synchronous reference frame). As elaborated in [97], dq^{+1} frame rotates in the positive direction and the other frame dq^{-1}, rotates in the negative direction. These two frames will have coupling and will interact with each other. The negative sequence is projected on the positive reference frame and, the positive sequence is reflected on the negative reference frame. Second-order oscillations appear, which need to be filtered.

A PLL elaborated in [98] and [97]; decoupled double synchronous reference frame (DDSRF) can be used to extract the positive sequence of the source voltage. The low-pass filters (LPFs) in DDSRF PLL cause an issue for variable frequency applications. If the fundamental frequency changes, as in this application, the LPF bandwidths need to be changed. These filters will be tuned to remove the second order oscillations, which would change with the variable frequency.

One way to address this is to use moving average filters (MAFs) [99, 100]. In the MAF, the window of the filter can be changed to adapt different frequencies. Applying this technique to the estimated back EMF of the generator will be interesting future work.

6.2.2 Extension of the Hybrid Modulation

When the hybrid modulation is used, the controller avoids overmodulation, as shown in Chapter 4. To achieve this, reactive current is injected. In order to improve

the efficiency of the converter even further, when the converter is entering overmodulation, the reactive current injection could be delayed, such that the converter operates with overmodulation, but still within the DO160 standard, not violating the harmonic limits. Therefore, in this case a certain amount of overmodulation (a small amount from the peak created by the special zero sequence) will be tolerated by the controller and the distortion in the currents will be a bit higher than with the hybrid modulation, but still less compared to the conventional methods. This will further reduce the amount of reactive current being used.

Extensive mathematical analysis is required to find the relationship between the reactive current that is required and the harmonic amplitudes of the input current waveform. Taking into account the harmonic limits from the DO-160 standard, a new boundary in the modulation vs. phase displacement plot would be derived. This implementation will require to perform real-time fast Fourier transform (FFT) of the input currents in the controller.

6.2.3 Min-max Zero Sequence Influence on the Converter

The min-max zero sequence is used to extend the modulation index and as an additional benefit, it reduces the low frequency capacitor voltage ripple. Nevertheless, further mathematical analysis is required to understand the mechanism of the harmonic reduction.

As illustrated in Fig. 6.1, the capacitor voltage ripple rms reduces from 491mV to 287mV with 100V dc-link voltage, when the min-max zero sequence is introduced (41.5% reduction). The reduction is from 634mV to 365mV, when the dc-link voltage is 125V.

6.2.4 Address the Current Zero Crossing Distortion Issue with Space-Vector Modulation and Model Predictive Control

In the conventional VOC, the PI controllers are tuned for one operating point of the Vienna rectifier. For variable frequency application, this can be further improved by having k_p, k_i values stored in a lookup table for different generator speeds. An alternative method would be to use model predictive control (MPC). The main ad-

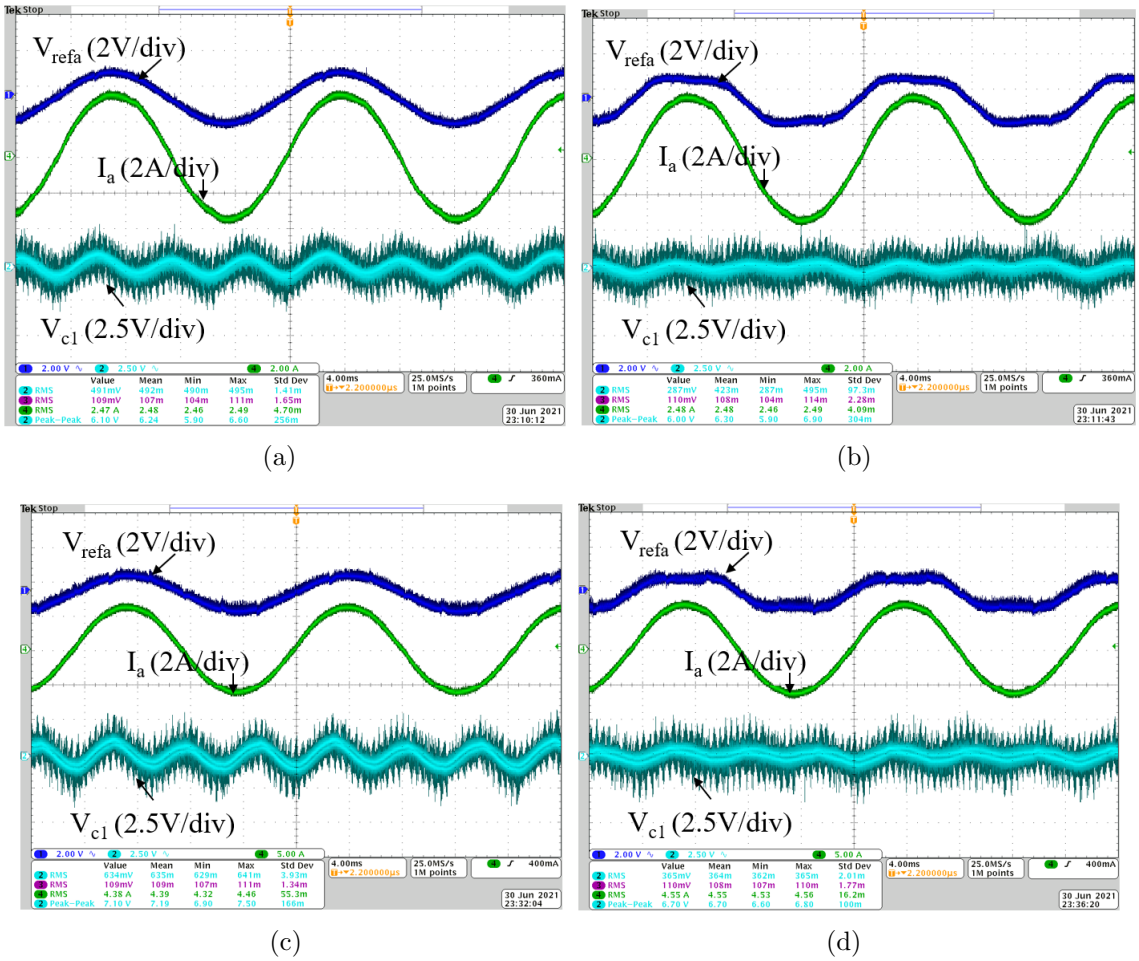

Figure 6.1: Main waveforms of the Vienna rectifier with the special zero sequence: (a) When min-max zero sequence is not injected (100V dc-link), (b) when min-max zero sequence is injected (100V dc-link), (c) when min-max zero sequence is not injected (125V dc-link) and (d) when min-max zero sequence is injected (125V dc-link).

vantage of MPC is that it can control multiple variables at the same time besides considering the constraints of the system. In the case of the Vienna rectifier, the constraints of the current direction can be included in the controller, i.e., if the current goes towards the converter only positive and middle voltages can be generated, while if it is in the opposite direction, only negative and middle voltages can be generated. With these constraints, MPC is expected to optimize the operation of the Vienna rectifier, similarly to what can be achieved with the solutions proposed in this thesis, but avoiding any transition mode.

The research presented in this PhD dissertation uses CB-PWM technique. Another modulation method to address the current zero crossing distortion in the Vienna rectifier would be SVM. Similar to MPC, the vectors that were not available for the modulation would be removed from the space-vector diagram and, therefore, not con-

sidered for the modulation. As a result, the space-vector diagram would be dynamic and only the vectors available at any time would be considered for the modulation.

6.2.5 Reliability

From surveys done in industry [101], the most fragile components of the converter are considered to be power semiconductor devices and capacitors. Therefore, much attention should be paid when selecting these components. A study in [102], shows that diode failure rate is very less where power device and capacitor failure rates are 34% and 20%, respectively.

For applications that demand high reliability, such as aircraft, film capacitors are preferred even though they have less capacitance per unit volume compared to electrolytic capacitors [103, 104]. Also, the capacitance reduction is less significant in film capacitors compared to Al-electrolyte ones during their lifetime [105].

In a study presented in [106], it is shown that IGBTs having higher blocking voltages are less robust compared to low-blocking voltage counterparts. Because the Vienna rectifier switches are blocking only half the dc-link voltage, the Vienna rectifier has a clear advantage over the two-level converter. According to the model in [106], the blocking voltage v_{block} of a device has a relationship with the reliability,

$$N_f \propto v_{block}^{-0.751} \tag{6.1}$$

where N_f is the number of cycles before failure. The Vienna rectifier would survive 1.68 times higher number of cycles before failure than the two-level converter, considering the fact that the Vienna rectifier requires active switches that block half the dc-link voltage.

From current stress aspect, the two-level converter is prone/less tolerant to shoot-through currents that might be triggered by erroneous drive signals [107], because it has active switches across the dc-link. This affects reliable converter operation. In the Vienna rectifier, inherently there would not be any shoot-through current as there are no switches connecting to top and bottom voltage levels. Then, regarding precharging, for both the two-level converter and the Vienna rectifier, additional circuitry is required for startup to control the inrush current.

In studies done in [108, 109], it is found that SiC MOSFETs are more robust

compared to Si MOSFETs and IGBTs in terms of single-event-burnout failures caused by terrestrial cosmic radiation. This is an important aspect for aerospace application as the cosmic ray intensity is up to 300 times stronger at aircraft cruising altitudes than at sea level [103].

In terms of components count, the two-level converter will win since the Vienna rectifier has 6 additional diodes (However, the Vienna rectifier has the least component count when compared with other three-level rectifier topologies).

From the aircraft zonal safety point of view, the reliability requirement of the power converter would vary, and further extensive analysis is required with mission profiles. As such, this study does not address all the challenges associated with the converter reliability, and it is included as future work.

Appendix A

Design Equations

A.0.1 Capacitor Sizing

The capacitance required at the output of the Vienna rectifier needs to be designed from two approaches, which are:

1. Minimum capacitance required based on the neutral point voltage ripple.

   The neutral point voltage ripple is discussed in [R1] where the maximum value occurs when the modulation index is unity. The maximum normalized voltage ripple can be represented as,

   $$\frac{\Delta V_{NPn}}{2} = \frac{\Delta V_{NP}/2}{I_{RMS}/fC} = 0.02973 \tag{A.1}$$

   where ΔV_{NP} is the peak-to-peak voltage ripple, I_{RMS} the RMS value of the input current, f the fundamental frequency and C the capacitance. Let us consider the 1-kW, 700 Vdc example system. As the standards do not specify a particular limit to the neutral point voltage ripple, a 5% voltage ripple amplitude is assumed and this gives a capacitance value of 49.3 μF. This is the capacitance value for each of the two capacitors connected to the dc-link. The relationship in (A.1) is for a neutral-point-clamped (NPC) converter, however, the result for the Vienna rectifier or a T-type converter would be approximately the same one.

   [R1] J. Pou, R. Pindado, D. Boroyevich, and P. Rodriguez, "Evaluation of the low frequency neutral-point voltage oscillations in the three-level inverter," *IEEE Trans. Ind. Electron.,* vol. 52, no. 6, pp. 1582-1588, Dec. 2005.

2. Minimum capacitance required from the dc-link energy buffer point of view.

   In this method, the capacitor is sized based on the energy it should buffer. If the rated power of a converter is P and the output voltage dips down to V_{dcmin} in time t_{hold} while the rated output voltage is V_{dc}, the buffered energy is given by,

$$E_{buffer} = Pt_{hold} = 0.5C(V_{dc}^2 - V_{dcmin}^2) \tag{A.2}$$

   by isolating the capacitance,

$$C = \frac{2Pt_{hold}}{V_{dc}^2 - V_{dcmin}^2} \tag{A.3}$$

   From the standard MIL-STD-704F, a 270-V aircraft power system cannot have more than 20 V dip for a time duration more than 30 ms. By extrapolating to a 700-V example system (the maximum voltage dip would be 51.85 V), the required capacitance for the 1 kW rectifier can be calculated by solving (A.3) as 142.8 μF.

   The above value is obtained considering the total capacitance C_{dc} in the dc-link. The C_{dc} consists of two series-connected capacitors. Therefore, the value for a single capacitor is double this amount, which is 285.6 μF.

Taking into account the two capacitance values, the more conservative should be selected (which is the higher capacitance, and it is the capacitance value from the energy buffer concept) to be used as the dc-link capacitor.

The aerospace standard mentioned above is for 270 V systems. The aircraft standards will have to be amended for power systems that use higher voltages and powers in the future.

A.0.2 Inductor Sizing

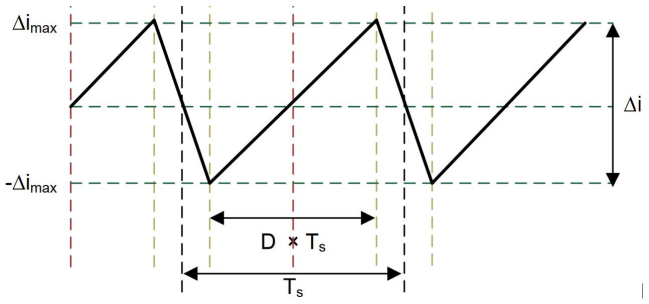

Figure A.1: Inductor current ripple.

The inductor current ripple can be calculated when the neutral point switch is on. Then,

$$\frac{V_{dc}}{2} - V_{in} = L\frac{\Delta i}{DT_s} \tag{A.4}$$

and by isolating the current ripple,

$$\Delta i = (\frac{V_{dc}}{2} - V_{in})\frac{DT_s}{L}. \tag{A.5}$$

By substituting $V_{in} = m(V_{dc}/2)\sin\omega t$ and $D = m\sin\omega t$

$$\Delta i = \frac{V_{dc}}{2} m\sin\omega t(1 - m\sin\omega t)\frac{T_s}{L}. \tag{A.6}$$

Differentiating with respect to time,

$$\frac{d\Delta i}{dt} = \frac{mV_{dc}T_s\omega}{2L}\cos\omega t(1 - 2m\sin\omega t). \tag{A.7}$$

The current ripple will be maximum when,

$$\sin\omega t = \frac{1}{2m}. \tag{A.8}$$

Thus, the inductance which gives this current ripple can be found by solving (A.6),

$$L = \frac{V_{dc}}{8f_s\Delta i_{max}}. \tag{A.9}$$

Substituting the system parameters,
Dc-link voltage $V_{dc} = 700$ V,

Switching frequency $f_s = 50$ kHz,

Maximum current ripple $\delta i_{max} = 0.58$ A,

the required inductance is calculated as 3 mH.

List of Publications

Journal papers:

[1] **D. A. Molligoda**, S. Ceballos, J. Pou, K. Satpathi, F. Sasongko, C. J. Gajanayake, and A. K. Gupta, "Hybrid modulation strategy for the Vienna rectifier," *IEEE Trans. Power Electron.*

(Accepted)

[2] **D. A. Molligoda**, S. Ceballos, J. Pou, K. Satpathi, F. Sasongko, C. J. Gajanayake, and A. K. Gupta, "Mitigating zero-crossing current distortion in the Vienna rectifier when operating with nonunity power factor," *IEEE Trans. Emerg. Sel. Topics Power Electron.*

(In preparation)

Conference papers:

[3] **D. A. Molligoda**, J. Pou, C. J. Gajanayake, and A. K. Gupta, "Analysis of the Vienna rectifier under nonunity power factor operation," in *Proc. Asian Conf. on Energy, Power and Transport. Electrific. (ACEPT)*, Singapore, Oct. 2018, pp.1–7.

[4] **D. A. Molligoda**, J. Pou, S. Ceballos, K. Satpathi, F. Sasongko, C. J. Gajanayake, and A. K. Gupta, "Current distortion mitigation in grid-connected Vienna rectifier during nonunity power factor operation," in *Proc. IEEE Ind. Electron. Soc. (IECON)*, 2020, pp.4085–4090.

[5] **D. A. Molligoda**, J. Pou, S. Ceballos, K. Satpathi, F. Sasongko, C. J. Gajanayake, and A. K. Gupta, "Hybrid modulation strategy to avoid zero crossing distortion in the Vienna rectifier," in *Proc. IEEE Energy Conversion Congress and Exposition - Asia (ECCE - Asia)*, 2021, pp.1245-1249.

References

[1] X. Roboam, B. Sareni, and A. D. Andrade, "More electricity in the air: Toward optimized electrical networks embedded in more-electrical aircraft," *IEEE Ind. Electron.. Mag.*, vol. 6, no. 4, pp. 6–17, Dec. 2012.

[2] Global market forecast 2018-2037 Airbus. [Online]. Available: https://www.airbus.com/aircraft/market/global-market-forecast.html

[3] Commercial market outlook 2018–2037 Boeing. [Online]. Available: https://www.boeing.com/commercial/market/commercial-market-outlook/

[4] P. Wheeler and S. Bozhko, "The more electric aircraft: Technology and challenges," *IEEE Electrification Magazine*, vol. 2, no. 4, pp. 6–12, Dec. 2014.

[5] V. Madonna, P. Giangrande, and M. Galea, "Electrical power generation in aircraft: Review, challenges, and opportunities," *IEEE Trans. Transport. Electrific.*, vol. 4, no. 3, pp. 646–659, Sep. 2018.

[6] G. Buticchi, S. Bozhko, M. Liserre, P. Wheeler, and K. Al-Haddad, "On-board microgrids for the more electric aircraft—technology review," *IEEE Trans. Ind. Electron.*, vol. 66, no. 7, pp. 5588–5599, Jul. 2019.

[7] B. Sarlioglu and C. T. Morris, "More electric aircraft: Review, challenges, and opportunities for commercial transport aircraft," *IEEE Trans. Transport. Electrific.*, vol. 1, no. 1, pp. 54–64, Jun. 2015.

[8] S. Bozhko, T. Yang, J.-M. Le Peuvedic, P. Arumugam, M. Degano, A. La Rocca, Z. Xu, M. Rashed, W. Fernando, C. I. Hill, C. Eastwick, S. Pickering, C. Gerada, and P. Wheeler, "Development of aircraft electric starter–generator system based on active rectification technology," *IEEE Trans. Transport. Electrific.*, vol. 4, no. 4, pp. 985–996, Dec. 2018.

[9] P. Wheeler, "Technology for the more and all electric aircraft of the future," in *Proc. IEEE International Conference on Automatica (ICA-ACCA)*, 2016, pp. 1–5.

[10] "AIR6127 managing higher voltages in aerospace electrical systems," *SAE International*, pp. 8–10, Apr. 2017.

[11] I. Christou and I. Cotton, "Methods for partial discharge testing of aerospace cables," in *Proc. IEEE International Symposium on Electrical Insulation*, Jun. 2010, pp. 1–5.

[12] I. Moir, A. Seabridge, and M. Jukes, *Civil Avionics Systems*. Wiley, 2013.

[13] "Commercial aircraft propulsion and energy systems research: Reducing global carbon emissions," *National Academies of Sciences, Engineering, and Medicine*, pp. 5–6, Jul. 2016.

[14] S. Gössling and A. Humpe, "The global scale, distribution and growth of aviation: Implications for climate change," *Global Environmental Change*, vol. 65, p. 102194, 2020.

[15] H. Ritchie, "Climate change and flying: what share of global CO2 emissions come from aviation?" *Our world in data*, Oct. 2020. [Online]. Available: https://ourworldindata.org/co2-emissions-from-aviation

[16] T. Schroter and D. Schulz, "The electrical aircraft network—benefits and drawbacks of modifications," *IEEE Trans. Aerosp. Electron. Syst.*, vol. 49, no. 1, pp. 189–200, Jan. 2013.

[17] J. Brombach and D. Schulz, "Electric power supply system for an aircraft, aircraft and airport power supply system," Nov. 1 2016, uS Patent 9,484,749.

[18] J. Yang, S. B. Lee, J. Yoo, S. Lee, Y. Oh, and C. Choi, "A stator winding insulation condition monitoring technique for inverter-fed machines," *IEEE Trans. Power Electron.*, vol. 22, no. 5, pp. 2026–2033, Sep. 2007.

[19] PFC VITA 62. [Online]. Available: https://www.brightloop.fr/en/pfcvita62

[20] DCHV MP. [Online]. Available: https://brightloop.fr/en/produits/dchv-mp/

[21] YASA Si400 Motor Controller. [Online]. Available: https://www.yasa.com/solutions/

[22] Inverters by Rinehart Motion Systems. [Online]. Available: https://www.phi-power.com/en/home/inverters/

[23] J. Lee and K. Lee, "A novel carrier-based PWM method for Vienna rectifier with a variable power factor," *IEEE Trans. Ind. Electron.*, vol. 63, no. 1, pp. 3–12, Jan. 2016.

[24] D. A. Molligoda, J. Pou, C. J. Gajanayake, and A. K. Gupta, "Analysis of the Vienna rectifier under nonunity power factor operation," in *Proc. Asian Conference on Energy, Power and Transportation Electrification (ACEPT)*, Oct. 2018, pp. 1–7.

[25] D. A. Molligoda, J. Pou, S. Ceballos, K. Satpathi, F. Sasongko, C. J. Gajanayake, and A. K. Gupta, "Current distortion mitigation in grid-connected Vienna rectifier during nonunity power factor operation," in *Proc. IEEE Ind. Electron. Soc. (IECON)*, 2020, pp. 4085–4090.

[26] K. Furmanczyk and M. Stefanich, "Power conversion technologies for reducing harmonics on the more electric aircraft," in *Proc. SAE International Power Systems Conference*, Nov. 2006. [Online]. Available: https://doi.org/10.4271/2006-01-3086

[27] S. Choi, P. N. Enjeti, and I. J. Pitel, "Polyphase transformer arrangements with reduced kVA capacities for harmonic current reduction in rectifier-type utility interface," *IEEE Trans. Power Electron.*, vol. 11, no. 5, pp. 680–690, Sep. 1996.

[28] F. Meng, L. Gao, S. Yang, and W. Yang, "Effect of phase-shift angle on a delta-connected autotransformer applied to a 12-pulse rectifier," *IEEE Trans. Ind. Electron.*, vol. 62, no. 8, pp. 4678–4690, Aug. 2015.

[29] J. Ferens, "Regulated ac to dc converter for aerospace applications," US Patent US 6 950 322 B2, Sep., 2005.

[30] G. Gong, M. L. Heldwein, U. Drofenik, J. Minibock, K. Mino, and J. W. Kolar, "Comparative evaluation of three-phase high-power-factor ac-dc converter concepts for application in future more electric aircraft," *IEEE Trans. Ind. Electron.*, vol. 52, no. 3, pp. 727–737, Jun. 2005.

[31] G. Gong, U. Drofenik, and J. W. Kolar, "12-pulse rectifier for more electric aircraft applications," in *Proc. IEEE International Conference on Industrial Technology*, Dec. 2003, pp. 1096–1101 Vol.2.

[32] J. C. Salmon, "Reliable 3-phase PWM boost rectifiers employing a stacked dual boost converter subtopology," *IEEE Trans. Ind. Appl.*, vol. 32, no. 3, pp. 542–551, May 1996.

[33] M. Hartmann, J. Miniboeck, H. Ertl, and J. W. Kolar, "A three-phase delta switch rectifier for use in modern aircraft," *IEEE Trans. Ind. Electron.*, vol. 59, no. 9, pp. 3635–3647, Sep. 2012.

[34] J. W. Kolar and F. C. Zach, "A novel three-phase utility interface minimizing line current harmonics of high-power telecommunications rectifier modules," *IEEE Trans. Ind. Electron.*, vol. 44, no. 4, pp. 456–467, Aug. 1997.

[35] J. Kolar, H. Ertl, and F. Zach, "A comprehensive design approach for a three-phase high-frequency single-switch discontinuous-mode boost power factor corrector based on analytically derived normalized converter component ratings," *IEEE Trans. Ind. Appl.*, vol. 31, no. 3, pp. 569–582, Jun. 1995.

[36] A. Nabae, I. Takahashi, and H. Akagi, "A new neutral-point-clamped PWM inverter," *IEEE Trans. Ind. Appl.*, vol. IA-17, no. 5, pp. 518–523, Sep. 1981.

[37] Y. Zhao, Y. Li, and T. A. Lipo, "Force commutated three level boost type rectifier," *IEEE Trans. Ind. Appl.*, vol. 31, no. 1, pp. 155–161, Jan. 1995.

[38] M. Leibl, J. W. Kolar, and J. Deuringer, "Sinusoidal input current discontinuous conduction mode control of the Vienna rectifier," *IEEE Trans. Power Electron.*, vol. 32, no. 11, pp. 8800–8812, Nov. 2017.

[39] M. Schweizer and J. W. Kolar, "Design and implementation of a highly efficient three-level T-Type converter for low-voltage applications," *IEEE Trans. Power Electron.*, vol. 28, no. 2, pp. 899–907, Feb. 2013.

[40] M. Schweizer, I. Lizama, T. Friedli, and J. W. Kolar, "Comparison of the chip area usage of 2-level and 3-level voltage source converter topologies," in *Proc. IEEE Industrial Electronics Conference*, Nov. 2010, pp. 391–396.

[41] A. R. Izadinia and H. R. Karshenas, "Current shaping in a hybrid 12-pulse rectifier using a Vienna rectifier," *IEEE Trans. Power Electron.*, vol. 33, no. 2, pp. 1135–1142, Feb. 2018.

[42] U. Borovic, S. Zhao, M. Silva, Y. E. Bouvier, M. Vasić, J. A. Oliver, P. Alou, J. A. Cobos, F. Árevalo, J. C. García-Tembleque, J. Carmena, C. García, and P. Pejović, "Comparison of three-phase active rectifier solutions for avionic applications: Impact of the avionic standard DO-160 F and failure modes," in *Proc. IEEE Energy Conversion Congress and Exposition (ECCE)*, Sep. 2016, pp. 1–8.

[43] T. Friedli, M. Hartmann, and J. W. Kolar, "The essence of three-phase PFC rectifier systems—Part II," *IEEE Trans. Power Electron.*, vol. 29, no. 2, pp. 543–560, Feb. 2014.

[44] J. Kolar, H. Ertl, and F. Zach, "Design and experimental investigation of a three-phase high power density high efficiency unity power factor pwm (VIENNA) rectifier employing a novel integrated power semiconductor module," in *Proc. Applied Power Electronics Conference (APEC)*, vol. 2, 1996, pp. 514–523.

[45] G. Rajendran, C. A. Vaithilingam, K. Naidu, and K. S. P. Oruganti, "Energy-efficient converters for electric vehicle charging stations," *SN Applied Sciences*, vol. 2, no. 4, pp. 1–15, 2020.

[46] L. Hang, H. Zhang, S. Liu, X. Xie, C. Zhao, and S. Liu, "A novel control strategy based on natural frame for Vienna-type rectifier under light unbalanced-grid conditions," *IEEE Trans. Ind. Electron.*, vol. 62, no. 3, pp. 1353–1362, Mar. 2015.

[47] Q. Wang, X. Zhang, R. Burgos, D. Boroyevich, A. M. White, and M. Kheraluwala, "Design and implementation of a two-channel interleaved vienna-type rectifier with 99no. 1, pp. 226–239, 2018.

[48] T. Tarasiuk, S. G. Jayasinghe, M. Gorniak, A. Pilat, V. Shagar, W. Liu, and J. M. Guerrero, "Review of power quality issues in maritime microgrids," *IEEE Access*, vol. 9, pp. 81 798–81 817, 2021.

[49] A. A. Qazalbash, S. M. Sharkh, N. T. Irenji, R. G. Wills, and M. A. Abusara, "Rotor eddy current power loss in permanent magnet synchronous generators feeding uncontrolled rectifier loads," *IEEE Trans. Magn.*, vol. 50, no. 6, pp. 1–9, Jun. 2014.

[50] K. Yamazaki and Y. Seto, "Iron loss analysis of interior permanent-magnet synchronous motors-variation of main loss factors due to driving condition," *IEEE Trans. Ind. Appl.*, vol. 42, no. 4, pp. 1045–1052, Aug. 2006.

[51] S.-M. Jang, H.-W. Cho, and Y.-H. Jeong, "Influence on the rectifiers of rotor losses in high-speed permanent magnet synchronous alternator," *Journal of Applied Physics*, vol. 99, no. 8, p. 08R315, Apr. 2006.

[52] A. G. M. Strollo and E. Napoli, "Optimal on-resistance versus breakdown voltage tradeoff in superjunction power devices: a novel analytical model," *IEEE Trans. Electron Devices*, vol. 48, no. 9, pp. 2161–2167, Sep. 2001.

[53] R. K. Williams, M. N. Darwish, R. A. Blanchard, R. Siemieniec, P. Rutter, and Y. Kawaguchi, "The trench power mosfet: Part i—history, technology, and prospects," *IEEE Trans. Electron Devices*, vol. 64, no. 3, pp. 674–691, Mar. 2017.

[54] T. Kostakis, P. J. Norman, S. J. Galloway, and G. M. Burt, "Demonstration of fast-acting protection as a key enabler for more-electric aircraft interconnected architectures," *IET Electr. Syst. Transp.*, vol. 7, no. 2, pp. 170–178, Jun. 2017.

[55] S. Wu, Q. Chen, Q. Li, X. Liu, H. Zhang, and L. Lin, "Design of aviation high impedance permanent magnet synchronous generator," *Mathematical Problems in Engineering*, vol. 2021, Apr. 2021.

[56] Z. Lim, Y. Liu, L. Zhang, J. Pou, R. Simanjorang, and A. Gupta, "Design of 100 kVA SiC power converter for aircraft electric starter generator," in *Proc. IEEE Southern Power Electronics Conference (SPEC)*, Dec. 2018, pp. 1–9.

[57] M. Standard, "Aircraft electric power characteristics," *Department of Defense Interface Standard (MIL-STD-704F)*, 2004.

[58] R. Teichmann and S. Bernet, "A comparison of three-level converters versus two-level converters for low-voltage drives, traction, and utility applications," *IEEE Trans. Ind. Appl.*, vol. 41, no. 3, pp. 855–865, Jun. 2005.

[59] M. Schweizer, T. Friedli, and J. W. Kolar, "Comparative evaluation of advanced three-phase three-level inverter/converter topologies against two-level systems," *IEEE Trans. Ind. Electron.*, vol. 60, no. 12, pp. 5515–5527, Dec. 2013.

[60] S. Bozhko, T. Yang, J.-M. Le Peuvedic, P. Arumugam, M. Degano, A. La Rocca, Z. Xu, M. Rashed, W. Fernando, C. I. Hill, C. Eastwick, S. Pickering, C. Gerada, and P. Wheeler, "Development of aircraft electric starter–generator system based on active rectification technology," *IEEE Trans. Transport. Electrific.*, vol. 4, no. 4, pp. 985–996, 2018.

[61] B. Wang, J. Cai, X. Du, and L. Zhou, "Review of power semiconductor device reliability for power converters," *CPSS Transactions on Power Electronics and Applications*, vol. 2, no. 2, pp. 101–117, Aug. 2017.

[62] J. W. Kolar and T. Friedli, "The essence of three-phase PFC rectifier systems—part i," *IEEE Trans. Power Electron.*, vol. 28, no. 1, pp. 176–198, Jan. 2013.

[63] T. Viitanen and H. Tuusa, "Space vector modulation and control of a unidirectional three-phase/level/switch Vienna rectifier with LCL-type AC filter,"

in *Proc. IEEE Annual Conference on Power Electronics Specialist, PESC '03*, Jun. 2003, pp. 1063–1068 vol.3.

[64] H. Xu, W. Yao, and S. Shao, "Improved SVPWM schemes for Vienna rectifiers without current distortion," in *Proc. IEEE Energy Conversion Congress and Exposition (ECCE)*, Oct. 2017, pp. 3410–3414.

[65] F. Wang, Y. Teng, Z. Yuan, and J. Xu, "A maximum power factor of control algorithms of three-level Vienna rectifier without current distortion at current zero-crossing point," in *Proc. IEEE International Power Electronics and Motion Control Conference (IPEMC-ECCE Asia)*, May 2016, pp. 2325–2331.

[66] A. Rajaei, M. Mohamadian, and A. Yazdian Varjani, "Vienna-rectifier-based direct torque control of PMSG for wind energy application," *IEEE Trans. Ind. Electron.*, vol. 60, no. 7, pp. 2919–2929, Jul. 2013.

[67] L. Dalessandro, S. D. Round, U. Drofenik, and J. W. Kolar, "Discontinuous space-vector modulation for three-level PWM rectifiers," *IEEE Trans. Power Electron.*, vol. 23, no. 2, pp. 530–542, Mar. 2008.

[68] D. Mukherjee and D. Kastha, "Voltage sensorless control of the three-level three-switch Vienna rectifier with programmable input power factor," *IET Power Electronics*, vol. 8, no. 8, pp. 1349–1357, Aug. 2015.

[69] H. Cheng, J. Kong, P. Wang, and C. Wang, "Hybrid control scheme for three-phase multilevel unidirectional rectifier under unbalanced input voltages," *IEEE Access*, vol. 7, pp. 29 989–30 001, Feb. 2019.

[70] C. Wang, J. Liu, H. Cheng, Y. Zhuang, and Z. Zhao, "A modified one-cycle control for Vienna rectifiers with functionality of input power factor regulation and input current distortion," *Energies*, vol. 12, no. 17, p. 3375, Sep. 2019.

[71] H. Cheng, J. Kong, X. Wang, P. Wang, T. Chen, and C. Wang, "A modified one-cycle control for Vienna rectifiers with functionality of input power factor regulation and input current distortion," *IET Power Electronics*, vol. 12, no. 17, p. 1816 – 1824, Jun. 2019.

[72] R. Burgos, R. Lai, Y. Pei, F. Wang, D. Boroyevich, and J. Pou, "Space vector modulator for Vienna-type rectifiers based on the equivalence between two- and three-level converters: A carrier-based implementation," *IEEE Trans. Power Electron.*, vol. 23, no. 4, pp. 1888–1898, Jul. 2008.

[73] Chongming Qiao and K. M. Smedley, "Three-phase unity-power-factor star-connected switch (Vienna) rectifier with unified constant-frequency integration control," *IEEE Trans. Power Electron.*, vol. 18, no. 4, pp. 952–957, Jul. 2003.

[74] R. Lai, F. Wang, R. Burgos, D. Boroyevich, D. Jiang, and D. Zhang, "Average modeling and control design for Vienna-type rectifiers considering the dc-link voltage balance," *IEEE Trans. Power Electron.*, vol. 24, no. 11, pp. 2509–2522, Nov. 2009.

[75] J. Alahuhtala, J. Virtakoivu, T. Viitanen, M. Routimo, and H. Tuusa, "Space vector modulated and vector controlled Vienna I rectifier with active filter function," in *Proc. Power Conversion Conference - Nagoya*, Apr. 2007, pp. 62–68.

[76] M. H. Johnson and D. C. Aliprantis, "Analysis and control of PMSG-based wind turbine with Vienna rectifier near current zero crossings," in *Proc. Power and Energy Conference at Illinois (PECI)*, Feb. 2014, pp. 1–8.

[77] W. Yao, Z. Lv, M. Zhang, and Z. Lin, "A novel SVPWM scheme for Vienna rectifier without current distortion at current zero-crossing point," in *Proc. IEEE International Symposium on Industrial Electronics (ISIE)*, Jun. 2014, pp. 2349–2353.

[78] A. M. Hava, R. J. Kerkman, and T. A. Lipo, "A high-performance generalized discontinuous PWM algorithm," *IEEE Trans. Ind. Appl.*, vol. 34, no. 5, pp. 1059–1071, Sep. 1998.

[79] J. Lee and K. Lee, "Carrier-based discontinuous PWM method for Vienna rectifiers," *IEEE Trans. Power Electron.*, vol. 30, no. 6, pp. 2896–2900, Jun. 2015.

[80] J. Lee and K. Lee, "Performance analysis of carrier-based discontinuous PWM method for Vienna rectifiers with neutral-point voltage balance," *IEEE Trans. Power Electron.*, vol. 31, no. 6, pp. 4075–4084, Jun. 2016.

[81] X. Li, J. Han, Y. Sun, M. Su, J. Lin, and S. Xie, "A generalized design framework for neutral point voltage balance of three phase Vienna rectifiers," *IEEE Trans. Power Electron.*, pp. 1–1, Oct. 2019.

[82] J. Minibock and J. W. Kolar, "Novel concept for mains voltage proportional input current shaping of a Vienna rectifier eliminating controller multipliers," *IEEE Trans. Ind. Electron.*, vol. 52, no. 1, pp. 162–170, Feb. 2005.

[83] D. Mukherjee and D. Kastha, "Voltage sensorless control of Vienna rectifier in the input current oriented reference frame," *IEEE Trans. Power Electron.*, pp. 1–1, 2018.

[84] B. Wang, G. Venkataramanan, and A. Bendre, "Unity power factor control for three-phase three-level rectifiers without current sensors," *IEEE Trans. Ind. Appl.*, vol. 43, no. 5, pp. 1341–1348, Sep. 2007.

[85] J. Pou, D. Boroyevich, and R. Pindado, "New feedforward space-vector PWM method to obtain balanced ac output voltages in a three-level neutral-point-clamped converter," *IEEE Trans. Ind. Electron.*, vol. 49, no. 5, pp. 1026–1034, 2002.

[86] Z. He, H. Ding, Z. Chen, Z. Xun, C. Liu, D. Zhang, and J. Shao, "A novel method to evaluate the influence of Vienna rectifier neutral-point voltage fluctuation on input current quality," *IEEE Trans. Power Electron.*, vol. 36, no. 7, pp. 8347–8358, Jul. 2021.

[87] J. Park, J. Lee, and K. Lee, "Sinusoidal harmonic voltage injection PWM method for Vienna rectifier with an LCL-filter," *IEEE Trans. Power Electron.*, vol. 36, no. 3, pp. 2875–2888, Mar. 2021.

[88] W. Cao, B. C. Mecrow, G. J. Atkinson, J. W. Bennett, and D. J. Atkinson, "Overview of electric motor technologies used for more electric aircraft (MEA)," *IEEE Trans. Ind. Electron.*, vol. 59, no. 9, pp. 3523–3531, Sep. 2012.

[89] S. Bozhko, M. Rashed, C. I. Hill, S. S. Yeoh, and T. Yang, "Flux-weakening control of electric starter–generator based on permanent-magnet machine," *IEEE Trans. Transport. Electrific.*, vol. 3, no. 4, pp. 864–877, Dec. 2017.

[90] H. Chen and D. C. Aliprantis, "Analysis of squirrel-cage induction generator with Vienna rectifier for wind energy conversion system," *IEEE Trans. Energy Convers.*, vol. 26, no. 3, pp. 967–975, Sep. 2011.

[91] J. Lee and K. Lee, "Predictive control of Vienna rectifiers for PMSG systems," *IEEE Trans. Ind. Electron.*, vol. 64, no. 4, pp. 2580–2591, Apr. 2017.

[92] J. Lee, K. Lee, and F. Blaabjerg, "Predictive control with discrete space-vector modulation of Vienna rectifier for driving PMSG of wind turbine systems," *IEEE Trans. Power Electron.*, pp. 1–1, Dec. 2019.

[93] B. Briane and S. Loudot, "Rapid reversible charging device for an electric vehicle," Dec. 23 2014, uS Patent 8,917,046.

[94] E. Ganev, "High-reactance permanent magnet machine for high-performance power generation systems," in *Proc. SAE International Power Systems Conference*, Nov. 2006. [Online]. Available: https://doi.org/10.4271/2006-01-3076

[95] D. V. Makarov, A. S. Khlebnikov, A. V. Geist, and P. A. Bachurin, "Generation system with variable frequency and constant amplitude," in *Proc. International Youth Conference on Energetics (IYCE)*, Jul. 2011, pp. 1–9.

[96] J. Wai and T. M. Jahns, "A new control technique for achieving wide constant power speed operation with an interior PM alternator machine," in *Proc. IEEE Industry Applications Conference, IAS Annual Meeting (Cat. No.01CH37248)*, vol. 2, Sep. 2001, pp. 807–814.

[97] R. Teodorescu, M. Liserre, and P. Rodriguez, *Grid converters for photovoltaic and wind power systems*. John Wiley & Sons, 2011, vol. 29.

[98] P. Rodriguez, J. Pou, J. Bergas, J. I. Candela, R. P. Burgos, and D. Boroyevich, "Decoupled double synchronous reference frame PLL for power converters control," *IEEE Trans. Power Electron.*, vol. 22, no. 2, pp. 584–592, Mar. 2007.

[99] E. Robles, S. Ceballos, J. Pou, J. L. Martín, J. Zaragoza, and P. Ibañez, "Variable-frequency grid-sequence detector based on a quasi-ideal low-pass filter stage and a phase-locked loop," *IEEE Trans. Power Electron.*, vol. 25, no. 10, pp. 2552–2563, Oct. 2010.

[100] E. Robles, J. Pou, S. Ceballos, J. Zaragoza, J. L. Martin, and P. Ibañez, "Frequency-adaptive stationary-reference-frame grid voltage sequence detector for distributed generation systems," *IEEE Trans. Ind. Electron.*, vol. 58, no. 9, pp. 4275–4287, Sep. 2011.

[101] S. Yang, A. Bryant, P. Mawby, D. Xiang, L. Ran, and P. Tavner, "An industry-based survey of reliability in power electronic converters," *IEEE Trans. Ind. Appl.*, vol. 47, no. 3, pp. 1441–1451, Jun. 2011.

[102] M. H. M. Sathik, S. Prasanth, F. Sasongko, and J. Pou, "Lifetime estimation of off-the-shelf aerospace power converters," *IEEE Aerospace and Electronic Systems Magazine*, vol. 33, no. 12, pp. 26–38, Dec. 2018.

[103] J. Harikumaran, G. Buticchi, G. Migliazza, V. Madonna, P. Giangrande, A. Costabeber, P. Wheeler, and M. Galea, "Failure modes and reliability oriented system design for aerospace power electronic converters," *IEEE Open Journal of the Industrial Electronics Society*, vol. 2, pp. 53–64, Dec. 2020.

[104] A. Wechsler, B. C. Mecrow, D. J. Atkinson, J. W. Bennett, and M. Benarous, "Condition monitoring of dc-link capacitors in aerospace drives," *IEEE Trans. Ind. Appl.*, vol. 48, no. 6, pp. 1866–1874, Dec. 2012.

[105] H. Wang and F. Blaabjerg, "Reliability of capacitors for dc-link applications in power electronic converters—An overview," *IEEE Trans. Ind. Appl.*, vol. 50, no. 5, pp. 3569–3578, Oct. 2014.

[106] R. Bayerer, T. Herrmann, T. Licht, J. Lutz, and M. Feller, "Model for power cycling lifetime of IGBT modules - Various factors influencing lifetime," in *Proc. International Conference on Integrated Power Electronics Systems*, 2008, pp. 1–6.

[107] J. Chen, X. Zhang, and C. Wen, "Harmonics attenuation and power factor correction of a more electric aircraft power grid using active power filter," *IEEE Trans. Ind. Electron.*, vol. 63, no. 12, pp. 7310–7319, Dec. 2016.

[108] C. Felgemacher, S. V. Araújo, P. Zacharias, K. Nesemann, and A. Gruber, "Cosmic radiation ruggedness of Si and SiC power semiconductors," in *Proc. International Symposium on Power Semiconductor Devices and ICs (ISPSD)*, 2016, pp. 51–54.

[109] H. Asai, I. Nashiyama, K. Sugimoto, K. Shiba, Y. Sakaide, Y. Ishimaru, Y. Okazaki, K. Noguchi, and T. Morimura, "Tolerance against terrestrial neutron-induced single-event burnout in sic mosfets," *IEEE Trans. Nucl. Sci.*, vol. 61, no. 6, pp. 3109–3114, Dec. 2014.